A COMBINED MODELING AND EXPERIMENTAL INVESTIGATION OF NANO-PARTICULATE TRANSPORT IN NON-ISOTHERMAL TURBULENT INTERNAL FLOWS

by

Mehdi Abarham

A dissertation submitted in partial fulfillment
of the requirements for the degree of
Doctor of Philosophy
(Mechanical Engineering)
in The University of Michigan
2011

Doctoral Committee:

Professor Dionissios N. Assanis, Co-Chair
Associate Research Scientist John W. Hoard, Co-Chair
Professor Arvind Atreya
Assistant Professor Krzysztof J. Fidkowski
Daniel J. Styles, Ford Motor Company

To Marjan

ACKNOWLEDGMENTS

I would first offer my sincerest gratitude to my advisers, Professor Dennis Assanis and associate research scientist John Hoard, for their support, friendship, encouragement, and guidance throughout my graduate studies. I deeply appreciate professor Assanis for his devotion to his students both in his lab and in his engines classes. I would also be grateful to John Hoard for his knowledgeable advice through past four years and his intensive help in constructing and developing the experimental apparatus that is described in chapter 5.

I would like to extend my appreciation to my exceptional doctoral committee: Professor Arvind Atreya, Professor Krzysztof Fidkowski, and EGR technical specialist Daniel Styles for their support and suggestions throughout the course of this work. I would especially like to acknowledge the physical insight that professor Fidkowski provided during his CFD class and the independent research study that I performed under his supervision.

This work was performed at the University of Michigan's Walter E. Lay Automotive Laboratory, under a grant from Ford Motor Company. I would also thank Daniel Styles, Dr. Eric Curtis, and Nitia Ramesh at Ford Motor Company for their helpful discussions during our monthly meetings. I would like to also thank Mr. Jimi Tjong from Ford Canada for providing the flow meter, air heater, and machined pieces.

I acknowledge Oak Ridge National Laboratory scientists, Scott Sluder, Dr. John Storey, and Dr. Michal Lance for their experimental work that made my modeling work progressive and valuable and for the discussions and suggestions.

I sincerely acknowledge Dr. Parsa Zamankhan for his advice and collaboration on the axi-symmetric model that is described in chapter 4.

I would like to thank all the members of the DNA research group. I especially thank research scientists Dr. Babajimopolous, Dr. George Lavioe, Dr. Stani Bohac, and Dr. Jason Martz for their feedback on my preliminary exam and PhD presentations. I truly acknowledge students: Sotiris Mamalis, Janardhan Kodavasal, Elliot Ortiz, Anastasis Amoratis for their valuable discussions and collaborations either on the research topics or on graduate course projects. I thank Amit Goje and Tejas Chafekar masters student who worked on the experimental apparatus and helped me in designing and constructing it. I would like to acknowledge Luke Hagen, AnneMarie Lewis, and Ashwin Salvi for their valuable help on the experimental study including running the engines for my tests and teaching me how to run the engine. I sincerely wish them success in their graduate studies and careers. I truly appreciate the help of Ashwin Salvi for reviewing this dissertation.

I would also like to thank my undergraduate assistants (UROP students), Steve Upplegger and Riely Schwader for helping me with the experimental part of the project presented in Chapter 5. Additionally, I would like to acknowledge Mihalis Manolidis for his efforts in constructing the test set up for a period of time he collaborated on this research project.

At the Department of Mechanical Engineering at the University of Michigan, I have become acquainted with a number of great faculty and staff. I would like to thank the staff particularly Laurie Stoianowski, Melissa McGeorge, Susan Clair, Michelle Mahler, Kent Pruss, Bill Kirpatrick, and William Lim for their administrative and technical assistance.

My journey through these years was much easier with the friendship of many bright friends and colleagues in the Department of Mechanical Engineering and many more outside the academic environment. I cannot list all their names here, but I would

like to express my feelings. I especially thank Dr. Saeed Jahangirian for his friendship and support over more than ten years.

Finally, I would like to thank my extended family: my parents, sisters (Minoo and Mahshid), in-laws, and wife. I would like to specially thank my mother, Shahnaz, for her love and support that have always been with me. We lost my beloved sister-in-law, Nadereh, whom I just had a chance to meet over a short trip; but I will never forget her kindness and beautiful smile.

Words fail me to express my appreciation to my best friend and wife, Marjan, whose dedication, love, passion, and persistent confidence in me, has taken the load off my shoulder. I am so fortunate to have her in my life.

TABLE OF CONTENTS

LIST OF FIGURES

LIST OF TABLES

ABSTRACT

Particles in particle-laden flows are subject to many forces including turbulent impaction, Brownian, electrostatic, thermophoretic, and gravitational. Our scaling analysis and experiments show that thermophoretic force is the dominant deposition mechanism for submicron particles.

One common example of industrial devices in which thermophoretic particle deposition occurs is exhaust gas recirculation (EGR) heat exchangers used on diesel engines. They are used to reduce intake charge temperature and thus reduce emissions of nitrogen oxides. The buildup of soot particles in EGR coolers causes a significant degradation in heat transfer performance (effectiveness) generally followed by the stabilization of cooler effectiveness (no more degradation) for longer exposure times.

To investigate the initial sharp reduction in cooler effectiveness, an analytical solution, computational one dimensional model and an axi-symmetric model are developed to estimate particulate deposition efficiency and consequently the overall heat transfer reduction in tube flows. Internal flows (tube/channel) are employed in this dissertation to resemble real EGR coolers. The analytical solution is employed for a parametric study and sensitivity analysis to highlight the effect of critical boundary conditions. The computational models are developed to solve the governing equations for exhaust flow and particles. Model output including predicted mass deposition along the tube and the tube effectiveness drop has been compared against experiments conducted at Oak Ridge National Laboratory with good accuracy. CFD models improve the output compared to the analytical solution while the axi-symmetric model is significantly closer to the experiments due to accurate calculations of near wall heat and mass fluxes.

Mechanisms responsible for the cooler effectiveness stabilization in long exposure times are not clearly understood. To address the stabilization trend, a visualization test rig is developed to track the dynamics of particulate deposition and removal in-situ, and a digital microscope records any events. Interesting results are observed for flaking/removal of the deposit layer at various boundary conditions. In contrast to conventional understanding, large particles (tens of microns) were also observed in diesel exhaust. Water condensation occurring at a low EGR cooler coolant temperature resulted in a significant removal of deposit in the form of flakes while thermal expansion alone did not remove the deposit layer.

CHAPTER 1

INTRODUCTION

There are many applications involved in understanding of nanoparticle-laden flows including gas cleaning, prevention of particle deposition on silicon wafers of semiconductors, pharmaceutical applications, and heat exchanger fouling (accumulation of material on solid surfaces i.e. particle deposition). Depending on the purpose of the application, particle deposition is desired (gas cleaning) or unwanted (microelectronics and pharmaceutical applications, and heat exchangers). Therefore, particle transport modeling helps to understand the physics and the process of particle deposition so that it can be prevented (mitigated) or enhanced depending on the application.

Although developed models in this study are general for particle transport in internal flows and can be used for similar applications, we focused on studying of the particle transport in heat exchangers. One common example of heat exchanger fouling is in exhaust gas recirculation (EGR) coolers used in diesel engines with the purpose of emission reduction. In the following sections, the aim of EGR cooler usage and the problem associated with them is introduced and plans are discussed on how to tackle the problem and propose solutions.

1.1 Exhaust Gas Recirculation (EGR) Cooler Fouling

Petroleum fuels are vastly used in the U.S. transportation system. Beside the massive consumption of these fuels, vehicles produce CO_2 emissions that have a drastic

effect on global warming. While diesel engines are very efficient and consequently produce less CO_2, one of their main shortcomings is their high level of nitrogen oxides (NO_x) emissions. Exhaust gas recirculation (EGR) has proven to be an effective way of reducing NO_x formation in diesel engines; however the performance of the EGR system has been shown to significantly degrade with particulate deposition (fouling). The aim of this thesis is to study the mechanisms of particulate deposition and removal in EGR coolers and to find ways to mitigate or prevent deposition and/or enhance removal mechanisms.

In practical engine systems, a portion of exhaust gas, known as EGR, is returned to the engine and mixed with incoming fresh air. Through the use of EGR, peak in-cylinder and flame temperatures can be lowered, leading to drastically lowered engine out NO_x emissions. Within the EGR cooler, engine coolant is used to cool the exhaust gas, which enhances the reduction of NO_x emissions. So, the presence of cooled surfaces will cause soot deposition and condensation of hydrocarbons and acids. The buildup of deposits in EGR coolers causes significant degradation in heat transfer performance, often on the order of 20-30% and accordingly clogging flow passages. Deposits also increase pressure drop across coolers. However, future emission standards will require increased EGR flow rates and reduced temperatures, requiring particulate deposition within the EGR cooler to be reduced or prevented so that the engine can meet future emission standards.

It is unlikely that EGR cooler deposits can be prevented from forming when soot and HC are present. It is generally felt that dry fluffy soot is less likely to cause major fouling than heavy wet soot. Experimental data indicates that majority of deposited mass is due to particulates and only a small fraction of hydrocarbons condense on tubes [1].

Most current diesel engines have a single EGR cooler, using engine coolant to cool the EGR. Some engines have more than one cooler; this is primarily driven by the amount of cooling required and the package space available. Some manufacturers have

designed engines to have more effective cooling by use of a second cooler and a second cooling system (FORD 6.7L diesel engine). Here, coolant can be supplied at 40-50°C so that the EGR outlet temperature can be reduced further than could be done with the normal cooling system.

In the following sections (extracted from [1]), we discuss what the deposits are, characterization of the deposit build, and deposit stabilization and recovery.

1.2 What Are Deposits

The deposits in the EGR cooler form a layer on the cooled surfaces, Figure 1.1 [2]. Here, deposits are shown after 200 hours of an EGR cooler fouling engine dynamometer test. The figure shows the inlet of the first EGR cooler. The deposits are black, and in this case fairly dry and fluffy in appearance. There is some evidence of flaking of the deposits, although it cannot be said with certainty whether this occurred while the engine ran or during handling and cutting.

Cooler deposits can also have a wet, oily appearance or in some cases can be hard and brittle in character. These differences evidently arise depending on the relative quantities of elemental soot particulate matter (PM), hydrocarbon (HC), acids, and perhaps the time-temperature history. These issues will be discussed in more detail in following sections.

Figure 1.1 – Deposits at EGR cooler inlet following 200 hour engine fouling test [2]

Lepperhoff and Houben [3] note that engine deposits (general deposits, not diesel EGR coolers specifically) are a combination of organics including carbon, HC, oxygen, and nitrogen, along with inorganics including sulfur and traces of barium and calcium. It is useful to examine the constituents of these deposits in more detail.

1.2.1 Soot

Deposits contain soot from the exhaust. The soot coming out of the engine is "elemental carbon"; that is, mainly carbon. It generally consists of small (20-30 nm) roughly spherical particles, agglomerated into larger particles. Maricq & Harris [4] show that diesel soot agglomerate size ranges about 20-300 nm (0.02-0.30 μm).

Many studies of diesel PM include measurement of "SOF" or soluble organic fraction. For EGR coolers, we must understand how this is measured. Most literature on PM includes the steps of mixing exhaust with dilution air and cooling to room temperature. During this process, some of the HC and sulfate in the gas will condense onto the surface of the soot particles. However, this does not generally happen to the soot arriving in hot exhaust gas at the EGR cooler inlet. Thus, "SOF" probably is not a large part of the soot in the EGR cooler unless the HC has separately condensed. Nonetheless, hydrocarbons associated with the deposits are sometimes incorrectly called SOF.

1.2.2 Hydrocarbons (HC)

Diesel exhaust contains a wide range of hydrocarbon and hydrocarbon-derived species. These include unburned and partially burned fuel and lube oil. Some of these compounds can condense on cooler surfaces. Condensation occurs when the surface of the cooler is below the dew point for the partial pressure of the compound. Thus, heavier species and higher concentration species will condense most.

Although some authors such as Lepperhof argue that a layer of HC on the surface is essential to act as a "glue" causing soot to stick to the surface, most authors agree that for particles as small as diesel soot, the soot sticks to the surface due to Van der Waals forces, whether or not there is HC present [5]. Nonetheless, it is clear that condensed HC will change the character of the deposit layer.

Hoard et.al. [2] analyzed the extractable fraction of the deposit HCs. Figure 1.2 shows the relative amounts (nanograms of each component per gram of deposit sample) of C_{10}-C_{17} alkane, C_{18}-C_{24} alkane, and light and heavy aromatics extracted from EGR cooler deposits. These are generally in the range of the heaviest fraction of diesel fuel, or the typical range of lube oil. Note that there are two EGR coolers in series in these data; the figure shows samples from inlet and outlet of each cooler.

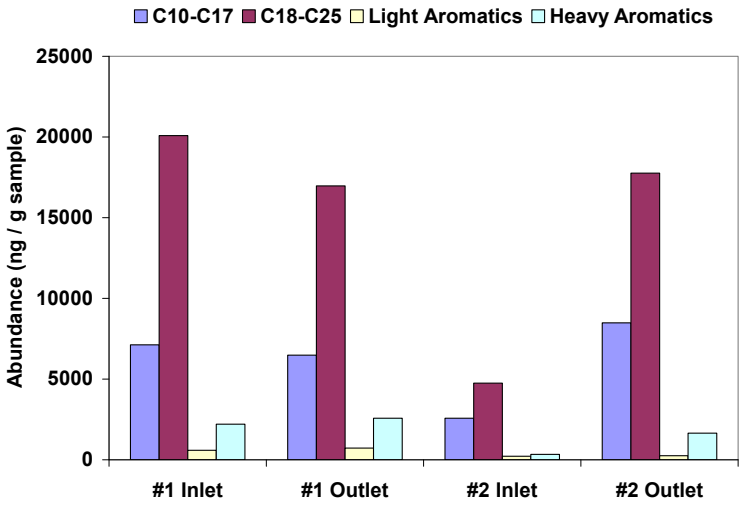

Figure 1.2 – Speciation of the extractable fraction of HC from EGR cooler deposit – Data from Hoard et.al. [2]

1.2.3 Acids

The relatively low temperature cooler surfaces can cause condensation of acids and water from the exhaust. McKinley [6] gives an excellent account of sulfuric acid

condensation. For typical fuel sulfur levels, the dew point for sulfuric acid is in the range of 100°C – i.e., close to normal operating temperature for an EGR cooler.

Girard et.al. [7] collected sulfuric acid condensate from an engine EGR system. With EGR cooler outlet temperature at 103°C, they collected 20-24 ml/hr liquid condensate; the condensate was 1.1-1.3% H_2SO_4.

Similarly, the dew point for nitric acid is around 40°C – potentially an issue for cold-coolant operation or for future engines with low temperature secondary EGR coolers. Organic acids such as formic and acetic acid can also be found in exhaust condensate.

Such acid condensation is of course a concern in material choices; typically a high grade stainless steel is required to resist the corrosive effects of these acid condensates. Stolz et.al. [8] show corrosion test results indicating that 904 stainless has better corrosion performance than 304 or 316L.

In addition, acids are known to contribute to chemical reactions with hydrocarbons, leading to hard deposits. It is possible that acids play a role in aging of deposits, although there does not seem to be any literature confirming this mechanism.

Although hydrocarbon and acids are important, it is shown that the majority of deposit is dry fluffy soot particles. Therefore, in this thesis, only soot deposition is considered to model the formed deposit. There is a developed model in Appendix A for condensation of hydrocarbons and acids in EGR coolers but it was not hooked to the soot deposition model. A comprehensive description when the HC subroutine is hooked to the soot deposition model is presented in [9] .

1.3 Characteristics of Deposit Build

Many authors have presented data on cooler effectiveness degradation with deposits. An example of cooler degradation is shown in Figure 1.3 ([2]). Here, a 2008-

level diesel engine having two EGR coolers in series is run on a three mode cooler fouling test, and the cooler effectiveness is plotted versus time. In the curve, the cooler effectiveness drops on a roughly exponential curve, reaching a steady state value at lower effectiveness than clean. At the condition shown, effectiveness drops roughly 15-20% from clean to dirty.

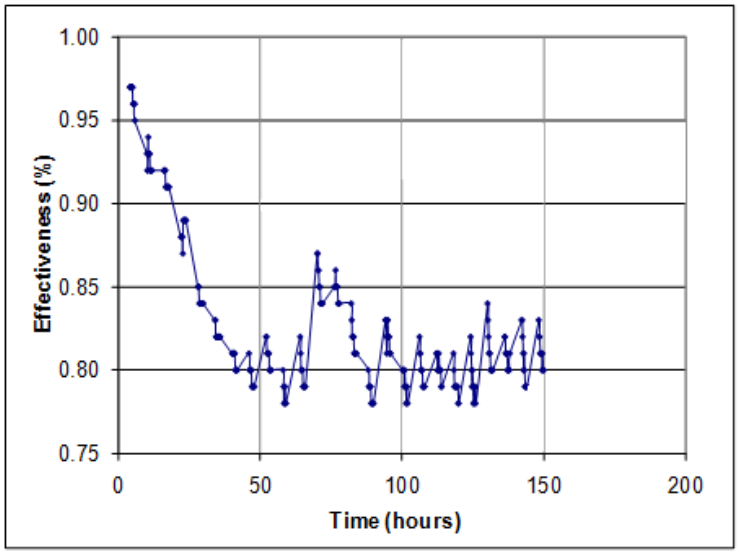

Figure 1.3 – EGR cooler system effectiveness versus engine running hours, Data from Hoard et.al. [2]

In addition to the data shown in above, Banzhaf and Lutz [10] show a 15% change in effectiveness over a 200 hour engine deposit test of a tube-in-shell "winglet" style cooler. Majewski and Pietrasz [11] report on a heat exchanger used to cool engine exhaust downstream of an oxidation catalyst. After 100 hours of operation the cooler heat transfer resistance R_f stabilized at 0.0053 m^2K/W.

Stolz et.al. [8] state that deposit build is worst at low speeds and loads. They also state (without showing data) that at typical driving conditions there is a self-cleaning process caused by abrasive high speed gas. They found vehicle aged coolers had deposit thickness 0.1-0.2 mm with no significant difference between inlet and outlet of the

cooler. Effectiveness loss is 15% for severe conditions, improving to 8-10% loss after recovery. They state that gas side pressure drop increases 5% with deposits.

Ewing et.al. [12] exposed simple straight tubes, as EGR cooler surrogates, to diesel exhaust. The tubes were then analyzed with neutron radiography as a non-invasive technique to measure the deposit thickness inside the tubes. Figure 1.4 from that paper shows the deposit thickness along the tube length (0 is the tube inlet) for a condition at Reynolds number = 7000 (turbulent flow). The deposit is thickest at the inlet. There is some wave-like structure to the deposit along the tube, perhaps indicating some deposit-relocation mechanism similar to sand dunes.

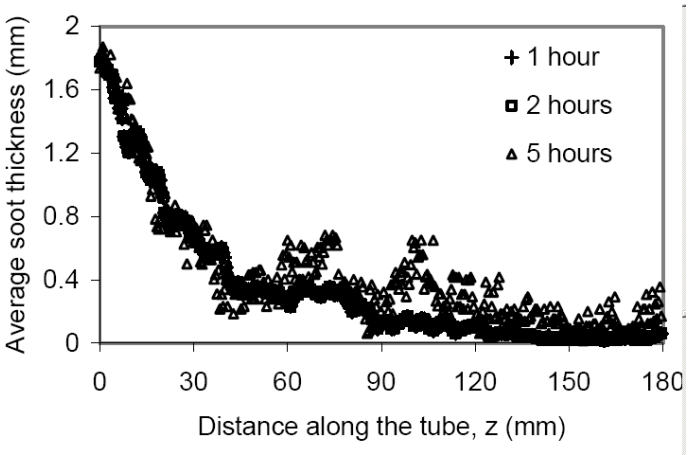

Figure 1.4 – Deposit thickness along a cooler tube ([12])

Stolz et.al. find no difference in deposit depth front to rear, while Ewing et.al. found a strong difference. It may be related to the test time. Ewing et.al. ran tests of 1, 2, and 5 hours duration – i.e., rather short times although Stolz ran 200 hours. If deposits initially are heavier at the front, the deposit layer will create an insulation effect, tending to reduce deposition rate as the deposit builds. Thus, the gas arriving downstream is hotter and dirtier, so the deposit will gradually even out over a long time.

Lepperhoff [3] measured deposit mass per unit area, deposit thickness, and heat transfer coefficient during 80 hours of deposit accumulation in a simulated EGR cooler

tube in diesel exhaust. He shows that the deposit thickness grows rapidly until reaching a steady value at about 20 hours. The heat transfer coefficient drops rapidly, stabilizing about the same time that the deposit thickness does. However, the deposit mass per unit surface area continues to increase over the 80 hour test. This seems to indicate that the heat transfer loss is related to properties other than the deposit mass. It is assumed that deposit porosity and density may change over time, with effect on heat transfer.

1.4 Stabilization and Recovery

It is common for EGR cooler effectiveness to degrade rapidly at first, then approach a steady state value exponentially. Such behavior can be seen in Figure 1.3 and in a large number of publications. The mechanisms leading to this stabilization are not clearly understood and there is no published article discussing deposit removal of sub-micron particles in the sub-sonic flow range. There may be deposit removal mechanisms, or it may be that the rate of deposition decreases or that the deposit layer thermal properties change as deposits build. It is not easily possible to determine whether either or both of these mechanisms is the reason, but in any case the exponential approach to steady thermal performance is typical of many heat exchanger systems ([13]).

Another behavior, rarely reported, is cooler recovery[1] – that is, a sudden improvement in thermal performance. Banzhaf & Lutz [9] state without showing data that "load changes between the operating points helped to reduce deposits which had been formed during the previous steady state operation". Andrews et.al. [14] report that particulate can store and be blown out of exhaust pipes and mufflers. Presumably, similar effects can happen with soot in EGR coolers. There is little real data on this recovery effect, and the little that exists is not very clear. This is a topic that seems to need more research.

[1] We use the term recovery to indicate at least partial recovery of clean cooler performance, and avoid the term regeneration since that is easily confused with diesel particulate filter (DPF) regeneration.

Bravo et.al. [15] developed a cooler aging cycle. They report (without showing data) that coolers are sometimes cleaned during transient operation. In a separate experiment [16] they tried a strategy that opens the EGR valve during decelerations in order to generate a large flow velocity in the cooler, in hopes that would blow deposits out of the cooler. The strategy was not successful, and they found no design or strategy that clearly improves the self-cleaning capability of the coolers.

Charnay et.al. [17] tested fouling of EGR coolers on a test cycle. They note that during steady idling conditions with EGR inlet temperature 120°C and engine coolant 20-25°C an oily layer built up in the EGR cooler. This layer disappeared during the following, higher speed/load/temperature mode of the test cycle. They report that the EGR cooler effectiveness recovered near original levels after engine shut down and restart. They hypothesize that a liquid layer, including water, may loosen the deposit adhesion during engine-off periods leading to an effectiveness recovery. Detailed data on this is not included in the paper.

Epstein [13] notes that most people assume there is a deposit particle removal process associated with the shear forces of gas flow over the layer. This is not a lifting force, but a force trying to "roll" the particle downstream. However, note that if an EGR cooler is tested on a test cycle with varying flow rates, and deposits build up then the highest flow rate must not be enough to remove the deposits completely. Otherwise, the deposits would not accumulate. The presence of heavy deposits in used EGR coolers implies that normal vehicle operation does not generate high enough flow (and thus shear velocity) to remove most of the deposits.

Although there is not a clear indication in the literature on what mechanisms may be responsible for self-cleaning of EGR coolers, the following potential mechanisms are suggested. Experiments should be run to determine which mechanisms are active. We address most of the following in chapter 5 of this thesis based on a series of visualization experiments that we designed and conducted.

- Blow Out – deposits accumulated under some conditions might blow off the surface at another, higher flow condition. This would be related to the shear force on the surface due to gas flow.
- Flaking – deposits might lose adhesion to the surface and flake off. This could be due to a factor reducing the strength of adhesion, such as water, liquid HC, and/or acids.
- Cracking – If the deposits harden with time, then the deposit layer might crack due to thermal or other stresses, causing portions to break off
- Evaporation or Oxidation – it is possible that some of the deposit material might be semi-volatile, and some operating conditions might raise temperature high enough for these components to evaporate. Oxidation of soot layers would require temperature above 500°C or so, unlikely to occur in an EGR cooler. For EGR valves, it is known that "hot side" locations (upstream of the EGR cooler) allow the EGR valve to reach temperatures where deposits are cleaned periodically.
- Wash Out – heavy condensation of water, HC, and/or acid might form a liquid film that would carry deposits out of the cooler
- Big particles bombardment - big particles or flakes coming from the cylinders might hit the formed deposit layer and cause the deposit removal

Each of these mechanisms has been briefly suggested in the literature, but there is no previous experimental data to show any are actually effective, nor how to intentionally create appropriate conditions to cause self-cleaning.

1.5 Dissertation Overview

The objective of this thesis is to study the deposition mechanisms of exhaust soot particles in EGR coolers and propose possible removal or recovery methods that are

applicable for real EGR coolers. Applicable methods for EGR coolers recovery reduces the cost of EGR coolers and helps auto-manufacturers meet future standard emissions. The document is organized as follows:

In chapter 2, the scaling analysis of different deposition mechanisms for small soot particles in exhaust flows are discussed and described in detail. Additionally, different removal mechanisms from literature for particles larger than soot particles are studied to see if they can potentially be responsible for removal in EGR coolers. Dominant deposition mechanism is understood for EGR coolers in this chapter but existing removal mechanisms for larger particles did not seem to be the reason for removal of small soot particles in EGR coolers.

Since EGR coolers are mainly shell-and-tube heat exchangers, we limited our study to fundamental investigation of particulate transport in turbulent tube flows that resembles real EGR coolers. Therefore, in chapter 3, an analytical study is done in order to predict the soot particle deposited mass and effectiveness drop of surrogate tubes at various boundary conditions. A parametric study and a sensitivity analysis are done to study the effect of critical boundary conditions including inlet gas temperature and pressure, wall temperature, inlet particle concentration, and gas mass flow rate on the particle deposition and heat transfer reduction of tubes. The results are compared with EGR flow experiments (in a controlled engine test set up) performed at Oak Ridge National Laboratory (ORNL) at the same boundary conditions.

In chapter 4, a one dimensional model in MATLAB and an axi-symmetric model in ANSYS-FLUENT are proposed to study the particulate deposition in turbulent tube flows. These two models are more accurate compared to the proposed analytical method and include more physics (gas properties variation along the tube, deposit layer properties variation, and deposit layer thickness variation in axial and radial directions) when the axi-symmetric model shows a significantly better prediction of the deposited mass gain and thickness compared to the analytical solution and the one dimensional model (52%

improvement compared to the analytical solution and 14% improvement compared to the 1D model). Although the results of CFD models are good for a relatively short exposure time, there is a need for either removal mechanisms or measurement of deposit layer properties when the layer builds up in order to predict the stabilization behavior of the fouled (deposited) layer. Therefore, we decided to study the dynamics of the fouling phenomenon in-situ.

In chapter 5, we describe a unique visualization experimental apparatus that we designed and constructed to monitor the deposition and removal of the deposit layer and potentially measure the deposit layer properties while it grows in-situ. We proposed two recovery methods based on our observation. Out of two, one method is published in this document and the other method (seems very promising for recovery of real EGR coolers) remains Ford confidential. This recovery method will be disclosed for a potential patent in the tech transfer office of the University of Michigan.

Finally, in Chapter 6, the major conclusions derived from this thesis and our contributions to the field are stated. Possible areas for future investigation are discussed as well.

1.6 References

[1] Hoard., J., Abarham, M., Styles, D., Giuliano, J., Sluder, S., Storey, J., "Diesel EGR cooler fouling", SAE transactions, International Journal of Engines 1(1):1234-1250, 2009.

[2] Hoard, J., Giuliano, J., Styles, D., Sluder, S., Storey, J., Lewis, S., Strzelec, A., Lance, M., "EGR Catalyst for Cooler Fouling Reduction", DOE Diesel Engine-Efficiency and Emission Reduction Conference, Detroit, MI, August 2007.

[3] Lepperhoff, G., Houben, M., "Mechanisms of Deposit Formation in IC Engines and Heat Exchangers". SAE paper 931032, 1993.

[4] M. Maricq, S. Harris, "The role of fragmentation in defining the signature size distribution of diesel soot", Aerosol Science 33: 935-942, 2002.

[5] Oliveria, R., "Understanding adhesion: a means for preventing fouling", Experimental Thermal and Fluid Science 14:316-322, 1997.

[6] McKinley, T. L., "Modeling Sulfuric Acid Condensation in Diesel Engine EGR Coolers". SAE paper 970636, 1997.

[7] Girard, J. W., Gratz, L. D., Johnson, J. H., Bagley, S. T., Leddy, D. G., "A Study of the Character and Deposition Rates of Sulfur Species in the EGR Cooling System of a Heavy-Duty Diesel Engine", SAE paper 1999-01-3566, 1999.

[8] Stolz, A., Fleischer, K., Knecht, W., Nies, J., Strahle, R., "Development of EGR Coolers for Truck and Passenger Car Application", SAE paper 2001-01-1748, 2001.

[9] Abarham, M., Hoard., J., Assanis, D., Styles, D., Curtis, E., Ramesh, N., Sluder, S., Storey, J., "Modeling of Thermophoretic Soot Deposition and Hydrocarbon Condensation in EGR Coolers", SAE transactions, International Journal of Fuels and Lubricants 2 (1): 921-931,2009.

[10] Banzhaf, M., Lutz, R., "Heat Exchanger for Cooled Exhaust Gas Recirculation", SAE paper 971822, 1997.

[11] Majewski, W. A., Pietrasz, E., "On-Vehicle Exhaust Gas Cooling in a Diesel Emissions Control System". SAE paper 921676, 1992.

[12] Ewing, D., Ismail, B., Cotton, J. S., Chang, J. S., "Characterization of the Soot Deposition Profiles in Diesel Engine Exhaust Gas Recirculation (EGR) Cooling Devices Using a Digital Neutron Radiography Imaging Technique", SAE paper 2004-01-1433, 2004.

[13] Epstein, N., "Elements of Particle Deposition onto Nonporous Solid Surfaces Parallel to Suspension Flows", Experimental Thermal and Fluid Science 14:323-334, 1997.

[14] Andrews, G. E., Clarke, A. G., Rojas, N. Y., Sale, T., Gregory, D., "The Transient Storage and Blow-Out of Diesel Particulate in Practical Exhaust Systems", SAE paper 2001-01-0204, 2001.

[15] Bravo, Y., Lazaro, J. L., Garcia-Bernad, J. L., "Study of Fouling Phenomena on EGR Coolers due to Soot Deposits: Development of a Representative Test Method", SAE paper 2005-01-1143, 2005.

[16] Bravo, Y., Moreno, F., Longo, O., "Improved Characterization of Fouling in Cooled EGR Systems", SAE 2007-01-1257, 2007.

[17] Charnay, L., Soderberg, E., Malmlof, E., Ohlund, P., Ostling, L., Fredholm, S., "Effect of fouling on the efficiency of a shell-and-tube EGR cooler", EAEC Congress Vehicle Systems Technology for the Next Century. Barcelona, 1999. Paper STA99C418.

CHAPTER 2

SCALING ANALYSIS OF PARTICLE DEPOSITION AND REMOVAL MECHANISMS

In this chapter, a scaling analysis of deposition and removal forces on a small particle (mean average diameter of exhaust soot particles) is presented. Different correlations in literature are employed and discussed and a scaling analysis is shown. This study led us through the modeling of the particle deposition based on the dominant mechanism and finding strategies to investigate particle removal in EGR coolers.

2.1 Deposition Mechanisms

Before describing deposition mechanisms, the soot particulate distribution in the exhaust flow must be analyzed. Harris and Maricq [1] studied the EGR particle distribution in many different engine conditions. A log-normal distribution for particle diameter is offered in the aforementioned work with the mean particle diameter of $\mu_g = 57.3$ nm and the standard deviation of $\sigma_g = 1.8$. Figure 2.1 illustrates the normalized particle distribution of diesel exhaust flow.

It is noted that the EGR soot particle range is between 10nm to 300nm. It is seen that almost 50% of soot particles have a size of 60 nm and less. This number (60 nm) is used to show how the deposition mechanism for small particles on this range differs from the deposition of larger particles.

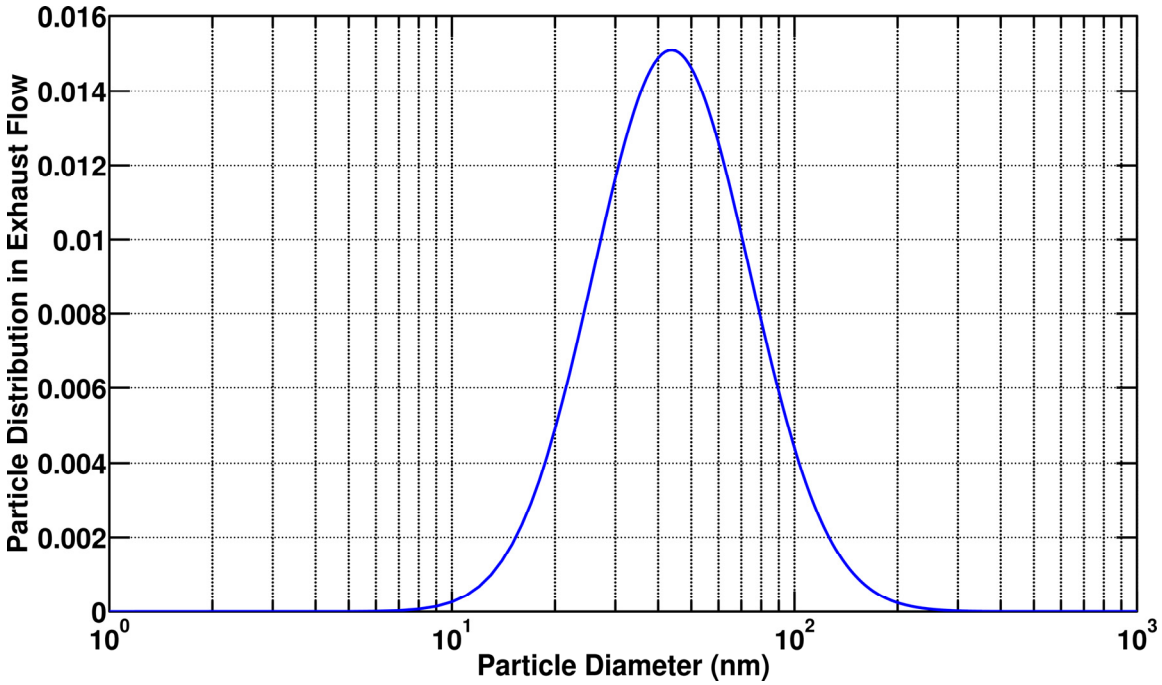

Figure 2.1 – EGR soot particles normalized distribution

In order to perform the scaling analysis of particle deposition and removal, some quantitative numbers are needed. Since most EGR coolers are tubes in shell type heat exchangers, this analysis is done for geometry similar to real EGR coolers tubes and the associated boundary conditions for a real EGR cooler (listed in Table 2.1). These numbers help us compare the mechanisms in the following sections. More detailed calculations are presented in the next chapter when deposition models are proposed.

Figure 2.2 shows a schematic of a surrogate tube in EGR cooler. The tube length (L), tube diameter (ID), averaged temperature ($\overline{T}$), soot particle concentration ($\overline{C}$), pressure ($\overline{P}$), velocity ($\overline{u}$), and wall temperature (T_w) are shown.

Table 2.1 – Geometry and boundary conditions of an EGR cooler tube

Tube inside diameter	5.5 mm
Tube length	0.3 m
Averaged gas temperature (K)	600 K
Wall temperature (K)	363 K
Averaged velocity (m/s)	25
Averaged pressure (kPa)	200
Averaged gas viscosity (kg/ms)	3.17×10^{-5}
Averaged gas density (kg/m3)	1.17
Particle concentration (mg/m3)	30
Particle density (kg/m3)	1770
Averaged sub-layer thickness (μm)	100
Averaged shear velocity (m/s)	1.7

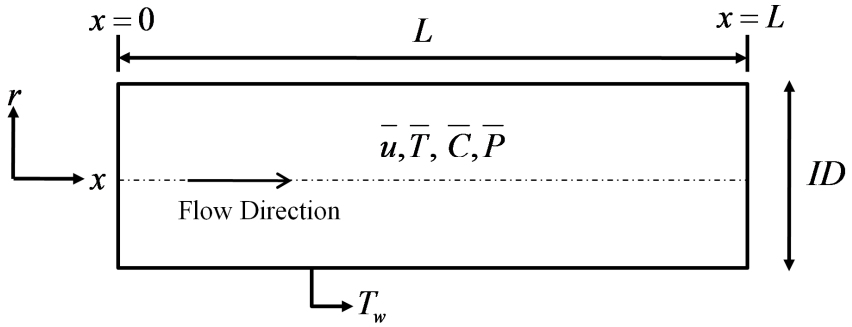

Figure 2.2 – Schematic of a surrogate tube and EGR flow

Total deposition flux of particles (J) toward the tube wall is defined as summation of all deposition fluxes based on the drift velocities (discussed in the following) as:

$$J = \sum_i \overline{C} V_i \tag{2.1}$$

There are a number of possible mechanisms by which particles may move from the gas flow onto the cooler surface. A comparison is made later between the deposition velocities of different mechanisms.

2.1.1 Thermophoresis

Thermophoresis is a particle motion generated by thermal gradients. Thermophoresis is the phenomenon that when a temperature gradient exists, particles move toward the cooler direction (Figure 2.3). This force arises from the fact that hotter gas molecules have higher velocity due to a larger kinetic energy. Thus, in a thermal gradient the gas on the hot side of the particle hits with higher force than the gas from the cooler side, and a net force is created toward the cooler region. As particles are transported from the bulk gas flow into the boundary layer near the surface, they enter a region of large thermal gradient and thus are thermophoretically driven toward the wall. Particles reaching the wall stick to the wall due to Van der Waals forces [2].

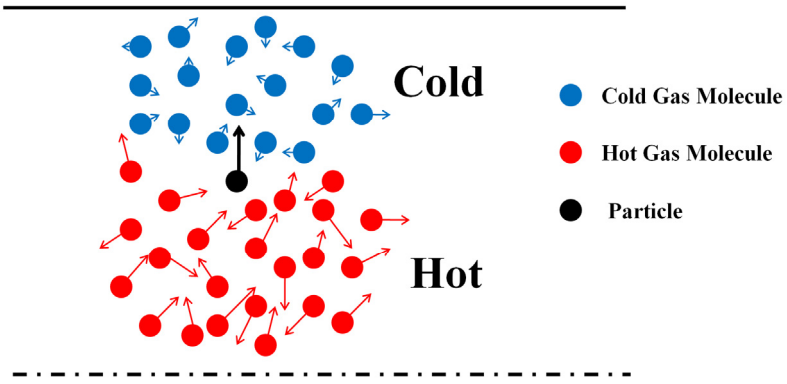

Figure 2.3 – Schematics of thermophoresis phenomenon

Researchers have studied thermophoresis and there are some correlations in literature for the thermophoretic force and velocity. Two common correlations are Brock-Talbot and modified Cha-McCoy-Wood (MCMW).

Brock-Talbot correlation

The thermophoretic drift velocity of a particle is defined as:

$$V_{th} = -K_{th} \frac{\nu}{\overline{T}} \vec{\nabla} \overline{T} \tag{2.2}$$

where ν is gas kinematic viscosity and K_{th} is the thermophoretic coefficient defined by:

$$K_{th} = \frac{2C_s C_c}{(1+3C_m Kn)} \times \frac{k_g / k_p + C_t Kn}{1+2k_g / k_p + 2C_t Kn} \tag{2.3}$$

k_g, k_p are gas and particulate thermal conductivity, respectively. Kn is Knudsen number $(=2\lambda/d_p)$, λ is the mean free path of a gas molecule and d_p is the particle diameter.

$$\lambda = \frac{2\mu}{\rho}\left(\frac{\pi MW_g}{8R\overline{T}}\right)^{0.5} \tag{2.4}$$

The correction factor (C_c) is also defined as:

$$C_c = 1 + K_n(AA + BBe^{-CC/Kn}) \tag{2.5}$$

The thermophoretic constants $AA, BB, CC, C_s, C_m, C_t$ are 1.2, 0.41, 0.88, 1.147, 1.146, and 2.20, respectively [3].

MCMW correlation

Thermophoretic force in the MCMW equation [4] is defined as:

$$F_{th} = 1.15 \frac{Kn}{4\sqrt{2}\alpha(1+\frac{\pi_1}{2}Kn)}.[1-\exp(-\frac{\alpha}{Kn})].(\frac{4}{3\pi}\phi\pi_1 Kn)^{1/2}\frac{k_b}{d_m^2}\nabla T d_p^2 \tag{2.6}$$

where:

$$\pi_1 = 0.18\frac{\frac{36}{\pi}}{(2-S_n+S_t)\frac{4}{\pi}+S_n}, \alpha = 0.22\left[\frac{\frac{\pi}{6}\phi}{1+\frac{\pi_1}{2}Kn}\right]^{1/2}, \phi = 0.25(9\gamma-5)\frac{c_v}{R} \tag{2.7}$$

In this study, the normal and tangential momentum accommodation coefficients are assumed $S_n = 1,\ S_t = 0$, respectively.

Thermophoretic drift velocity in this correlation is calculated as:

$$V_{th} = \frac{F_{th}\tau}{m_p} = \frac{F_{th}\tau}{\rho_p \pi d_p^3/6} \tag{2.8}$$

where τ is the particle relaxation time defined by:

$$\tau = (\frac{\rho_p d_p^2 C_c}{18\mu}) \tag{2.9}$$

It is usual to choose Brock-Talbot equations in articles; however, there is a criterion for employing that equation. He and Ahmadi [5] studied the thermophoretic deposition of particles and compared Brock-Talbot equation with the MCMW correlation. By comparing the two correlations with experimental measurements ([6],[7]), they showed that Brock-Talbot equation deviates from experimental results when particles are very small and the Knudsen number is larger than 2.

When the particle diameter equals to the mean free path of gas molecules, the Knudsen number is 2. So, if the particle diameter is less than the mean free path of gas molecules, the gas medium is not considered continuum anymore. It is recommended by He and Ahmadi [5] to use Brock-Talbot equation when Kn<2 and the MCMW equation when Kn>2.

According to the given boundary condition in Table 2.1, the mean free path of EGR gas molecules is calculated to be 78 nm (close to the exhaust soot particle mean diameter of 57 nm). Figure 2.4 compares the two correlations for a wide range of Knudsen numbers corresponding to the range of soot particles in the exhaust flows.

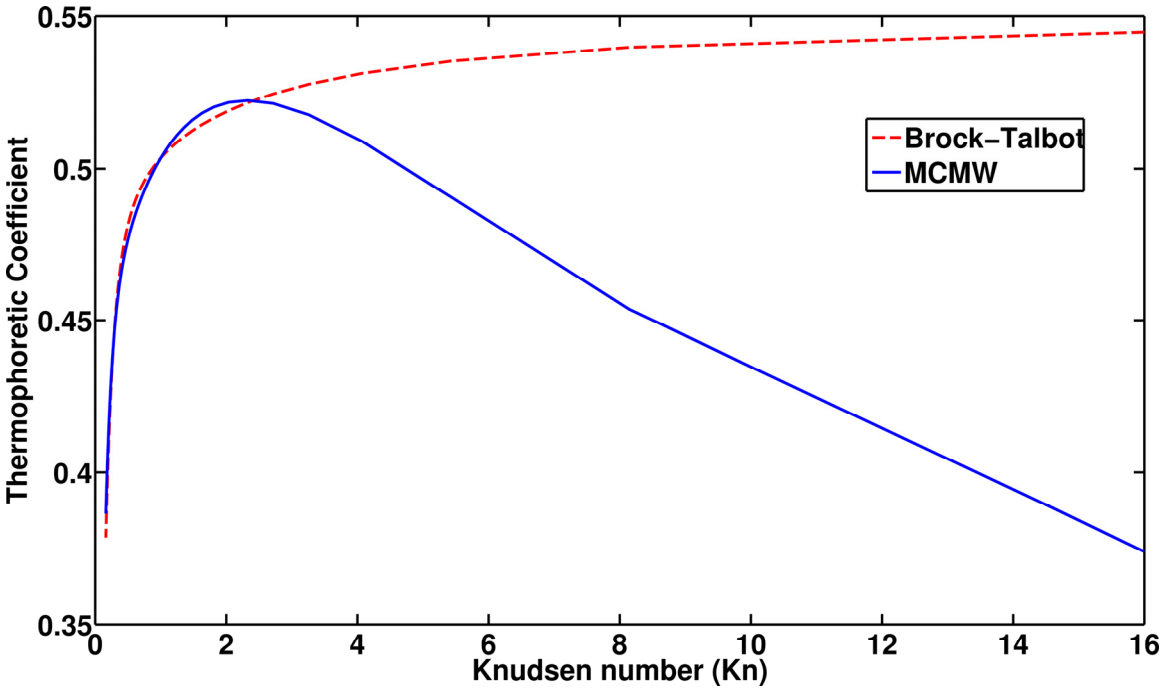

Figure 2.4 – MCMW and Brock-Talbot correlations comparison

Since more than 50% of particles have a diameter less than 60 nm, using Brock-Talbot equation over-predicts the thermophoretic deposition by a few percent. So, instead of taking the mean particle diameter, a weighted thermophoretic coefficient can be calculated for the whole range of soot particles. The fraction of each particle is calculated based on the accumulative distribution given in Figure 2.1. Also, the thermophoretic coefficient of each particle can be calculated from the Brock-Talbot formula (for Kn<2) and the MCMW (for Kn>2). Then, an equivalent thermophoretic coefficient for the given range of particle diameter (1 nm to 1000 nm) is:

$$K_{th} = \sum_{i=1}^{1000} K_{th,i}.Fraction_i \tag{2.10}$$

Finally, considering the above correlation for the thermophoretic coefficient, we are able to find the thermophoretic drift velocity of soot particles at the following temperature gradient:

$$\nabla T = \frac{u^{*2}(\bar{T} - T_w)}{\nu(\bar{u} - u^*)} \tag{2.11}$$

Results of all deposition velocities are compared at the end of the section.

2.1.2 Fickian Diffusion

Submicron particles could be easily moved by the eddy motion toward the wall. The migration of particles from a higher concentration region to a lower one is called diffusion. Diffusion can be well described by the well-known Fick's law. There are many theoretical and experimental studies on deposition of ultrafine particles by diffusion from a stream ([8]-[13]). The deposition velocity due to diffusion in a turbulent flow is [14]:

$$V_d = 0.057 u^* Sc_p^{-2/3} \tag{2.12}$$

Where Schmidt number of particles is defined as the ratio of gas kinematic viscosity to the Brownian diffusion coefficient:

$$Sc_p = \frac{\nu}{D_B} \tag{2.13}$$

The particles diffusion coefficient is also defined by:

$$D_B = \frac{k_b \overline{T} C_c}{3\pi\mu d_p} \tag{2.14}$$

where k_b is the Boltzmann constant ($1.38 \times 10^{-38}\ J/K$).

2.1.3 Turbulent Impaction

Inertial impaction due to turbulence is sometime called turbulent impaction, eddy impaction, or turbophoresis. Similar to thermophoresis, particle is subject to a higher force where turbulence is higher. For many heat exchangers operating in dusty flows, particles can be inertially deposited. This occurs when the particle is large enough that it cannot easily follow rapid changes in the gas flow direction. However, small particles have very short relaxation times and thus follow the flow. A measure for the inertia of a

particle is the particle relaxation time τ defined in (2.9). The particle relaxation time should be compared to the smallest time scale of the flow that is the Kolmogrov scale k_K and the largest time scale of the flow k_L. When the particle relaxation time is larger than the largest time scale, the particle transport is controlled inertially but when it is between the two aforementioned scales, the transport is under the control of eddies. The two scales are defined by:

$$k_K = \sqrt{\frac{\nu L}{U^3}} \tag{2.15}$$

$$k_L = \frac{L}{U} \tag{2.16}$$

L and U are taken as the tube diameter and the averaged gas velocity, respectively (given in Table 2.1). So, the Kolmogrov time scale is $\sim 2\times10^{-6}$ s and the largest time scale is $\sim 1\times10^{-4}$ s. Substituting above numbers, we find out that the inertia is important for particles of $\sim 5\,\mu m$ and larger while transport starts to be controlled by eddies for submicron particles. Another way of comparison is to find the drift velocity due to the inertial impaction for a turbulent flow as [8]:

$$V_t = 4.5\times10^{-4} u^* (\tau / (\nu / u^{*2}))^2 \tag{2.17}$$

2.1.4 Electrostatics

Electrostatic forces can be another mechanism of particle deposition. There are two types of electrostatic forces: the Coulomb force, and the image forces. Charged particle transportation under the effect of an electric field is called the Coulomb effect while the image force is a polarization phenomenon that occurs when a charged particle is moved towards a conducting surface. There have been many attempts to simulate charge particle trajectories in the presence of an electric field ([15]-[18]) but there is little literature on investigating the effect of image forces. The reason is the image forces in

general are not comparable with the Coulomb forces in different applications. The migration velocity due to the Coulomb force is:

$$V_e = \frac{neE}{f} \tag{2.18}$$

n is the number of elementary charges on the particles and e is the elementary charge ($1.602 \times 10^{-19} C$). Since there is not an external electric field in EGR coolers, the Coulomb force is zero for the soot particles in exhaust. Applying an external electric field results in a higher soot deposition as discussed in [19].

Researchers showed that 60-80% of soot particles in EGR coolers are electrically charged with almost equal numbers of positively and negatively charged particles which leaves the exhaust flow electrically neutral [20]. The charge arises due to the adsorption of ions in the medium or dissociation of molecules on the solid surface (image forces). The drift velocity caused by the electrostatic image forces is:

$$V_i = \frac{K_E n^2 e^2}{4f} \phi(\varepsilon) \frac{1}{y^2} \tag{2.19}$$

y is the distance from the surface and K_E is the electrostatic coefficient ($9 \times 10^9 Nm^2 / C^2$) and f is the drag coefficient:

$$f = \frac{3\pi d_p \mu}{C_c} \tag{2.20}$$

Dielectric constant factor (ϕ) for the bulk gas (assumed as the dry air) and the deposit layer (assumed as the graphite):

$$\phi(\varepsilon) = \frac{\varepsilon_2 - \varepsilon_1}{\varepsilon_2 + \varepsilon_1}, \varepsilon_1 = 1.0059, \textit{ dry air}, \varepsilon_2 = 15, \textit{ graphite} \tag{2.21}$$

Number of charges acquired by a particle of diameter d_p:

$$n = \frac{d_p k_b \overline{T}}{2K_E e^2} \ln(1 + \frac{\pi K_E d_p \bar{c}_i e^2 N_i t}{2k_b \overline{T}}) \tag{2.22}$$

N_i is the ion concentration and $\bar{c}_i$ is the thermal speed of the ions in m/s. It is assumed that charged particles are at equilibrium with Boltzmann charge distribution:

$$f(n) = \left(\frac{K_E e^2}{\pi d_p k_b \bar{T}}\right)^{1/2} \exp\left(-\frac{K_E n^2 e^2}{d_p k_b \bar{T}}\right) \tag{2.23}$$

$f(n)$ is the fraction of particles of a given diameter d_p having n elementary charges (either positive or negative). Maricq [20] has measured n for the soot particles of a diesel engine exhaust stream to be 4 (positive or negative). If the viscous sub-layer thickness is assumed to estimate the drift velocity, we are able to estimate the image force drift velocity.

2.1.5 Gravitational

Gravitational drift velocity of particles can be simply defined based on gas to particle density ratio as [8]:

$$V_g = \left(1 - \frac{\rho_g}{\rho_p}\right) g \tau \tag{2.24}$$

2.1.6 Summary of Deposition Mechanisms

Figure 2.5 shows a schematic of the particles soot deposition and the possible particles removal in tube flows. Convection and diffusion bring particle from the core main flow to the edge of the viscous sub-layer and the thermophoresis is responsible for particle deposition.

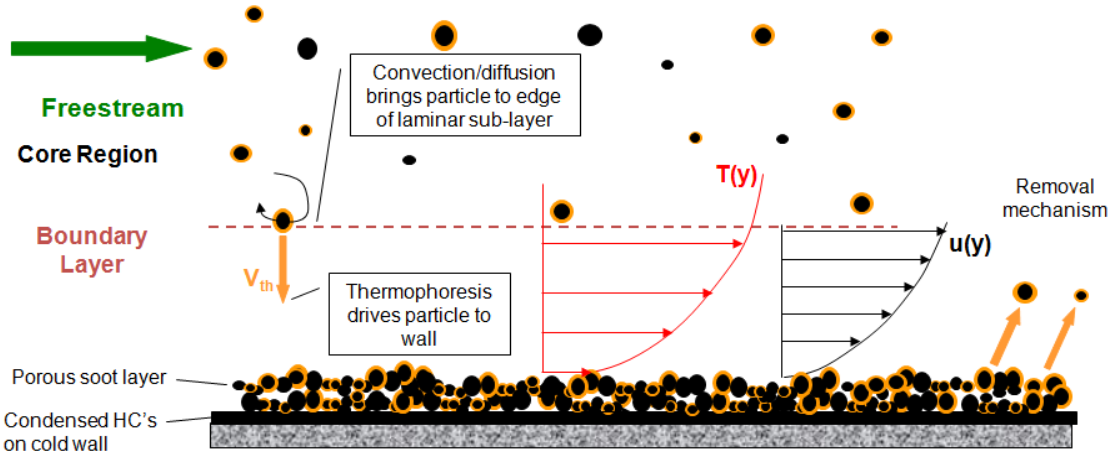

Figure 2.5 – Schematics of particles deposition and removal in a tube flow

Figure 2.6 illustrates a comparison made among different deposition mechanisms for submicron particles (a logarithmic graph). The drift velocity caused by the electrostatic image forces, gravitational forces and turbulent impaction are much smaller than the other two mechanisms. The diffusion mechanism is more significant for smaller particles (10-50 nm) in the submicron range due to their lower Schmidt numbers. Diffusion velocity for small particles (less than 50nm) is one order of magnitude less than the thermophoretic velocity but it is not comparable with the thermophoretic velocity for larger particles at all. It is clear that the thermophoretic velocity is the dominant mechanism for deposition of soot particles in the exhaust gas stream of a diesel engine (we will show this experimentally in chapter 5). A similar calculation was done for a lower gas averaged temperature of 400°C (not presented) and the results still show the dominancy of thermophoresis for this range particle diameter. Diffusion is taken into account in our one dimensional and axi-symmetric modeling studies that are described in chapter 4.

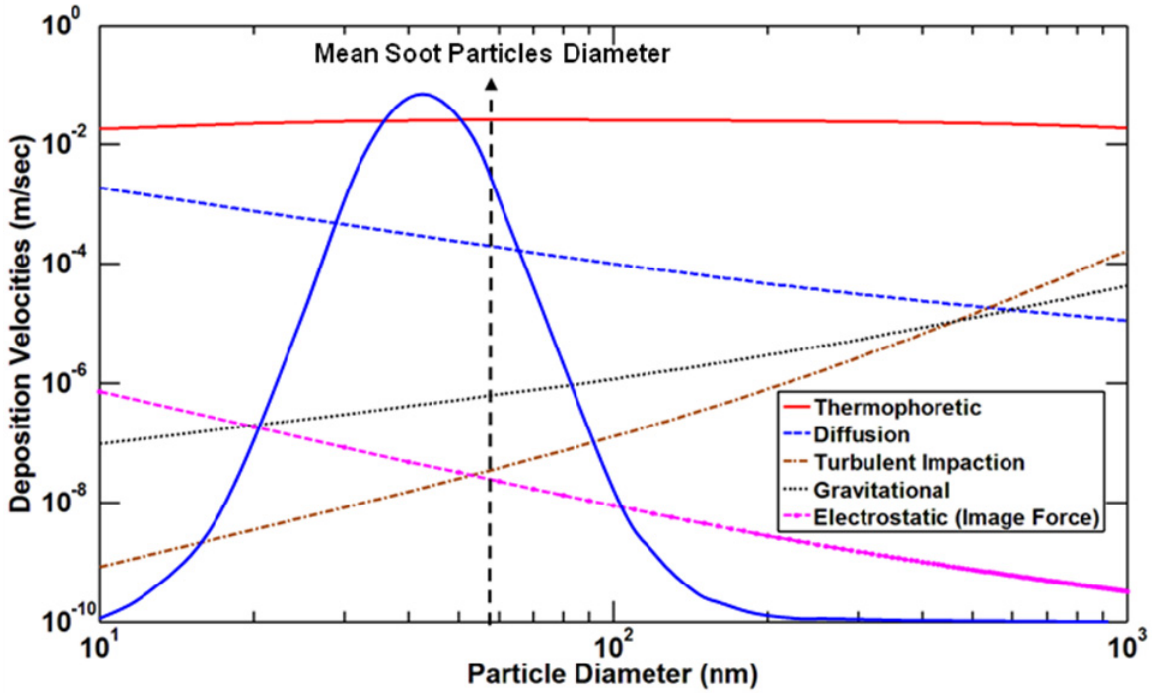

Figure 2.6 – Comparison of various deposition mechanisms for submicron particles at the given condition in Table 2.1

As a summary, the scaling analysis reveals that the thermophoresis is the dominant deposition mechanism for exhaust soot particles. When particles land on the wall, Van der Waals forces are responsible to keep them attached to each other or onto the surface as many researchers believe. Van der Waals forces include forces between dipole and quadrupoles molecules produced by either the polarization of the atoms and molecules in the material or by presenting an induced polarity [21] .

Hamaker [2] extended London's theory to the interaction between solid bodies. His theory is constructed based on the atomic and molecular interaction and calculates the attraction between larger bodies. The theory utilizes a constant called Hamaker constant that takes care of the properties of bodies. Hamaker constants are available in the literature for many materials.

Kennedy and Harris computed Van der Waals interaction energy for a vast number of particles of silver and water in the range of nanometer. Based on their calculation, particle collision rates have been deduced [22]. Oliveria [23] believes that

adhesion of particulates is an essential factor in the formation of fouling (particle deposition and hydrocarbon and acid condensation). He explained this phenomenon in terms of colloid chemistry and discussed the physicochemical factors that play an important role in fouling.

2.2 Removal Mechanisms

It is common for EGR cooler effectiveness to degrade rapidly at first, then approach a steady state value exponentially. Similar behavior can be seen in a large number of publications for particles with larger diameter than that of exhaust soot particle. There may be some removal mechanism or the rate of deposition decreases as the deposit layer grows. If such a removal mechanism has the characteristic that the mass removal rate is proportional to the total deposit mass, then an exponential approach to the steady state value where removal rate equals deposit rate occurs.

It is not easily possible to determine whether either or both of these mechanisms is the reason, but in any case the exponential approach to steady thermal performance is typical of many heat exchanger systems. Although there is not a clear indication in the literature on what mechanisms may be responsible for self-cleaning of EGR coolers, the following potential mechanisms are suggested for a wide range of particle diameters. The analysis in this chapter led us towards an experimental study that is discussed in chapter 5 in order to determine if any removal mechanism exists or if there is any recovery method to clean the fouled coolers.

In a review article a complete study of soot particulate deposition and removal in exhaust flows is done by Hoard et. al. [24] and in another work a scaling analysis is performed to find the dominant deposition and removal mechanism for soot particles in EGR flows [25]. Kern and Seaton [26] believe that the shear force is the only important factor to cause particles reentrainment. Hubbe observed that submicron particles might be

re-entrained due to shear force [27]. Taborek et. al. [28] also believe that wall shear force is responsible for the deposited particles removal . In contrast, some researchers believe that for small particles in the range of exhaust soot particles Van der Waals force is strong enough to prevent re-suspension of particles to the flow ([29],[30]). Charnay et. al. [31] state that in some cases water condensation in the cooler can loosen deposits and cause some effectiveness recovery; no data is shown to support the statement.

Epstein [32] notes that most people assume there is a deposit particle removal process associated with the shear forces of gas flow over the layer. This is not a lifting force, but a force trying to roll the particle downstream. Bridgewater [33] mentioned that the structure of the deposit layer may undergo some changes due to the thermal stress at the surface. This may affect particle removal. The stored thermal stress can induce planes of weakness in the deposit layer which causes particles removal.

Cleaver and Yates [34] hypothesize that particles can be removed and re-entrained to the main flow by the updraft generated during the fluid ejection. Turbulent burst can create enough lift to remove particles. In case of turbulent burst assumption, the sub-layer flow is not steady state anymore. Yung et. al [35] showed the role of turbulence burst in particle removal from the viscous sub-layer by utilizing flow visualization techniques. Their result shows that a rolling mechanism due to the drag force was more dominant than vertical lift forces, and turbulent burst effect was insignificant in particles removal in contrast to what Cleaver hypothesized.

Kaftori et. al [36] in agreement with Yung also believes that particle removal occurs as a result of the turbulent burst which consists of random sequence of ejections from the boundary layer into the main fluid flow. Reeks and Hall [37] presented dominance of the drag force over the lift force by measurement of tangential and normal adhesive force. They found out that the drag force had a much greater effect by a factor of 100 over the lift force. Kallay et. al.[38] also studied the kinetics of adhesion and removal of uniform spherical particles.

The differences in results may be due to the fact that researchers' experiments were conducted on different thermo-hydraulic conditions and particles size and materials. That is the reason they proposed different conclusions.

Deposits might lose adhesion to the surface and flake off. This could be due to a factor reducing the strength of adhesion, such as water, liquid HC, and/or acids. Kalghatgi ([39]-[41]) investigated the effect of water drops on combustion chamber deposits. Although his research was not directly related to EGR cooler deposit, one can find it really helpful in understanding the flake off mechanism. As a summary, one can conclude the following from his articles:

- Combustion chamber deposit flakes off when exposed to water. Water is a critical factor that seems to be much more effective than other organic solvents in flaking particles.
- Deposit flaking could be due to thermal stress and it may occur locally.
- Deposit flake off was usually seen after cold starts rather than during engine operation
- Water disappears below the deposit surface and the deposit cracks continue to propagate in sudden bursts for a further 10 minutes.
- It can be hypothesized that the water runs along the cracks and forces the deposit apart. It could also be due to water reaction chemistry with deposit layers at the surface.
- There is a thin layer of deposit still left on the metal surface after each flaking.
- Young deposits do not flake.
- Deposits must go through a thermal history before they can be flaked.
- There is not a firm correlation between deposit thickness and deposit flaking tendency.

Thermal history and the age of deposits are critical factors in deposit flaking. This field is an important area that needs to be investigated in more detail beyond the scope of this thesis.

A scaling analysis is conducted in this part of the chapter to compare variable correlations and theories for removal of small particles. Initially we did a simple calculation to identify forces that can potentially overcome Van der Waals forces acting on a particle attached to the wall or the deposit layer (Figure 2.7). Acting forces on a particle are listed as ([39],[42]):

Drag force:

$$F_D = 8\rho\nu^2(\frac{u^* d_p}{\nu})^2 = 8\rho\nu^2 \,\mathrm{Re}_p^2 \tag{2.25}$$

Lift force:

$$F_L = 0.076\rho\nu^2(\frac{d_p u^*}{\nu})^3 \tag{2.26}$$

Weight:

$$F_w = \frac{\pi}{6}(\rho_p - \rho_g)\, g\, d_p^3 \tag{2.27}$$

Van der Waals Force:

$$F_v = \frac{A_H d_p}{12 Z_0^2} \tag{2.28}$$

Hamaker's constant (A_H) is assumed to be $10^{-20} J$ and the distance between particles (Z_0) is assumed to be 1/50 of the particle diameter (it can even be less and the Van der Waals forces can be stronger).

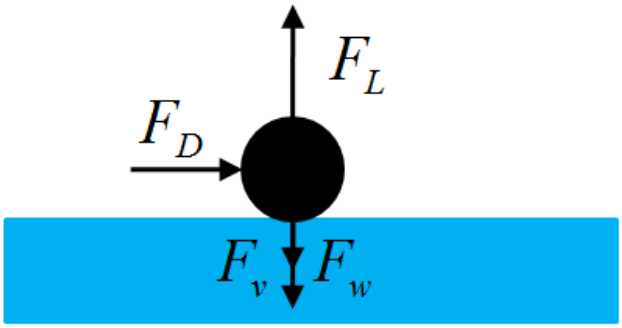

Figure 2.7 – Forces acting on a particle attached to the surface

Figure 2.8 shows a comparison among the aforementioned forces for a range wider than the range of EGR soot particles (logarithmic scale). It is seen that the lift force and the weight are not comparable with the drag and Van der Waals forces for submicron particles (particle distribution is also demonstrated on the graph).

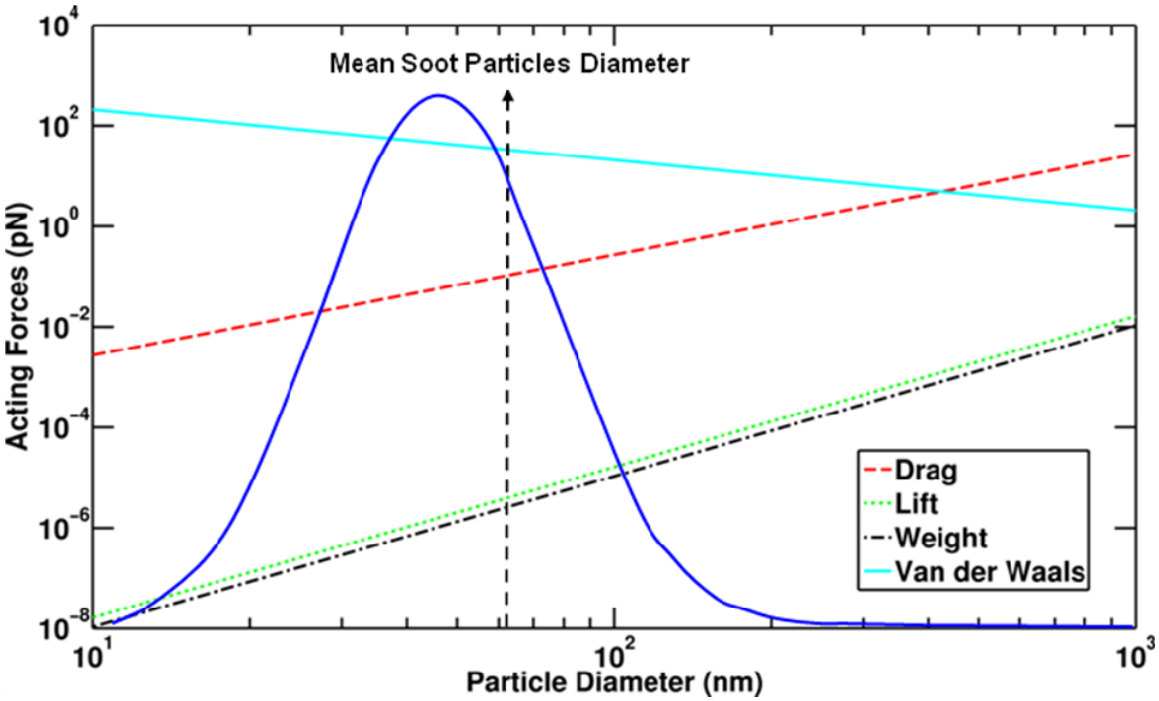

Figure 2.8 – Forces acting on submicron particles

It seems that Van der Waals forces are strong enough for smaller particles so that removal by drag or lift forces seem unlikely. In the following, a hypothesis on removal mechanisms based on current correlations in literature is presented.

2.2.1 Turbulent Burst

Cleaver and Yates [43] investigated the effect of the turbulent burst and the caused lift force on the re-entraining of particles to the main flow. Although the lift force is proven to be small (Figure 2.8), they believe that the turbulent burst applies an updraft force normal to the wall in a time duration. They claimed that the duration of this force is enough to move a particle through one diameter. This movement is larger than the range of adhesion force and the particle can be removed to the main flow. This force is defined as:

$$F_C = 10.1\rho\nu^2\left(\frac{d_p u^*}{\nu}\right)^3 \tag{2.29}$$

They proposed a criterion for particles removal. The criterion is achieved by equating Van der Waals force and the updraft force due to turbulent burst $F_v = F_C$:

$$\tau_w d_p^{4/3} > \beta \tag{2.30}$$

Where:

$$\beta = \left(\frac{\nu\rho^{0.5} A_H}{10.1\times 12 Z_0^2}\right)^{\frac{2}{3}} \tag{2.31}$$

Figure 2.9 shows a comparison made between Van der Waals force and the updraft force for the given boundary condition. It is seen that they just are barely equal for larger particles that are not in the EGR soot particle distribution.

Also, Figure 2.10 depicts the shear force required to satisfy the criterion for the range of EGR soot particles. According to the given boundary condition in Table 2.1, the averaged shear on the deposit layer is 3.4 Pa that is significantly lower than the criterion for the turbulent burst removal. Although the distance between particles is a critical factor in determining the criterion and it has not been really measured, it seems really unlikely that soot particles can be removed by the turbulent bursts or the velocity of EGR flow on

this range (25 m/s). There are a few articles on particle removal by supersonic flows to confirm this claim ([44]-[46]).

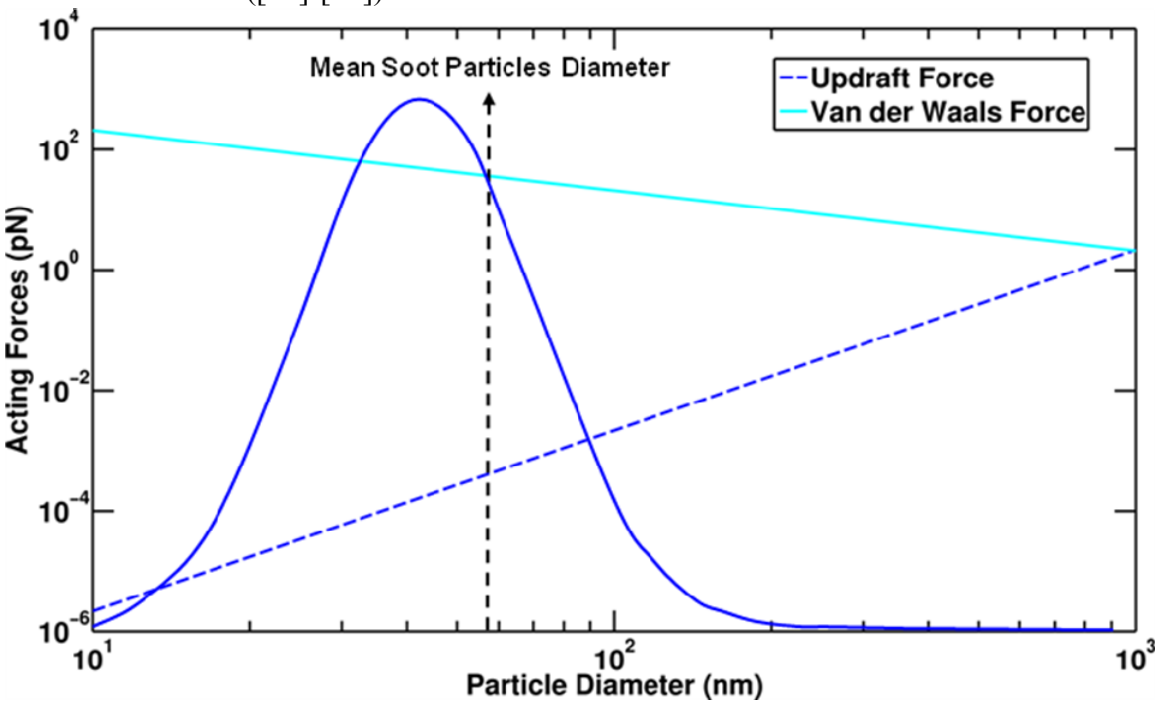

Figure 2.9 – Comparison of the updraft force and Van der Waals force

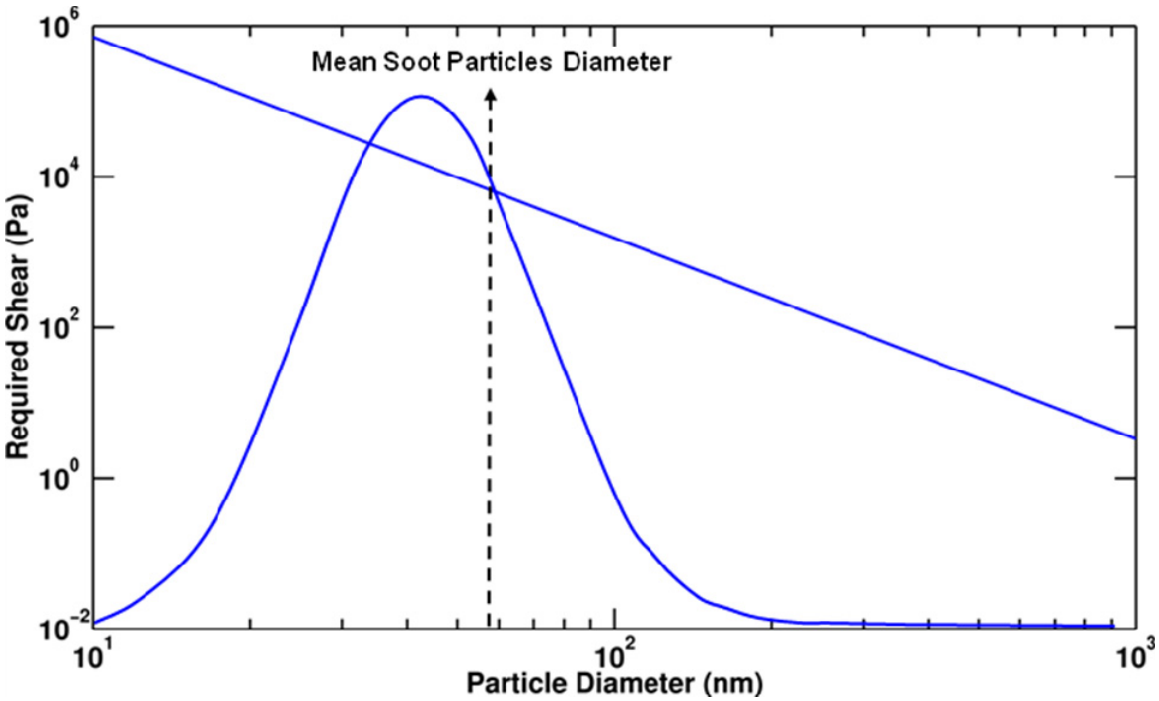

Figure 2.10 – Required shear to remove the particles with different diameters based on the turbulent burst criterion

2.2.2 Removal due to the Drag Force

The only force that is comparable with Van der Waals is the drag force (Figure 2.8). There is a hypothesis which says the drag force is responsible for particles removal. Philips [47] developed a force balance model for particles re-entrainments into the main flow. He categorized the mechanisms in four groups for large, intermediate, small particles and a mechanism for unrealized regimes. His force balance requires:

$$F_C \text{ or } F_D = F_v + F_w - F_L \tag{2.32}$$

Weight and the lift are not comparable with the rest of the two, and the updraft force is not responsible for removal as discussed in the previous section. Yung et. al.[35] performed an experiment and showed that if the drag force is larger than the adhesion force for small particles, removal occurs. So, the criterion for removal based on his claim is:

$$\tau_w d_p > \eta \tag{2.33}$$

where:

$$\eta = \frac{A_H}{96 Z_0^2} \tag{2.34}$$

Figure 2.11 shows the required shear force to remove submicron particles based on Yung's theory. It is noted that for removing 60 nm particles a shear of 1200 Pa is required. This is significantly larger than the shear force given in Table 2.1. To remove the particles by drag force, a mean velocity of 355 m/s (Mach number of 0.75 at 600K) is required to remove 60 nm particles. It seems unlikely to remove the soot particles at regular EGR flows with a low velocity.

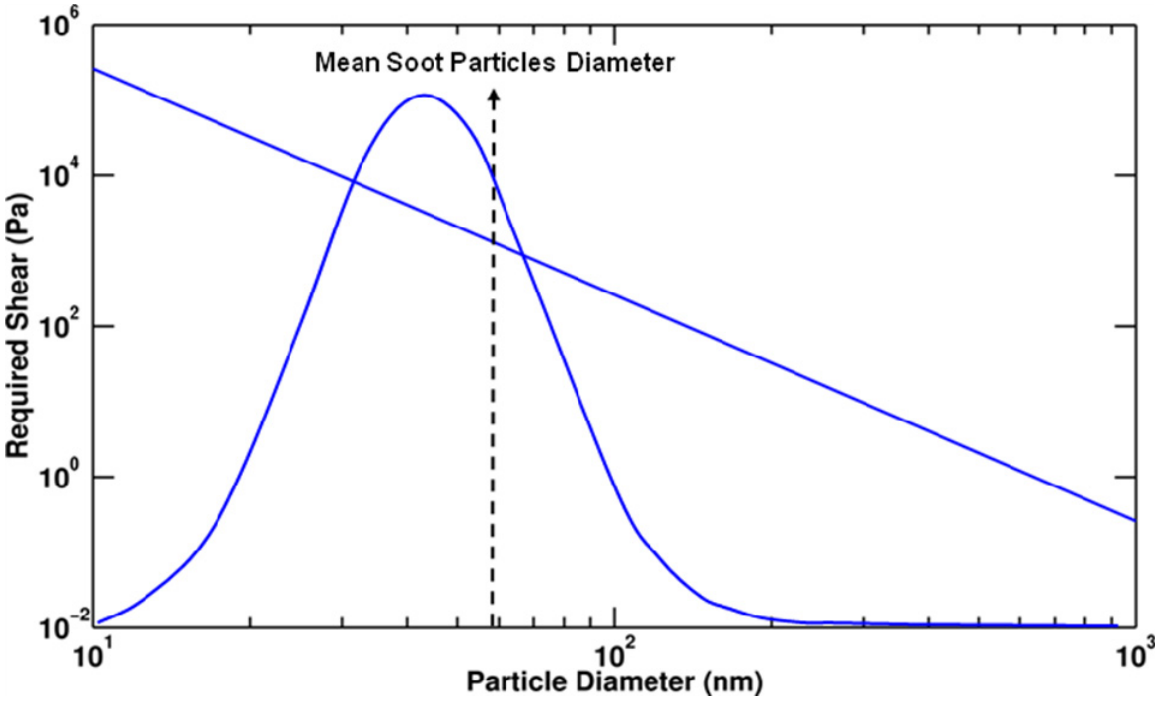

Figure 2.11 – Required shear to remove the particles with different diameters based on Yung's hypothesis

2.2.3 Removal due to Water Condensation

There is a possibility that in low wall temperatures in EGR coolers, water condensation causes particle removal as Kalghatgi mentioned. There could also be a wash-out mechanism that removes the deposit layer. The criterion to have the water condensation is that the mole fraction of water in the main flow is equal or larger than the mole fraction at the surface of the deposit layer or the tube wall. The mole fraction at the interface (y_{gi}) is defined by:

$$y_{gi} = \frac{P_v}{P_{total}} \tag{2.35}$$

Also, water vapor pressure is calculated based on Antoine coefficients of water:

$$Log_{10} P_v = AA - \frac{BB}{T_{\text{int}\,erface} + CC} \tag{2.36}$$

Antoine coefficients for water are: $AA = 10.23, \mathrm{BB} = 1750, \mathrm{CC} = 235$. Pressure in the equation is in Pascal and the surface temperature is in Celsius. Figure 2.12 demonstrates water vapor pressure at various temperatures.

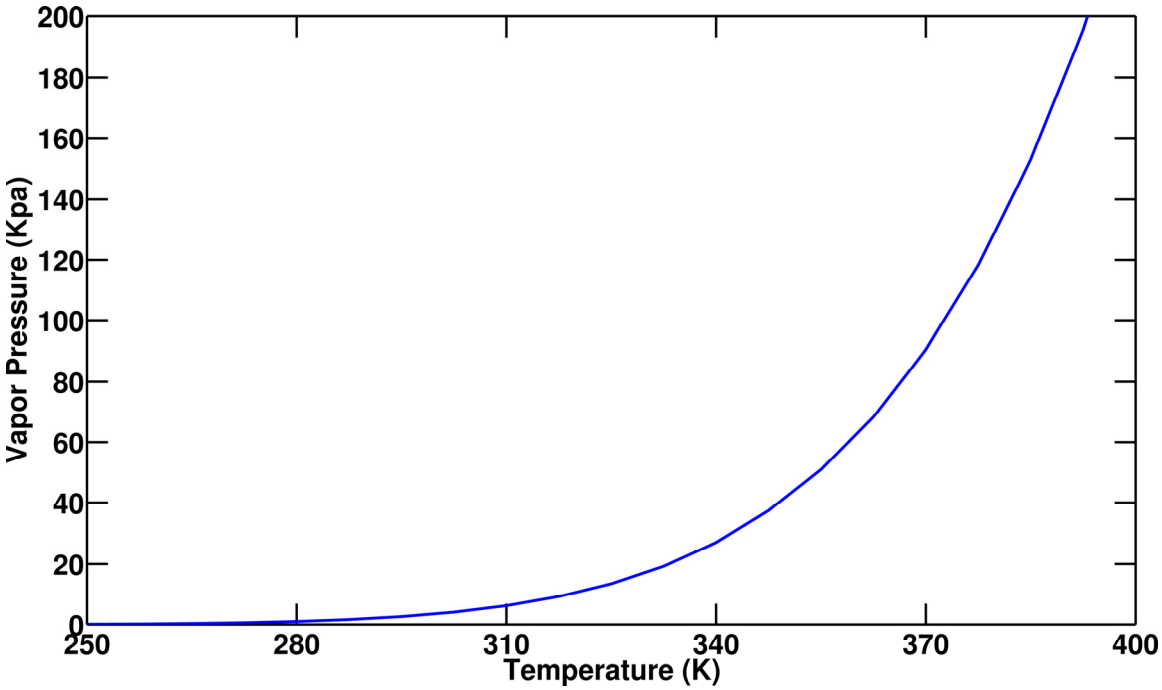

Figure 2.12 – Water vapor pressure vs. temperature

To find the water mole fraction in the main flow: the diesel fuel H:C ratio CH = 1.809 and the dry based mole fraction of carbon dioxide based on the experimental measurements of Oak Ridge National Laboratory are used at the ideal chemical reaction in the diesel engine as below:

$$CH_{1.809} + 4.12(O_2 + 3.76N_2) \rightarrow CO_2 + 0.9045H_2O + 15.491N_2 + 2.667O_2$$

Air/Fuel ratio in conducted experiments is 40.95. The dry based mole fractions of species are also given by experimental measurements as:

$$(X_{CO_2} = 4.984\%, X_{H_2O} = 4.508\%, X_{O_2} = 13.294\%, X_{N_2} = 77.214\%)$$

The mole fraction of CO, NOx, HC, and all other existing species in the exhaust gas are negligible for this purpose and ignored. Now, having the mole fraction of water in the main flow (0.04508) and an averaged pressure of the flow (Table 2.1), we can find

the critical interface temperature at which (and below) condensation occurs ($T_{critical-\text{int}erface} = 42^{\circ}C$). This temperature is likely to be the coolant temperature of EGR coolers especially at cold start of the engine.

2.2.4 Chemical Reactions and Aging

Deposit layer can be hardened and cracked over time due to being exposed to ambient and loosing volatile fraction of the mass. Cracked deposit is more prone to removal by shear. There can also be surface chemistry [48] or chemical reactions in the deposit layer that cause the properties to change over time. Hydrocarbon, acid, and water condensation can change the deposit morphology and change all calculations presented above. This subject needs more investigations that require long tests to monitor the layer when exposed to the ambient, hydrocarbons, or acids. The possible reactions and behavior of the layer can be recorded to understand the physics of such reactions. This is not the scope of this thesis and is not discussed further.

2.2.5 Kinetic Energy (Thermal Force)

Based on the kinetic theory, when particles are attached, Van der Waals force is larger than thermal forces between them. So, a criterion for particles removal can be that the kinetic energy of attached particles must be larger than Van der Waals potential energy. Then,

Kinetic energy:

$$K.E. = \frac{1}{2}mv^2 = \frac{3}{2}k_b\overline{T} \tag{2.37}$$

Van der Waals potential energy:

$$\varphi = \frac{A_H d_p}{12Z_0} \tag{2.38}$$

$$\frac{3}{2}k_b T_{\text{int}erface} > \frac{A_H d_p}{12 Z_0} \tag{2.39}$$

or,

$$T_{\text{int}erface} > \frac{A_H d_p}{18 Z_0 k_b} \tag{2.40}$$

Another important fact is that the deposit layer is less dense and is fluffier on the top layers compared to the layers closer to the wall. Figure 2.13 (courtesy of Michael Lance – Oak Ridge National Laboratory [49]) shows two images of the deposit layer, one from the gas-deposit interface and one from the deposit-metal interface. The images show that the layer near the metal is denser compared to the fluffy layer at the gas-deposit interface. It means that Van der Waals force for the top layer can be less compared to that of the bottom layer. The top layer deposit can be more prone to removal due to smaller binding forces.

Therefore, we hypothesize that the reason for seeing less dense (fluffier) layers with weaker bind forces on the top side of the deposited layer is the larger kinetic energy compared to the bottom layers due to higher temperatures. This makes particles at the gas-deposit interface more prone to removal if (2.40) is valid for the interface temperature. Interface temperature acts like a cut-off mechanism for removing particles. It is noted that the fluffy layer seems to have a larger distance Z_0 between particles. Shear force does not seem to be an effective factor in submicron particles removal and the thermal force could be more possibly the reason. We do not yet have any experimental evidence to verify this hypothesis. We show in the last chapter (future work) what is planned to prove or disapprove the kinetic theory hypothesis.

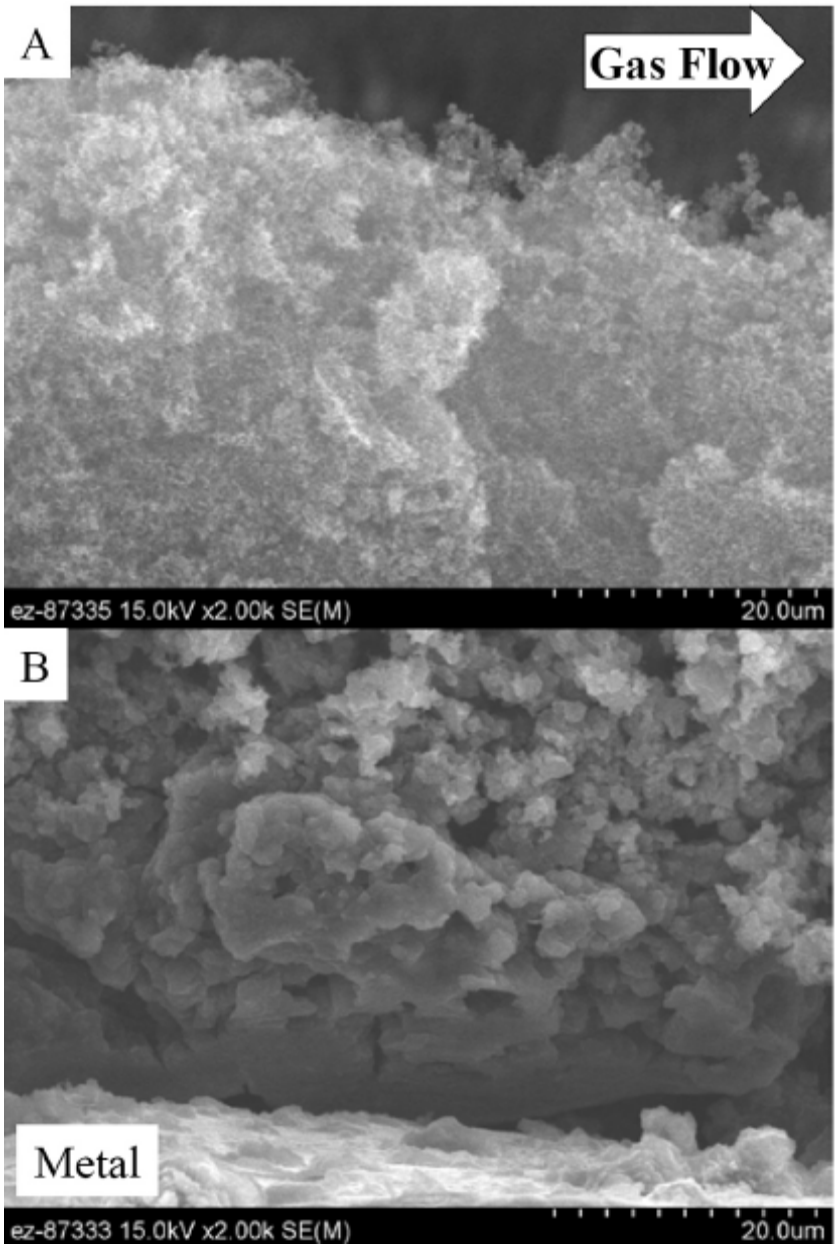

Figure 2.13 – Image As is from the gas deposit interface and image B is from the deposit metal interface (Courtesy of Michael Lance – Oak Ridge National Laboratory [49])

2.2.6 Other Removal Mechanisms

There are other mechanisms including laser-assisted methods ([50]-[51]) or hypersonic flows to remove small particles from surfaces but these methods are not practical recovery methods for cleaning of EGR coolers. The behavior of small particle

collision with the surface is a complex problem. Some researchers even believe there is no removal of already landed submicron particles [52].

As a summary, the scaling analysis shows that current proposed mechanisms in literature including the drag force and the turbulent burst seem not to be applicable for submicron particles. Water condensation is a strong candidate for the deposit removal at low wall (coolant) temperatures (below $40^{\circ}C$). Experimental evidence to prove this theory is presented in chapter 5.

2.3 Particles Sticking Probability

Sticking probability of particles is not fully understood and there is not a unique equation that covers a wide range of particle size. Authors have proposed many formulas that may not work for different cases. Watkinson and Epstein [53] proposed a sticking probability as a ratio of adhesion force to the shear stress. Beal ([54]-[55]) showed that the sticking probability for small particles remains constant but it decreases with a non-dimensional parameter called stopping distance. Stopping distance is a critical distance from the wall in which the particles are detached from an eddy and are projected in a free-flight motion across the viscous sub-layer to impact with the wall. In other word, the stopping distance is defined as the distance which a particle travels through a stagnant fluid when it is projected with an initial velocity.

Van Beek et. al. studied the gas side fouling of waste recovery boilers which is mainly caused by particulate matter. They calculated the deposition rate and discussed the sticking coefficient of particles in the range of submicron and micrometers [56]. There are many other articles discussing the sticking probability of particles for different applications ([57]-[63]). Overall, the sticking probability for small particles on the range of EGR soot particles seems to be 100% but this field needs more experimental investigation.

2.4 Surface Roughness Effect

Based on the literature and ORNL experiments, the deposit layer is not uniformly distributed. It is also seen that deposit flake off and a relevantly large roughness occurs in the layer. So, it is worth looking at the criterion for the surface roughness. A roughness Reynolds number is defined for the surface in [64] by:

$$\mathrm{Re}_k = \frac{u^* k_s}{\nu} \tag{2.41}$$

where k_s is a length dimension to describe the roughness size. After some simplifications,

$$\mathrm{Re}_k = \frac{k_s \bar{u}\sqrt{\frac{f}{8}}}{\nu} = \frac{k_s \bar{u}\sqrt{\frac{f}{8}}}{\nu} = \frac{\mathrm{Re}\sqrt{\frac{f}{8}}}{ID/k_s} \tag{2.42}$$

If $\mathrm{Re}_k < 5$, the surface behaves as perfectly smooth. If $5 < \mathrm{Re}_k < 70$, some of the smooth characteristics of a smooth surface persist. For larger roughness Reynolds numbers, the surface is fully rough and sub-layer disappears entirely and viscosity is no longer important. Following calculations show how rough the surface could be in our simulation to be considered as a perfect smooth or rough surface, respectively.

$$\mathrm{Re}_k = \frac{u^* k_s}{\nu} < 5 \rightarrow k_s <\sim 100\mu m \tag{2.43}$$

$$\mathrm{Re}_k = \frac{u^* k_s}{\nu} > 70 \rightarrow k_s >\sim 140mm \tag{2.44}$$

Although it is occasionally seen in the experiments a large flake that causes a roughness larger than $100\mu m$, assuming a smooth surface is a rational assumption.

2.5 Concluding Remarks

Different particle deposition mechanisms were discussed and compared for EGR soot particles. The scaling analysis showed that the thermophoresis is the dominant

mechanism compared to the rest. Also, possible removal mechanisms offered in literature were studied and compared analytically to find if they can potentially be in charge of re-entraining EGR soot particles to the main flow. We hypothesize that the higher surface temperature may cause the higher kinetic energy of soot particles at the gas-deposit surface and make their bond forces weaker. That could be the reason that the outer layer of deposit is always fluffier and more prone to removal. Also, water condensation can be a strong wash-out mechanisms to remove the deposit layer and act as a recovery method.

2.6 Nomenclature

A_H	Hamaker's constant
$\overline{C}$	Averaged particle concentration (kg / m^3)
$\bar{c}_i$	Thermal speed of ions (240 m/s)
c_v	Volume specific heat (J / kgK)
D_B	Particle diffusion coefficient (m^2 / s)
d_p	Soot particle diameter (m)
d_m	Molecular diameter (m)
E	Parallel component of electric field to the flow (V/m)
e	Elementary charge ($1.602 \times 10^{-19}\ C$)
F_C	Updraft burst Force (N)
F_D	Drag Force (N)
F_L	Lift Force (N)
F_v	Van der Waals Force (N)
F_w	Weigth (N)
f	Drag coefficient
g	Gravity (N/kg)
K_E	Electrostatic Constant ($9 \times 10^9 Nm^2 / C$)
k_b	Boltzmann's constant $1.38 \times 10^{-23} m^2 kgs^2 / K$
k_g	Gas thermal conductivity (W/mK)
Kn	Knudsen number
k_K	Kolmogrov time scale (s)
k_L	Largest time scale of the flow (s)
k_p	Particle thermal conductivity (W/mK)
K_{th}	Thermophoretic coefficient
MW_g	Gas molecular weight (kg/mol)
m_p	Particle mass (kg)

N_i	Ion concentration
n	Number of elementary charges on the particle
$\overline{P}$	Averaged gas pressure (Pa)
R	Gas constant (J/mol K)
Re_p	Particle Reynolds number
Sc_p	Particles Schmidt number
S_n, S_t	Normal and tangential momentum accommodation coefficients
$\overline{T}$	Averaged gas temperature (K)
T_w	Inner tube wall temperature (K)
t	Elapsed time of particles in the tube (s)
$\overline{U}$	Averaged gas velocity (m/s)
u^*	Shear velocity (m/s)
V_d	Fickian diffusion velocity (m/s)
V_g	Gravitational deposition velocity (m/s)
V_i	Image force drift velocity (m/s)
V_t	Turbulent impaction velocity (m/s)
V_{th}	Thermophoretic velocity (m/s)
y	Distance from the surface (m)
Z_0	Distance between particles molecules (m)

Greek

γ	Specific heat ratio
λ	Particle mean free path (m)
μ	Viscosity of the bulk flow (kg / ms)
μ_g	Mean particle diameter (nm)
ρ	Density of the bulk flow (kg / m^3)
ρ_p	Particle layer density (kg / m^3)
σ_g	Standard deviation
τ	Particle Relaxtation time

τ_w	Wall or deposit layer Shear stress (Pa)
ν	Bulk gas kinematic viscosity (m^2 / s)
$\phi(\varepsilon)$	Dielectric constant factor

2.7 References

[1] Harris, S. J., Maricq, M. M., "The role of fragmentation in defining the signature size distribution of diesel soot", J. of Aerosol Science 33:935-942, 2002.

[2] Hamaker, H. C., "The London-Van der Waals attraction between spherical particles", Physica IV 10:1058-1072, 1937.

[3] Talbot, L., Cheng, R.K., Schefer, R.W., Willis, D.R., "Thermophoresis of particles in a heated boundary layer", Journal of Fluid Mechanics 101(4):737-758, 1980.

[4] Cha, C. Y., McCoy, B. J., "Thermal force on aerosol particles", The Physics of Fluids 17 (7): 1376-1380, 1974.

[5] He, C, Ahmadi, G., "Particle deposition with thermophoresis in laminar and turbulent duct flows", Aerosol Science and Technology 29:525-546, 1998.

[6] Li, W., Davis, E.J., "Measurement of the thermophoretic force by electrodynamics levitation: Microspheres in air", Journal of Aerosol Sciences 26(7):1063-1083, 1995.

[7] Li, W., Davis, E.J., "The effects of gas and particle properties on thermophoresis", Journal of Aerosol Sciences 26(7):1085-1099, 1995.

[8] Ingham, D. B., "Diffusion of aerosols from a stream flowing through a short cylindrical pipe", J. Aerosol Sci. 15(5):637-641, 1984.

[9] Shaw, D. A., and Hanaratty, T. J., "Turbulent mass transfer rates to a wall for large Schmidt numbers", AICHE Journal 23(1):28-37, 1977.

[10] Magnaudet, J., and Calmet, I., "Large-eddy simulation of high-Schmidt number mass transfer in a turbulent channel flow", Phys. Fluids 9(2):438-455, 1997.

[11] Martoen, T., Zhang, Z., Yang, Y., "Particle diffusion with entrance effects in a smooth-walled cylinder", J. Aerosol sci. 27(1):139-150, 1996.

[12] Cohen, B. S., Asgharian, B., "Deposition of ultrafine particles in the upper airways: an empirical analysis", J. Aerosol Sci. 21(6):789-797, 1990.

[13] Zahmatkesh, I., "On the importance of thermophoresis and Brownian diffusion for the deposition of micro-and nanoparticles". Int. Commun. Heat Mass 35(3):369–375, 2008.

[14] N. B. Wood, "The mass transfer of particles and acid vapour to cooled surfaces", Journal of Institute of Energy 76:76-93, 1981.

[15] Lai, A. C. K., "Investigation of electrostatic forces on particle deposition in a test chamber", Indoor and Built Environment 15:179-186, 2006.

[16] Turner, J. R., Fissan, H. J., "Convective diffusion of particles in external forces fields: The role of electrostatics on particle removal from turbulently-mixed gases", Chemical Engineering Science 44(5):1255-1261, 1989.

[17] Chen, F., Lai, A. C. K., "An Eulerian model for particle deposition under electrostatic and turbulent conditions", J. Aerosol Science 35:47-62, 2004.

[18] Soltani, M., Ahmadi, G., "Charged particle trajectory statistics and deposition in a turbulent channel flow", Aerosol Sci. and Technol. 31(2-3):170-186, 1999.

[19] Cruz a, E. D., Chang, J. S., Berezin, A. A., Ewing, D., Cotton, J. S., Bardeleben, M., "Electrical effect of soot depositions in a co-axial wire pipe flow", J. of electrostatics 67:128-132, 2009.

[20] Maricq, M. M., "On the electrical charge of motor vehicle exhaust particles", J. of Aerosol Science 37:858-874, 2006.

[21] Bott, T.R., Fouling of heat exchangers, New York, Elsevier, 1995.

[22] Kennedy, I. M., Harris, S.J., "Direct numerical simulation of aerosol coagulation with van der Waals forces", Journal of colloid and Interface Science 130(2):489-497, 1989.

[23] Oliveria, R., "Understanding adhesion: a means for preventing fouling", Experimental Thermal and Fluid Science 14:316-322, 1997.

[24] Hoard., J., Abarham, M., Styles, D., Giuliano, J., Sluder, S., Storey, J., "Diesel EGR cooler fouling", SAE transactions, International Journal of Engines 1(1):1234-1250, 2009.

[25] Abarham, M., Hoard., J., Assanis, D., Styles, D., Curtis, E., Ramesh, N., "Review of soot deposition and removal mechanisms in EGR coolers", SAE transactions, International Journal of Fuel and Lubricants 3(1):690-704, 2010.

[26] Kern, D.Q., Seaton, R.E., "Theoretical analysis of thermal surface fouling", Brit. Chem. Eng. 4(5):258-262, 1959.

[27] Hubbe, M., "Detachment of colloidal hydrous oxide spheres from flat solids exposed to flow 2. Mechanism of release". Colloids and Surfaces 16(3-4):249–270, 1985.

[28] Taborek, J., Aoki, T., Ritter, R., Palen, J., and Knudsen, J., "Fouling: the major unresolved problem in heat transfer", 1972.

[29] Bowen, B., and Epstein, N., "Fine particle deposition in smooth parallel-plate channels". Journal of colloid and interface science 72(1):81–97, 1979.

[30] Adomeit, P., and Renz, U., "The influence of liquid flow rate on particle deposition and detachment". In Eng. Foundation Conf. on Fouling Mitigation of Industrial Heat Exchangers, 1995.

[31] Charnay, L., Soderberg, E., Malmlof, E., Ohlund, P., Ostling, L., Fredholm, S., "Effect of fouling on the efficiency of a shell-and-tube EGR cooler", EAEC Congress Vehicle Systems Technology for the Next Century. Barcelona, 1999. Paper STA99C418.

[32] Epstein, N., "Elements of particle deposition onto nonporous solid surfaces parallel to suspension flows", Experimental Thermal and Fluid Science 14:323-334, 1997.

[33] Bridgewater, J., Loo, C.E., "Removal of crystalline scale: mechanisms and the role of thermal stress", 1st UK heat transfer conf. Symposium series No. 86:455-463, 1984.

[34] Cleaver, J. W., Yates, B., "A sub-layer model for the deposition of particles from a turbulent flow", Chem. Eng. Sci. 30:983-992, 1975.

[35] Yung, B. P. K., Merry, H., Bott, T. R., "The role of turbulent bursts in particle re-entrainment in aqueous systems", Chem. Eng. Sci. 44(4):873-882, 1989.

[36] Kaftori, D., Hetsroni, G., Banerjee, S., "Particle behavior in the turbulent boundary layer. I. Motion, deposition, and entrainment", Phys. Fluids 7(5):1095-1106, 1995.

[37] Reeks, M. W., Hall, D., "Kinetic models for particle resuspension in turbulent flows: Theory and measurements", Aerosol Science 32:1-31, 2001.

[38] Kallay, N., Nelligan, J. D., Matijevic, E., "Particle adhesion and removal in model systems", J. Chem. Soc., Faraday Trans. 1 79:65-74, 1983.

[39] Kalghatgi, G.T., Price, R.J., "Combustion chamber deposit flaking", SAE 2000-01-2858, 2000.

[40] Kalghatgi, G.T., "Combustion chamber deposit flaking-Studies using a road test procedure", SAE 2002-01-2833, 2002.

[41] Kalghatgi, G.T., "Combustion chamber deposit flaking and startability problems in three different engines", SAE 2003-01-3187, 2003.

[42] Schmitz, P., Cardot, J., "Adhesion and removal of particles from charged surfaces under a humidity-controlled air stream", Particles on Surfaces: Detection, Adhesion and Removal 7: 189-196, 2002.

[43] Cleaver, J. W., Yates, B., "Mechanism of detachment of colloidal particles from flat substrate in a turbulent flow", Journal of collide and Interface Science 44(3):464-474, 1973.

[44] Dunbar, T.J., Peri, M.D.M., Varghese, I., Cetinkaya, C., "Submerged Laser-induced Plasma amplification of shockwaves using shock tubes for nanoparticle removal", J. Adhes. Sci. Technol 21(14):1425-1437, 2007.

[45] Dunbar, T., Cetinkaya, C., "Underwater Pressure Amplification of Laser-Induced Plasma Shockwaves for Particle Removal", Appl. Phys. Lett. 91(5), 2007.

[46] Dunbar, T., Maynard, B., Thomas, D. A. , Murthy Peri, M. D., Varghese, I., Cetinkaya, C., "Pressure Amplification of Laser-Induced Plasma Shockwaves with Shock tubes for Nanoparticle Removal", J. Adhes. Sci. Technol. 21(1):67-81, 2007.

[47] Philips, M., "A force balance model for particle entrainment into a fluid stream", Journal of physics D: Applied physics 13:221-233, 1980.

[48] Turner, C. W., Klimas, S. J., "The effect of surface chemistry on particulate fouling under flow-boiling conditions", Heat exchanger fouling: Fundamental approaches and technical solutions, Davos, Switzerland, July 8-13, 2001.

[49] Lance, M., Sluder, C., Lewis, S., Storey, J., "Characterization of field-aged EGR cooler deposit", SAE paper 2010-01-2091, 2010.

[50] Vereecke, G., Röhr, E., Heyns, M. M., "Laser-assisted removal of particles on silicon wafers", J. Appl. Phys. 85(7):3837-3843, 1999.

[51] Lu, Y. F., Zheng, Y. W., Song, W. D., "An energy approach to the modeling of particle removal by pulsed laer irradiation", Appl. Phys. A 68:569-572, 1999.

[52] Vaˇsaacute, F., Kaˇst´anek, F., Bowen, B., Chen, C., and Epstein, N., "Fine particle deposition in laminar and turbulent flows". The Canadian Journal of Chemical Engineering, 73(6):785–792, 1995.

[53] Watkinson, A. P., Epstein, N., "Particulate fouling of sensible heat exchangers", 4th International Heat Transfer Conference, Versailles, France, Volume 1, pp. HE1.6 1-12, Elsevier Science Publishers BV, Amsterdam (1971).

[54] Beal, S. K., "Turbulent agglomeration of suspensions", Journal of Aerosol Science 3:113-125, 1973.

[55] Beal, S. K., "Correlations for the sticking probability and erosion of particles", J. of Aerosol Sci. 9:455-461, 1978.

[56] Van Beek, M. C., Rindt, C. M., Winjers, J. G., Van Steenhoven, A. A., "Analysis of fouling in refuse waste incinerators", Heat transfer Engineering 22:22-31, 2001.

[57] Insepov, Z. A., Zhankadamova, A. M., "Molecular dynamics calculation of the sticking coefficient of gases to surfaces", Z. Phys. D - Atoms, moleculaes and clusters 20:145-146, 1991.

[58] Hsu, J. P., Lin, D. P., Tseng, S., "The sticking probability of colloidal particles in polymer-induced flocculation", Colloid. Polym. Sci. 273:271-278, 1995.

[59] Kisliuk, P., "The sticking probabilities of gases chemisorbed on the surfaces of solids", J. Phys. Chem. Solids 3:95-101, 1957.

[60] Li, C., Hsieh, J. H., "effects of variable sticking coefficients on the stability of reactive sputtering process", J. Phys. D: Appl. Phys. 37:1065-1073, 2004.

[61] Subbarao, K. K. S., Rindt, C. C., Steenhoven, A. A., "Preliminary study of particulate fouling in a high temperature controlled experimental facility", Proceedings of International Conference on Heat Exchanger Fouling and Cleaning VIII, Schladming, Austria, June 14-19, 2009.

[62] Konstandopoulos, A., "Deposit growth dynamics: particle stickingand scattering phenomena". Powder Technology 109(1-3):262–277, 2000.

[63] Sato, S., Chen, D., and Pui, D., "Molecular Dynamics Study ofNanoparticle Collision with a Surface- Implication to Nanoparticle Filtration". Aerosol and Air Quality Research 7(3):278–303, 2007.

[64] Kays, W. M., Crawford, M. E., Convection heat and mass transfer, 3rd Ed., McGraw-Hill, New York, 1993.

CHAPTER 3

ANALYTICAL STUDY OF THERMOPHORETIC PARTICLE DEPOSITION

It was shown in chapter 2 that the dominant deposition mechanism for nano-particles in non-isothermal flows is thermophoresis. It was also discussed that most EGR coolers are tubes in shell type of heat exchangers. To understand the physics of particle transport under thermophretic forces, we limited our study to a simple non-isothermal tube flow and we proposed an analytical method to estimate thermophoretic particulate deposition efficiency and its effect on overall heat transfer coefficient of tube flows in transition and turbulent flow regimes [1]. The proposed analytical solution is validated against experiments conducted at Oak Ridge National Laboratory.

3.1 Introduction

There are many industrial applications involved in thermophoretic particulate deposition including gas cleaning, prevention of particle deposition on silicon wafers of semiconductors, and heat exchangers. Accordingly, there have been many attempts to propose analytical correlations for thermophoretic soot particle depositions in laminar and turbulent tube flows. Analytical solutions provide proportionality and functionality of variables especially for complex problems where many variables are involved.

Considerable theoretical work with experimental validation has been done by Walker et. al. [2], Batchelor and Shen [3] to study thermophoretic particulate deposition in laminar tube flows. There are also experimental investigations of thermophoretic particle deposition in laminar flow regime for a wide range of particle diameter ([4]-[7]).

The experimental data agrees well with theoretical models when Talbot equation [8] for thermophoretic coefficient is employed. Another effort is the work done by Lin and Tsai [9] for investigation of the thermophoretic deposition efficiency under developing flow at the entrance region. They found that the thermal entrance region of the pipe makes the thermophoretic deposition efficiency slightly higher than the fully developed case for a long pipe. They also developed empirical equations to predict thermophoretic efficiency of a laminar flow in a circular pipe in fully developed and developing flow under laminar flow conditions.

Besides laminar flow regimes, there is considerable work in the literature addressing thermophoretic deposition of particles under turbulent tube flow regimes as listed in the following. Chiou [10] focused on developing the theoretical and analytical models for turbulent thermophoretic deposition in tube flows. Byers and Calvert [11] studied thermophoretic deposition of particles in turbulent flow with the aspect of air cleaning. Their experiments were done to cover a wide range of particle size from 300nm to 1.3 micrometer. They proposed an analytical correlation to predict the particle deposition efficiency based on the experiments. Singh and Byers [12] extended the field by conducting experiments in the transition regime.

Nishio et. al. [13] performed experiments to study thermophoretic deposition of aerosol particles in pipe flows at various Reynolds numbers in laminar and turbulent flow regimes. They also proposed analytical correlations for the particle deposition and compared them with their experimental results. They also investigated the effect of different parameters including temperature gradient between hot fluid and coolant and the fluid velocity.

Romay et. al. [14] studied the thermophoretic deposition of aerosol particles under laminar and turbulent pipe flows. They performed the experiment for variable gas inlet temperature, different particle sizes, and mass flow rates correlating to laminar, transition, and turbulent Reynolds numbers in a pipe flow. They proposed an analytical

correlation for the deposition efficiency and compared it with other correlations in the literature ([3],[11],[12]).

A steady-state model has been developed by Housiadas and Drossinos [15] to predict thermophoretic particle deposition in laminar and turbulent pipe flow. Their results suggest that the 1D boundary layer approximation in turbulent flow is adequate, in general. The 1D model and 2D Lagrangian model in their work provide the same level of accuracy until the gas to wall temperature difference is large. In that case, the 2D model shows significant improvements.

He and Ahmadi [16] studied the thermophoretic deposition of particles in laminar and turbulent duct flows and compared the Brock-Talbot equation with the modified Cha-McCoy-Wood correlation. They also compared these two correlations with experimental measurements (Li and Davis [17],[18]) for a wide range of Knudsen numbers. They also studied the dominant mechanisms of soot deposition for different Knudsen numbers.

In another work, Chen conducted an analytical study on thermophoretic motion of two free aerosol particles with constant temperatures [19]. The particles can have different surface properties, diameter, and temperature. For the case that particles have the same diameter, particle interactions drives the pair system approaching each other if the particle temperature is less than the temperature of the surrounding. But if the temperature of the particles is higher than the surrounding temperature, the thermophoretic force will have a repulsive effect between the particles.

Lin [20] developed an analytical procedure to predict the particle deposition efficiency by considering the thermophoretic velocity in the conservation equations of particles. Lin investigated the effect of significant variables, including the temperature difference between the inlet gas and the wall, particle size, and Lewis number, on thermophoretic deposition efficiency.

Teng and Renger [21] also investigated soot deposition in EGR coolers. They proposed analytical correlations for particulate deposition efficiency and the effectiveness

for turbulent particle-laden flows but they did not include the effect of the formed layer on the effective tube diameter and the deposition rate. Besides aforementioned theoretical and analytical approaches, there are studies that are relevant to the subject ([22]-[24]).

Although analytical correlations for thermophoretic particle deposition have been proposed before, the objective of this study is to develop a novel correlation for cases where:

- The tube diameter reduction due to the deposit layer and thermal resistance of the deposit layer are taken into account in the solution
- The proposed solution is applicable to longer exposure times compared to steady-state solutions previously reported in literature and this method accounts for time varying parameters

This approach is to solve the energy equations for the bulk gas flow and the mass conservation of particles for a simple turbulent tube flow with different boundary conditions including gas inlet temperature, gas mass flow rate, and inlet particulate concentration.

The Oak Ridge National Laboratory experiments employing engine exhaust gas in a controlled test set up are used to verify the proposed analytical solution of this study [25]. Engine exhaust gas carries submicron soot particles and that makes it suitable for verification purposes of the analytical method. The exhaust gas was divided in a few tubes with designed Reynolds numbers to correlate transition and turbulent flow regimes.

The heat transfer coefficient (or effectiveness) of the tube, and soot mass deposited along the tube were compared to the experimental measurements for a relatively short exposure time (3 hours). The comparison shows an agreement between the analytical solution and experimental measurements with good accuracy; however, there are still improvements to be considered.

Although this solution is compared with engine exhaust flows representative of diesel engine exhaust gas recirculation (EGR) coolers, it can be generally used for

prediction of thermophoretic deposition of submicron particles in turbulent flows for a short exposure time.

3.2 Governing Equations

In this part, the analytical method for thermophoretic particulate deposition in turbulent and transition tube flows is described. Hot gas passes through the tube that has a constant wall temperature. The schematic of the tube is shown in Figure 3.1. The tube length (L), the inner diameter of a clean tube (ID), the transient inner diameter due to particulate deposition ($D(t)$), the inlet temperature (T_0), the inlet concentration of particles (C_0), the interface temperature at the deposit-gas interface ($T_{\text{int}erface}$), and the wall temperature (T_w) are depicted. Gas temperature (T), particle concentration (C), tube diameter, heat transfer coefficient, and gas velocity are functions of time since this problem is a transient problem. By finding the transient diameter of the tube, the conductive thermal resistance of the deposit layer and consequently the heat transfer coefficient (or effectiveness) drop of the tube can be calculated.

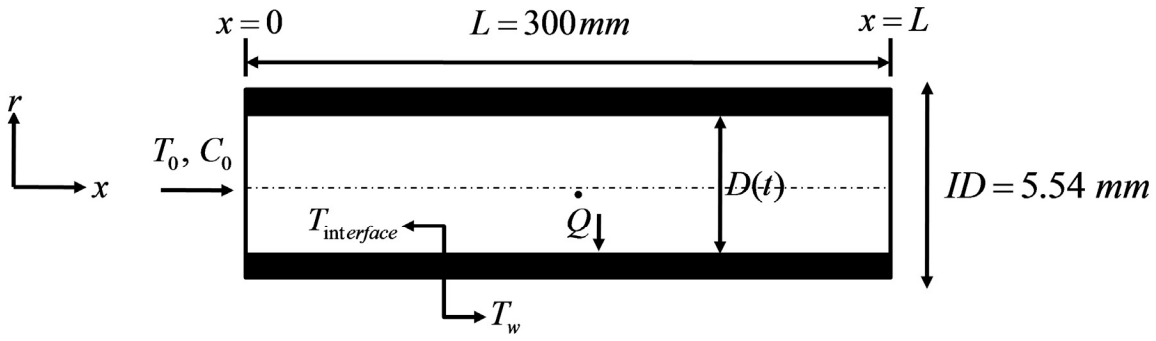

Figure 3.1 – A schematic of the model

The assumptions in developing the solution are:

- Constant wall temperature – A constant wall temperature is an appropriate assumption since the liquid coolant temperature typically changes only a

few degrees across the cooler, and the coolant-to-metal thermal resistance is much less that the gas-to-metal

- The particles do not affect the flow field due to their low mass fraction within the bulk gas
- The radial variations of temperature and particle concentration in main equations (energy and concentration) are neglected compared to the axial changes
- The bulk gas flow has low viscosity
- The deposit layer has a uniform radial and axial distribution in the tube and has a smooth surface (Figure 3.1). This assumption is made to simplify the equations and it seems to give reasonable results that will be discussed later in this chapter.

3.2.1 Energy Equation for Bulk Gas

By neglecting the axial conduction in the gas phase (large Peclet number) and the transient term (quasi steady assumption), the convection heat transfer along the axis will be equal to the amount of heat that is transferred to the tube walls ($\dot{Q}$). Considering the thermal resistance of the deposit layer and the heat transfer to the wall, the energy equation for an elemental tube segment (dx) can be written as:

$$\dot{Q} = \frac{T - T_w}{R_{convection} + R_{conduction}} = \frac{T - T_w}{\frac{1}{h\pi D dx} + \frac{\ln(ID/D)}{2\pi k_d dx}} \tag{3.1}$$

$$-\frac{\pi}{4} D^2 \rho U C_p dT = \frac{(T - T_w)}{\frac{1}{h\pi D} + \frac{\ln(ID/D)}{2\pi k_d}} dx \tag{3.2}$$

In the above equations, the convection thermal resistance of the gas flow ($R_{convection}$) and the conduction thermal resistance ($R_{conduction}$) of the deposit layer are taken

into account. It is also assumed that the state variables (i.e. interface temperature, tube diameter, gas velocity (U), density (ρ), specific heat (C_p), and gas convection heat transfer coefficient (h)) are not functions of x and they just vary with time (t). Constant values are considered for deposit properties. By integrating equation (3.2) along the tube length, the temperature can be calculated as:

$$\int_{T_0}^{T} \frac{dT}{T - T_w} = \int_{0}^{x} \frac{1}{(-\frac{\pi}{4} D^2 \rho U C_p)(\frac{1}{h\pi D} + \frac{\ln(ID/D)}{2\pi k_d})} dx \tag{3.3}$$

$$T = T_w + (T_0 - T_w) \exp(\frac{-4hx}{\rho U C_p D(1 + hD \ln(ID/D)/2k_d)}) \tag{3.4}$$

3.2.2 Particle Mass Conservation

Deposition is mainly due to thermophoresis for submicron particles as discussed in chapter 2. Neglecting the diffusion and other deposition mechanisms, and equation the convective and thermophoretic terms, the particle mass conservation in the tube can be expressed as:

$$-\frac{\pi}{4} D^2 U dC = C V_{th} \pi D dx \tag{3.5}$$

By reorganizing terms in equation (3.5) and introducing the definition for the thermophoretic velocity (V_{th}):

$$V_{th} = -\frac{K_{th}\nu}{T} \nabla T = -\frac{K_{th}\nu}{T} \frac{dT}{dr} \tag{3.6}$$

We get,

$$\frac{dC}{C} = -\frac{4V_{th}}{UD} dx = \frac{4}{UD} \frac{K_{th}\nu}{T} \frac{dT}{dr} dx \tag{3.7}$$

The thermophoretic velocity correlation was shown in chapter 2. For thermophoresis to occur, a temperature gradient in the radial direction is required. In

turbulent flows, temperature and concentration variations in radial direction just occur in a thin layer near the wall. Hence, the temperature gradient can be defined by equating the heat fluxes at the gas-deposit interface as:

$$\frac{dT}{dr} = (-\frac{h}{k_g})(T - T_{\text{int}erface}) \tag{3.8}$$

The convection heat flux between the gas and the deposit interface must also be equal to the conduction heat flux through the deposit layer.

$$\frac{T - T_{\text{int}erface}}{1/h\pi D} = \frac{T_{\text{int}erface} - T_w}{\ln(ID/D)/2\pi k_d} \tag{3.9}$$

So, the interface temperature is:

$$T_{\text{int}erface} = \frac{T + 2k_d T_w/(hD\ln(ID/D))}{1 + 2k_d/(hD\ln(ID/D))} \tag{3.10}$$

Substituting the interface temperature and the temperature gradient in the particle concentration equation (3.7) results in:

$$\frac{dC}{C} = K_{th}\,\text{Pr}\frac{dF}{F} \tag{3.11}$$

Where Pr is Prandtl number and

$$\begin{aligned} F &= T_w + (T_0 - T_w)\exp(\frac{-4hx}{\rho UC_p D(1 + hD\ln(ID/D)/2k_d)}), \\ dF &= (T_0 - T_w)(\frac{-4hdx}{\rho UC_p D(1 + hD\ln(ID/D)/2k_d)}) \times \\ &\exp(\frac{-4hx}{\rho UC_p D(1 + hD\ln(ID/D)/2k_d)}) \end{aligned} \tag{3.12}$$

Integrating equation (3.11) along the length (from 0 to x) yields:

$$C = C_0[\frac{T_w}{T_0} + (1 - \frac{T_w}{T_0})\exp(\frac{-4hx}{\rho UC_p D(1 + hD\ln(ID/D)/2k_d)})]^{K_{th}\,\text{Pr}} \tag{3.13}$$

Then, the particle deposition efficiency over the entire tube length can be defined as:

$$\eta_d = 1 - \frac{C_L}{C_0} = 1 - [\frac{T_w}{T_0} + (1 - \frac{T_w}{T_0}) \exp(\frac{-4hL}{\rho U C_p D(1 + hD \ln(ID/D)/2k_d)})]^{K_{th} \Pr} \tag{3.14}$$

where C_L is the outlet particulate concentration.

3.2.3 Transient Tube Diameter due to Particulate Deposition

Particulates create a growing layer of deposits after landing on the tube wall over time. Although the rate of deposition seems to be larger in the inlet compared to the outlet due to larger particulate concentration and larger driving force (temperature gradient), it is assumed that the layer is formed uniformly in the axial and radial directions in order to simplify the problem and make it solvable. Then the rate of mass deposition of the layer in terms of particulate deposition efficiency and particulate inlet concentration can be evaluated as:

$$\frac{dMass_{deposit}}{dt} = \eta_d C_0 \frac{\pi D^2}{4} U \tag{3.15}$$

Considering the deposit layer forming inside the tube (a hollow cylinder), equation (3.15) can be rewritten as:

$$\rho_d \frac{\pi}{4} L \frac{d(ID^2 - D^2)}{dt} = \eta_d C_0 \frac{\dot{m}}{\rho} \tag{3.16}$$

Assuming that the bulk gas mass flow rate ($\dot{m}$) is constant over time and substituting the deposition efficiency, one obtains:

$$\frac{DdD}{\{1 - [\frac{T_w}{T_0} + (1 - \frac{T_w}{T_0}) \exp(\frac{-4hL}{\rho U C_p D(1 + hD \ln(ID/D)/2k_d)})]^{K_{th} \Pr}\}} = -\frac{2C_0 \dot{m}}{\pi L \rho \rho_d} dt \tag{3.17}$$

The convective heat transfer coefficient and the velocity of the bulk gas flow are also functions of the transient tube diameter. The heat transfer coefficient can be calculated from the Nusselt number (Nu) definition for fully turbulent tube flows as [26]:

$$Nu = \frac{hD}{k_g} = \frac{\mathrm{Re}\,\mathrm{Pr}\,f/8}{1.07 + 12.7(f/8)^{0.5}(\mathrm{Pr}^{2/3} - 1)}, \quad 10^4 < \mathrm{Re} < 5 \times 10^6, 0.5 < \mathrm{Pr} < 2000 \tag{3.18}$$

Since the Nusselt number in equation (3.18) is applicable for turbulent flows, its use in transient regimes may cause errors or deviations from experimental results. There is a modified version of the aforementioned Nusselt number that covers the transition region but it is not employed in this study for simplicity. The Reynolds number is defined by:

$$\mathrm{Re} = \frac{4\dot{m}}{\pi \mu D} \tag{3.19}$$

The reduction of the tube diameter due to deposition changes the Reynolds number over time. For results presented later in this paper, $\mathrm{Re}_{t=0}$ is defined to represent the Reynolds number for a clean tube without the deposit layer as:

$$\mathrm{Re}_{t=0} = \frac{4\dot{m}}{\pi \mu ID} \tag{3.20}$$

The friction coefficient (f) is a function of the tube diameter, but the effect of the tube diameter variation on f due to particulate deposition is small. Consequently, the variation of the friction factor with the tube diameter (Reynolds number) can be neglected and f can be treated as a constant for the sake of simplicity.

$$f = \left(0.79 \ln \mathrm{Re}_{t=0} - 1.64\right)^{-2} \qquad 3000 \prec \mathrm{Re} \prec 5 \times 10^6 \tag{3.21}$$

The gas velocity is extracted from the continuity equation as:

$$U = \frac{4\dot{m}}{\pi\rho} D^{-2} \tag{3.22}$$

Substituting all the definitions in equation (3.17) and some manipulation yield:

$$\frac{DdD}{1-[A_1 + (1-A_1)\exp(\frac{-A_2 D^{-1}}{1+A_3 D^{-1}\ln(ID/D)}]^{K_{th}\,\mathrm{Pr}}} = -\frac{2C_0\dot{m}}{\pi L\rho\rho_d} dt \tag{3.23}$$

where,

$$\begin{aligned} A_1 &= \frac{T_w}{T_0} \\ A_2 &= (\frac{4k_g\,\mathrm{Pr}}{\mu C_p})(\frac{f/8}{1.07+12.7(f/8)^{0.5}(\mathrm{Pr}^{2/3}-1)})L \\ A_3 &= k_g(\frac{4\dot{m}}{\pi\mu})\frac{\mathrm{Pr}}{2k_d}(\frac{f/8}{1.07+12.7(f/8)^{0.5}(\mathrm{Pr}^{2/3}-1)}) \\ \frac{A_2}{A_3} &= \frac{2k_d\pi L}{\dot{m}C_p} \end{aligned} \tag{3.24}$$

Equation (3.23) is nonlinear and does not have an analytical solution unless some simplifications and assumptions are made. Accordingly, a Taylor expansion is employed for the exponential term as follows:

$$e^x = \sum_{n=0}^{\infty}\frac{x^n}{n!} = 1 + x + \frac{x^2}{2!} + \ldots \quad for\ \ all\ \ x \tag{3.25}$$

The first two terms in equation (3.25) are selected and the rest will be the error of this estimation. So, after simplifications equation (3.23) can be rewritten as:

$$\frac{DdD}{1-[1-\frac{(1-A_1)A_2}{D+A_3\ln(ID/D)}]^{K_{th}\,\mathrm{Pr}}} = -\frac{2C_0\dot{m}}{\pi L\rho\rho_d} dt \tag{3.26}$$

Another Taylor expansion is utilized to estimate the power term in equation (3.26) as:

$$(1+x)^{\alpha} = \sum_{n=0}^{\infty} \binom{\alpha}{n} x^n, \text{for all } \alpha, |x| < 1, \binom{\alpha}{n} = \prod_{k=1}^{n} \frac{\alpha - k + 1}{k} = \frac{\alpha(\alpha-1)...(\alpha-n+1)}{n!} \tag{3.27}$$

Since the criteria for using the proposed expansion are met, applying it simplifies equation (3.26) to:

$$\frac{DdD}{\Pr K_{th} \frac{(1-A_1)A_2}{D + A_3 Ln(ID/D)}} = -\frac{2C_0 \dot{m}}{\pi L \rho \rho_d} dt \tag{3.28}$$

Now, the ODE in equation (3.28) is linearized and can be integrated as:

$$\int_{ID}^{D} [D^2 + A_3 DLn(ID/D)] dD = \int_{0}^{t} -\frac{2C_0 \dot{m} \Pr K_{th} (1-A_1) A_2}{\pi L \rho \rho_d} dt \tag{3.29}$$

After applying the initial condition $D(t=0) = ID$, the result for the tube diameter can be expressed as:

$$\{D^3 - ID^3 + 3A_3 (\frac{D^2}{4} - \frac{ID^2}{4} + \frac{D^2}{2} Ln(ID/D))\} = -\frac{6(1-A_1)A_2 C_0 \dot{m} \Pr K_{th}}{\pi L \rho \rho_d} t \tag{3.30}$$

Taylor series expansion is used again to simplify the natural logarithmic term:

$$Ln(1+x) = \sum_{n=1}^{\infty} (-1)^{n+1} \frac{x^n}{n} \quad for \ |x| < 1, \ x \neq -1 \tag{3.31}$$

where,

$$\frac{ID}{D} = 1 + \frac{2\Delta}{D}, \quad \frac{2\Delta}{D} < 1 \tag{3.32}$$

So, the result becomes:

$$\{D^3 - ID^3 + \frac{3A_3}{4}(-D^2 + 2DID - ID^2)\} = -\frac{6(1-A_1)A_2 C_0 \dot{m} \Pr K_{th}}{\pi L \rho \rho_d} t \tag{3.33}$$

Equation (3.33) can be rewritten as:

$$D^3 - ED^2 + FD - J = Kt \tag{3.34}$$

where,

$$
\begin{aligned}
E &= \frac{3\dot{m}\,\mathrm{Pr}\,k_g f}{16\pi\mu k_d\left(1.07+12.7(f/8)^{0.5}(\mathrm{Pr}^{2/3}-1)\right)} \\
F &= \frac{3\dot{m}\,\mathrm{Pr}\,k_g f\,ID}{8\pi\mu k_d\left(1.07+12.7(f/8)^{0.5}(\mathrm{Pr}^{2/3}-1)\right)} \\
J &= ID^3 + \frac{3\dot{m}\,\mathrm{Pr}\,k_g f\,ID^2}{16\pi\mu k_d\left(1.07+12.7(f/8)^{0.5}(\mathrm{Pr}^{2/3}-1)\right)} \\
K &= -3(1-\frac{T_w}{T_0})\frac{k_g\,\mathrm{Pr}\,C_0\,\dot{m}\,\mathrm{Pr}\,K_{th} f}{\mu C_p \pi\,\rho\rho_d\left(1.07+12.7(f/8)^{0.5}(\mathrm{Pr}^{2/3}-1)\right)}
\end{aligned}
\tag{3.35}
$$

Solving equation (3.34) results in three solutions for the transient tube diameter, as follows:

$$
\begin{cases}
D(t)=\dfrac{E}{3}-\dfrac{2^{1/3}(-E^2+3F)}{3(2E^3-9EF+27Kt+27J+\sqrt{4(-E^2+3F)^3+(2E^3-9EF+27Kt+27J)^2}\,)^{1/3}} \\
\quad+\dfrac{(2E^3-9EF+27Kt+27J+\sqrt{4(-E^2+3F)^3+(2E^3-9EF+27Kt+27J)^2}\,)^{1/3}}{3\times 2^{1/3}} \\
D(t)=\dfrac{E}{3}+\dfrac{(1+i\sqrt{3})(-E^2+3F)}{3\times 2^{2/3}(2E^3-9EF+27Kt+27J+\sqrt{4(-E^2+3F)^3+(2E^3-9EF+27Kt+27J)^2}\,)^{1/3}} \\
\quad-\dfrac{(1-i\sqrt{3})(2E^3-9EF+27Kt+27J+\sqrt{4(-E^2+3F)^3+(2E^3-9EF+27Kt+27J)^2}\,)^{1/3}}{6\times 2^{1/3}} \\
D(t)=\dfrac{E}{3}+\dfrac{(1-i\sqrt{3})(-E^2+3F)}{3\times 2^{2/3}(2E^3-9EF+27Kt+27J+\sqrt{4(-E^2+3F)^3+(2E^3-9EF+27Kt+27J)^2}\,)^{1/3}} \\
\quad-\dfrac{(1+i\sqrt{3})(2E^3-9EF+27Kt+27J+\sqrt{4(-E^2+3F)^3+(2E^3-9EF+27Kt+27J)^2}\,)^{1/3}}{6\times 2^{1/3}}
\end{cases}
\tag{3.36}
$$

Depending on the parameters and variables of the problem, the above set can give either three real numbers or one real number and two conjugate complex numbers. In each of the two cases, it is really trivial to detect the physically meaningful solution for the transient diameter so that it is not a complex or negative number, or larger than the clean tube inner diameter (ID).

Due to the fact that non-linear terms are repeatedly expanded by Taylor expansions to first order terms for simplification of equation (3.23), a comparison is made with the numerical solution of equation (3.23) with the results presented in equation (3.36). Figure 3.2 shows how the transient tube diameter is predicted by employing Taylor expansions. To perform a quantitative comparison some values are selected for critical parameters including inlet gas temperature (380°C), the tube wall temperature (90°C), inlet gas pressure (200 kPa), Initial Reynolds number (8000), and inlet particle concentration (30 mg/m^3). It is seen that the linearized solution of (3.23) for the time-dependent tube diameter is less than what numerical solution of the non-linearize original ODE in (3.23) predicts. There is a small error percentage involved in calculation of the tube diameter after 3 hours (2.1%) and the difference between absolute values is ($110\mu m$) which is quite small relative to the tube diameter. The deposited particulate thickness predicted by the numerical solution is $274\mu m$ while the analytical solution predicts it to be $384\mu m$ for 3 hours of exposure time. This error cannot be avoided if an analytical solution is desired. This analytical method is a simple fast way to perform a parametric study and a sensitivity analysis of the important boundary condition on the results.

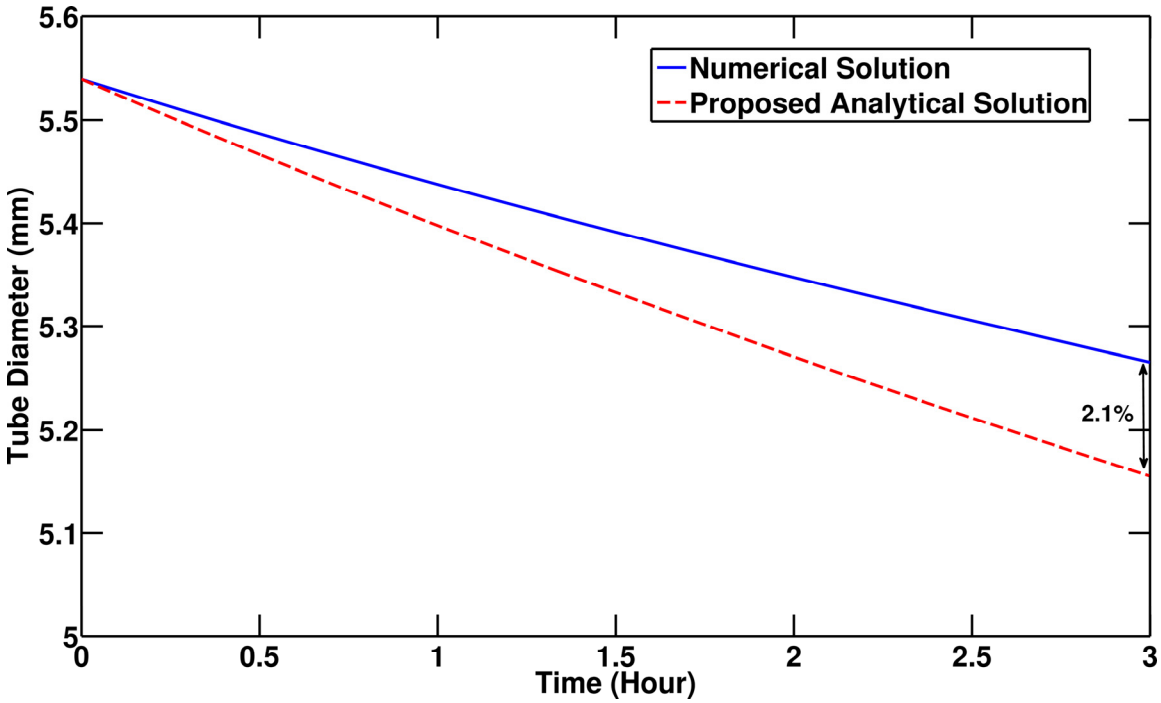

Figure 3.2 – Comparison between the numerical and analytical solutions of the transient tube diameter. $T_0 = 400^\circ C$, $T_w = 90^\circ C$, $C_0 = 30\,mg/m^3$, $P_0 = 200Kpa$, $\mathrm{Re}_{t=0} = 10000$

Having the transient tube diameter or the deposit thickness $\Delta = 0.5(ID - D(t))$, the tube effectiveness (actual heat transfer divided by the maximum possible heat transfer) can be computed as:

$$\varepsilon(t) = \frac{T_0 - T_L(t)}{T_0 - T_w} \tag{3.37}$$

where, $T_L(t)$ is the gas outlet temperature defined as:

$$T_L(t) = T_w + (T_0 - T_w)\exp\left(\frac{-4h(t)L}{\rho U(t) C_p D(t)(1 + h(t)D(t)\ln(ID/D(t))/2k_d)}\right) \tag{3.38}$$

Effectiveness drop ($\varepsilon|_{t=0} - \varepsilon|_{t=tend}$) is a metric to quantify the loss of thermal performance of the tubes. It is defined as the difference between the effectiveness at the start of deposition experiment (for a clean tube) minus the effectiveness at the end of the experiment. Since the diameter is a function of time, all other parameters including the effectiveness can be calculated as a function of time and explicit functions are defined.

The deposit mass gain can also be obtained from a geometrical estimation (deposit layer is a hollow cylinder along the tube length):

$$Mass_{deposit}(t) = \frac{\pi}{4}\rho_d L(ID^2 - D(t)^2) \tag{3.39}$$

3.2.4 Boundary Conditions

The inlet gas temperature, pressure, mass flow rate, inlet particle concentration, and tube wall temperature are constant in each case. So, the boundary conditions for this problem are listed as:

$$\dot{m}(0,t) = \dot{m}$$
$$T(0,t) = T_0$$
$$C(0,t) = C_0$$
$$P(0,t) = P_0$$
$$T\big|_{r=ID/2} = T_w$$
$$C\big|_{r=D/2} = 0$$

3.3 Exhaust Gas Thermodynamic and Transport Properties

Since the diesel fuel H:C ratio CH = 1.809 for experiments used for verification is known, and the dry based mole fraction of carbon dioxide based on the experimental measurements, the ideal chemical reaction in the diesel engine is as below [9]:

$$CH_{1.809} + 4.12(O_2 + 3.76N_2) \rightarrow CO_2 + 0.9045H_2O + 15.491N_2 + 2.667O_2$$

Air/Fuel ratio in conducted experiments is 40.95. Using the aforementioned reaction, one can determine the mole fraction of each species in the exhaust gas: It is noted that the dry based mole fraction of CO_2 is also given by experimental measurements and it is comparable with the following calculations:

$X_{CO_2} = 4.984\%$

$X_{H_2O} = 4.508\%$

$X_{O_2} = 13.294\%$

$X_{N_2} = 77.214\%$

The mole fraction of CO, NOX, HC, and all other existing species in the exhaust gas are negligible for this purpose. Utilizing the calculated mole fraction, one can find the gas flow properties including specific heat, viscosity, and thermal conductivity. Specific heat (molar based) of the main EGR flow can be found as:

$$\overline{C}_{p_{Mix}} = \sum_{\alpha=1}^{N} \overline{C}^{\circ}_{p_\alpha} X_\alpha \tag{3.40}$$

$$\frac{\overline{C}^{\circ}_{p_\alpha}}{R} = \sum_{m=1}^{M} a_{m\alpha} T_\alpha^{m-1} \tag{3.41}$$

For gas-phase species, the standard state is an ideal gas at 1 atmosphere. The coefficients (a_m) of individual specific heat of each species are extracted from CHEMKIN [28].

The Lennard-Jones Formula (in cgs units) is used to predict the viscosity of each species.

$$\mu_\alpha = 2.6693 \times 10^{-5} \frac{(MT)^{1/2}}{\sigma^2 \Omega_\mu} \tag{3.42}$$

while the viscosity of the main flow, as a mixture of different species, is:

$$\mu_{mix} = \sum_{\alpha=1}^{N} \frac{X_\alpha \mu_\alpha}{\sum_{\beta=1}^{\beta=1} X_\beta \phi_{\alpha\beta}} \tag{3.43}$$

$$\phi_{\alpha\beta} = \frac{1}{\sqrt{8}} (1 + \frac{M_\alpha}{M_\beta})^{-1/2} \left[1 + (\frac{\mu_\alpha}{\mu_\beta})^{1/2} (\frac{M_\beta}{M_\alpha})^{1/4} \right]^2 \tag{3.44}$$

The data for collision diameter of each species ($\phi_{\alpha\beta}$) is extracted from CHEMKIN [29]. Also, the definition of the collision integral is [30]:

$$\Omega_{\mu} = \frac{1.16145}{T^{*0.14874}} + \frac{0.52487}{\exp(0.7732T^{*})} + \frac{2.16178}{\exp(2.43787T^{*})} \tag{3.45}$$

$$T^{*} = \frac{kT}{\varepsilon} \tag{3.46}$$

$\frac{\varepsilon}{k}$: an intermolecular force parameter of each species (from CHEMKIN [29])

Thermal conductivity of a gas mixture containing polyatomic molecules can be estimated as [31]:

$$K_{Mix} = \frac{1}{2}\left[\sum_{\alpha=1}^{N} X_{\alpha} K_{\alpha} + \left(\sum_{\alpha=1}^{N} X_{\alpha} / K_{\alpha}\right)^{-1}\right] \tag{3.47}$$

$$K_{\alpha} = (C_{P\alpha}^{\circ} + \frac{5}{4}\frac{R}{M_{\alpha}})\mu_{\alpha} \tag{3.48}$$

It is noted that exhaust gas flow properties in this analytical study are calculated at the average temperature of the inlet flow and the wall.

$$T_{avg} = \frac{1}{2}(T_0 + T_w) \tag{3.49}$$

After linearizing, the properties of the exhaust gas as a function of temperature and pressure are listed as:

$$R_g = \frac{R}{MW_g},\ MW_g = 28.89\ \frac{g}{mol} \tag{3.50}$$

$$\rho = \frac{P_0}{R_g T_{avg}} \tag{3.51}$$

$$\mu = 3.07 \times 10^{-7} T_{avg}^{0.7126} \tag{3.52}$$

$$C_p = 0.2168 T_{avg} + 960.49 \tag{3.53}$$

$$k_g = 5.43 \times 10^{-5} T_{avg} + 0.01084 \tag{3.54}$$

$$\Pr = \frac{C_p \mu}{k_g} \tag{3.55}$$

Above correlations are valid for a temperature range between 298 K and 1000 K.

3.4 Deposit Layer Properties

There was little or no data in the literature to describe the thermal properties of EGR cooler deposits before Lance et. al. at Oak Ridge National Laboratory measured deposit thermal properties of EGR cooler deposit [32]. They measured the thermal diffusivity of the deposited soot cake by milling a window into the tube and using the Xenon flash lamp method. The heat capacity of the deposit was also measured and it was slightly higher than graphite, presumably due to the presence of hydrocarbons.

By combining above measurements, they calculated the deposit thermal conductivity to be 0.041 W/mK (averaged value), only~1.5 times that of air and much lower than the 304 stainless steel tube (14.7 W/mK). The most important factor in their measurement is density, which was measured to be just 2% that of the density of the primary soot particles (or 98% porous). Experiments are being done at Oak Ridge to also measure the mechanical strength of deposits.

Deposited soot layer properties are provided from the experimental data [32] to the model and listed in Table 3.1. Soot particle density and thermal conductivity are also listed in Table 3.2.

Table 3.1 – Properties of the deposited soot layer

Density	$\rho_d = 35\,Kg/m^3$
Thermal conductivity	$k_d = 0.041 W/mK$
Porosity	98%

Table 3.2 – Properties of soot particles

Mean diameter	$d_p = 57\,nm$
Density	$\rho_p = 1770\,Kg/m^3$
Thermal conductivity	$k_p = 0.5\,W/mK$

Maricq & Harris [33] showed that diesel engine soot agglomerate size ranges between 20 and 300 nm. They also showed that the mean particle size is 57 nm in most experimental conditions; hence, that is the number used to represent the particle diameter in this article.

3.5 Test Case for Verification of the Solution (ORNL Experiments)

To verify the model, a particle-laden EGR engine flow is selected for verification of this solution. The Oak Ridge National Laboratory has run EGR flow experiments in a controlled engine test set up. Details of the test set up and measurement procedures are fully described in Sluder et. al. [25]. The exhaust gas was divided to a few tubes at different designed boundary conditions (Table 3.3). In all selected experiments, the tube wall temperature was kept at $90^{\circ}C$ and HC level was enough low in order to prevent water or hydrocarbon condensation in the tube. Also, the gas inlet absolute pressure was kept at 196 Kpa.

Hot gas flow passes through the tube and the coolant circulates around it in the outer tube to keep a constant wall temperature. The coolant temperature rise is negligible (~2^{o} C). This low rise in coolant temperature is due to the large heat capacity of the coolant compared to that of exhaust gas flow. The tubes are made of stainless steel that has a large thermal conductivity compared to that of soot and exhaust gas. After each time exposure (3 hours), the sample tubes were removed from the fixture and analyzed.

Table 3.3 – Boundary conditions for selected experiments

Experiment No.	Initial Reynolds number ($\mathrm{Re}_{t=0}$)	Inlet Soot Concentration (mg/m3)	Inlet temperature ($^{\circ}$C)
1	4500	7.5	220
2	4000	7.5	380
3	4500	30	220
4	4000	30	380
5	9000	7.5	220
6	8000	7.5	380
7	9000	30	220
8	8000	30	380

3.6 Results and Discussion

In this part, the results of the analytical approach are described and discussed. Before verification of the solution, a parametric study is done to highlight the effects of boundary conditions on thermophoretic particle deposition.

3.6.1 Parametric Study

For this parametric study, the geometry in Figure 3.1 and the aforementioned layer information are used. In each case, all boundary conditions except one were kept constant in order to magnify the effect of the varying boundary condition on particulate mass deposited. It is also noted that the unit of the particulate concentration is defined as kg per m^3 of the gas flow and not based on the particulate number or particulate mass fraction.

Figure 3.3 shows the effect of the gas inlet temperature on the amount of particulate mass deposited along the tube. Increasing the inlet temperature while the wall

temperature is constant results in increasing the thermophoretic driving force applied to particulates in the main flow. Also, increasing the inlet temperature decreases the gas density and increases the volumetric flow at a constant inlet pressure and the initial Reynolds number. Therefore, to have a constant particle concentration, the number of particles must be larger in a larger volumetric flow rate. As a result, the larger inlet temperature yields more deposited mass along the tube over the selected exposure time (3 hours) due to larger driving forces and number of particles.

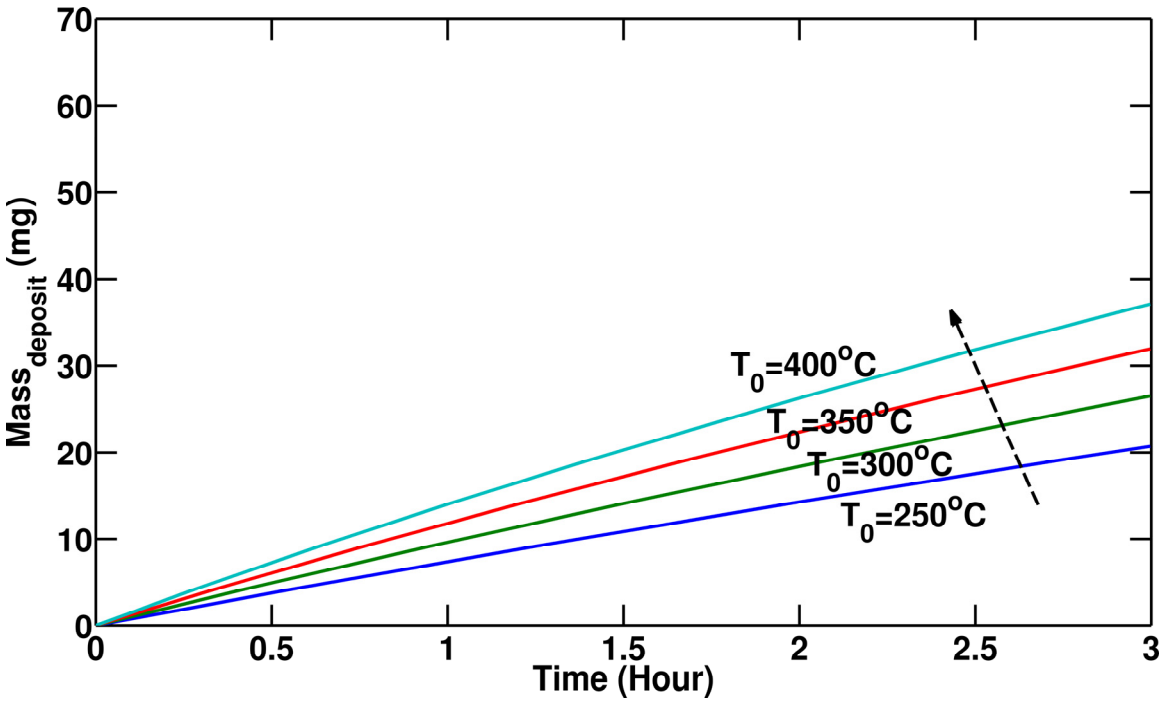

Figure 3.3 – Variation of particulate mass deposited with gas inlet temperature (T_0).
$\mathrm{Re}_{t=0} = 10000$, $T_w = 90^\circ C, C_0 = 30 mg/m^3, P_0 = 200 Kpa$

While the gas temperature and pressure are kept constant, gas properties do not vary. Figure 3.4 shows that by increasing the initial Reynolds number (gas mass flow rate) for a clean tube (defined in (3.20)), the deposit mass increases. This is due to the fact that a larger initial Reynolds number means a larger mass flow rate while the inlet temperature is constant (referring to (3.20). A larger mass flow rate results in a larger volumetric flow for a constant inlet gas temperature (density). To satisfy the constant

concentration constraint in this graph, the number of particles (quantity of particles not their size) must be also larger. This results in larger deposition of particulate.

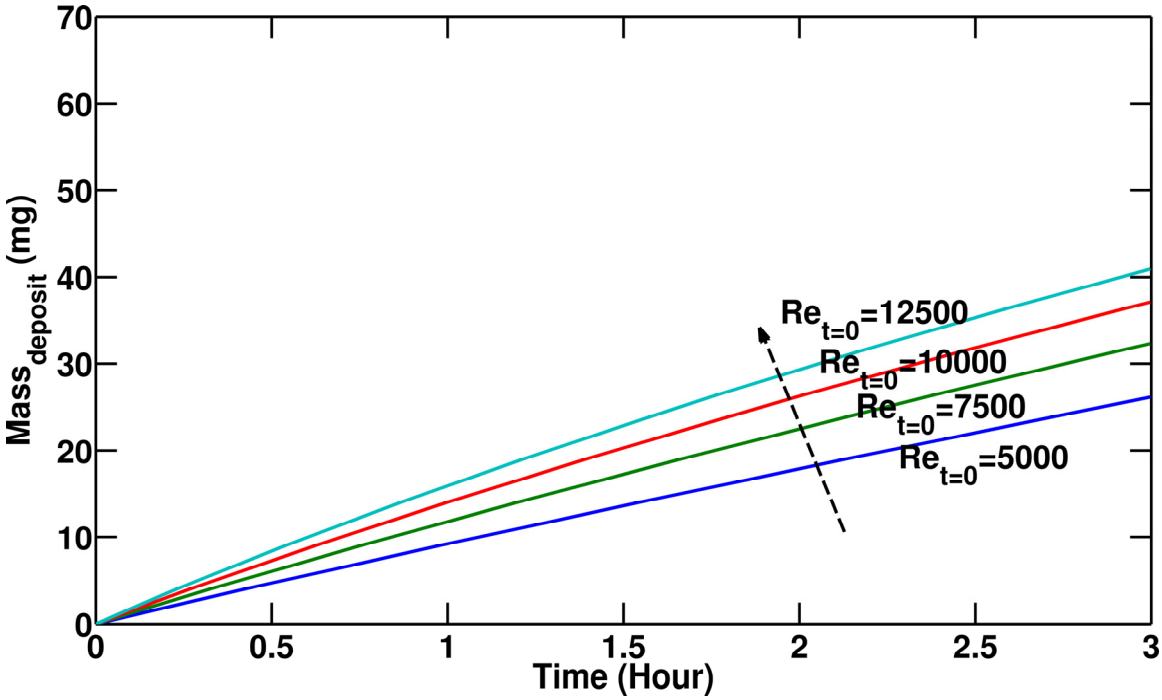

Figure 3.4 – Variation of particulate mass deposited with initial Reynolds number ($\mathrm{Re}_{t=0}$). $T_0 = 400^\circ C$, $T_w = 90^\circ C$, $C_0 = 30\,mg/m^3$, $P_0 = 200Kpa$

An expected trend is illustrated in Figure 3.5 . Increasing the inlet particulate concentration when the mass flow rate and the gas temperature are constant results in a larger mass deposited along the tube due to the presence of more particles in the main flow. The effect of gas inlet pressure on deposited mass along the tube is presented in Figure 3.6. Increasing the inlet pressure increases the gas density while gas inlet temperature is kept constant. For a constant mass flow rate, increasing gas density lowers the volumetric flow rate. Thus the number of particles carried by the flow must be lesser to keep the particulate concentration constant. Therefore, a lesser inlet particulate number due to higher gas inlet pressure causes less particulate deposition.

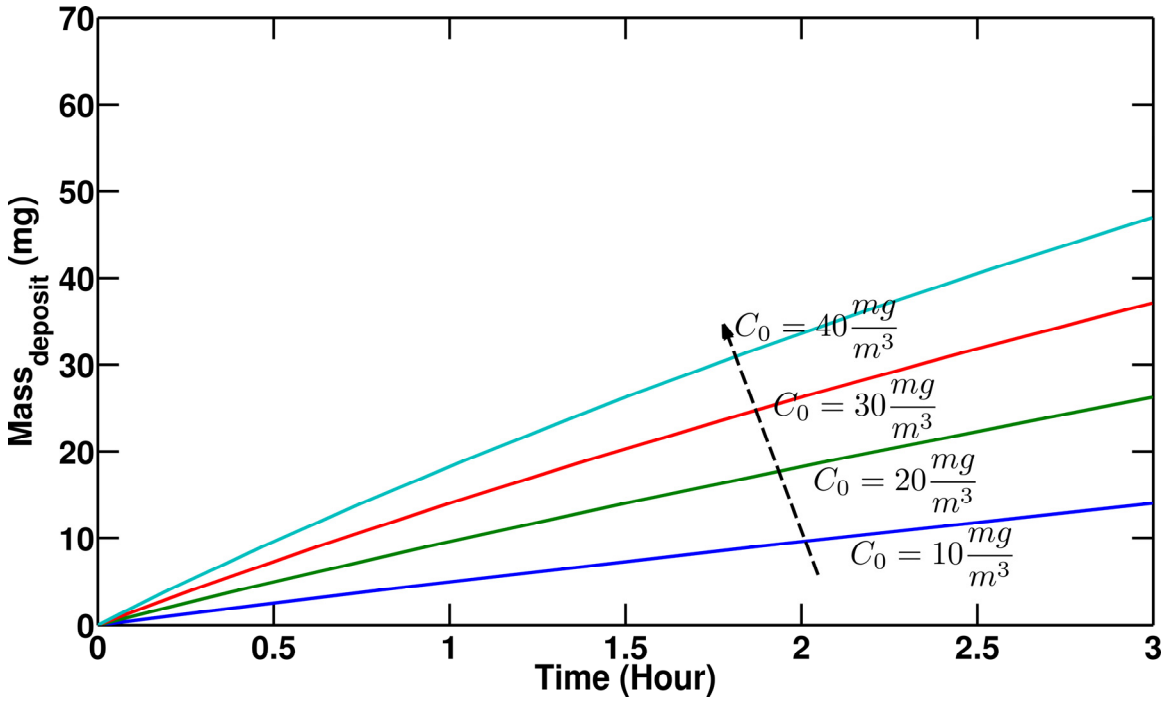

Figure 3.5 – Variation of particulate mass deposited with particulate inlet concentration (C_0). $\mathrm{Re}_{t=0} = 10000$, $T_0 = 400^\circ C$, $T_w = 90^\circ C$, $P_0 = 200 Kpa$

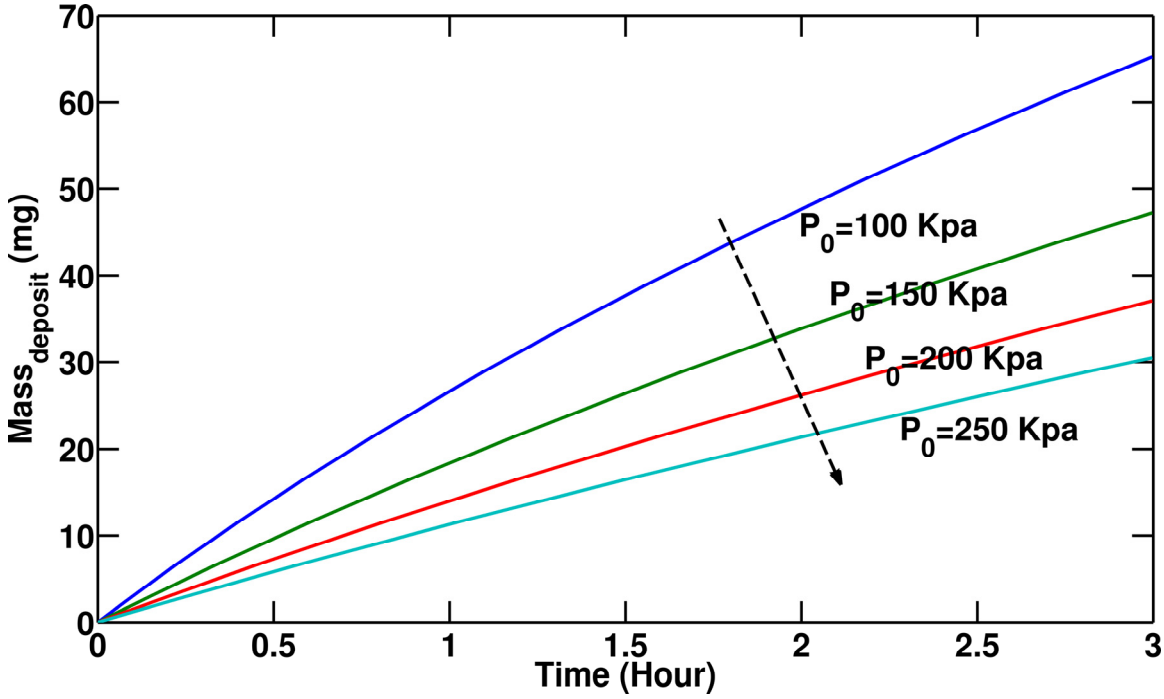

Figure 3.6 – Variation of particulate deposited mass with gas inlet pressure (P_0). $\mathrm{Re}_{t=0} = 10000$, $T_0 = 400^\circ C$, $T_w = 90^\circ C$, $C_0 = 30 mg/m^3$

3.6.2 Sensitivity Analysis

To investigate how changes in variables ($k_d, \rho_d, T_0, P_0, C_0, \dot{m}$) affect the model output (deposited mass gain and effectiveness drop), a sensitivity analysis is performed. The analysis in section 3.6.1 shows that each variable affects the results of deposited mass gain in a monotonic manner. For the sensitivity analysis, the variable values are randomly selected based on a normal distribution where the means correspond to the average values from the orthogonal experiments by Oak Ridge National Laboratory (ORNL) and the standard deviation is set to be 20% of the mean. This sampling was conducted 1000 times (it shows similar results with even a lower number). The mean of the deposited mass gain is 12 mg and the standard deviation is 5.6 mg, about 46% of the mean. We are also interested in how each parameter correlates with the model output (deposited mass gain and effectiveness drop). Therefore, we calculated the partial rank correlation coefficient (PRCC). PRCC is a robust measure of sensitivity for nonlinear but monotonic relationships between a certain input and the output. A positive PRCC implies that the input is correlated with the output and increasing the input increases the output as well. A negative PRCC means the input parameter is negatively correlated with the output and increasing the input results in the output reduction. A zero value for PRCC shows input and output are uncorrelated.

As shown in Figure 3.7, the deposited mass gain show negligible correlation with the deposit properties k_d, ρ_d. Observations from these results include:

- Increasing deposit thermal conductivity results in a better heat transfer and larger temperature gradients at the wall a small increase in deposition due to thermophoresis.
- Increasing deposit layer density means a smaller thickness for the same deposited mass and a smaller conduction thermal resistance (slightly larger temperature gradient at the wall). So, larger deposit layer density

delivers slightly larger deposition and that is the reason the PRCC is positive.

- Inlet temperature, particle concentration, and gas mass flow rate are positively correlated and have larger effects on the deposited mass gain while gas pressure is negatively correlated as discussed before. Inlet temperature shows the most effect on deposited mass gain.

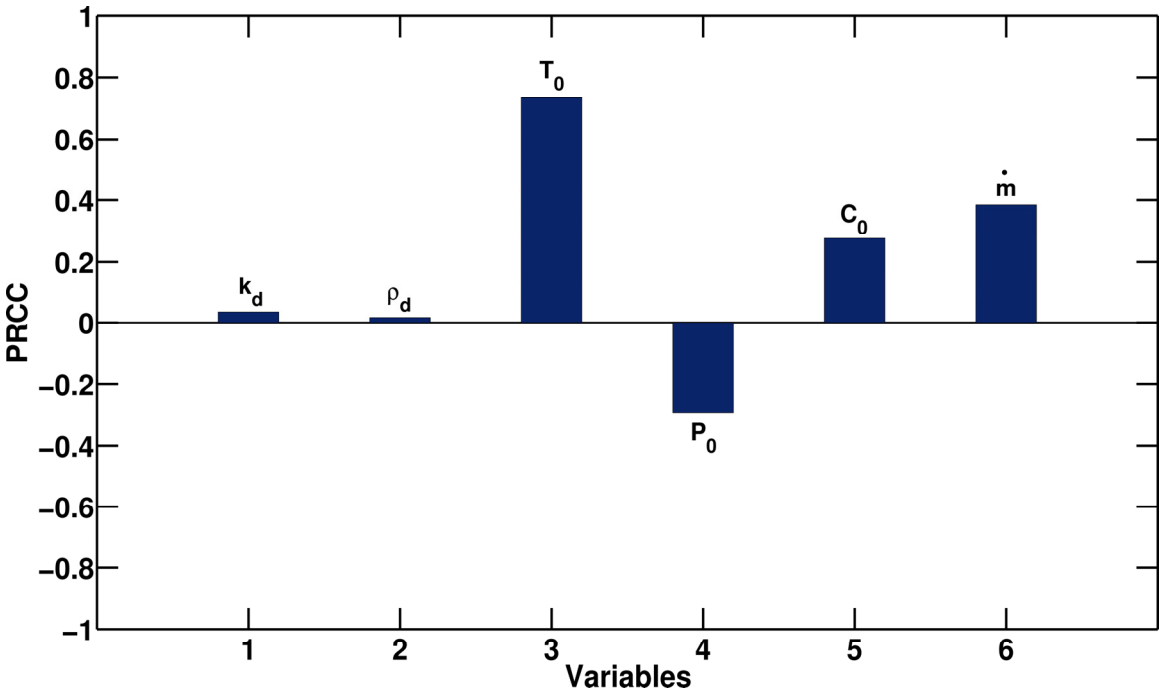

Figure 3.7 – PRCC values for different parameters $k_d, \rho_d, T_0, P_0, C_0, \dot{m}$ effect on deposited mass gain

Similar analysis is done (Figure 3.8) for the effectiveness reduction of the tube after 3 hours exposure. It can be seen from the graph that inlet gas temperature, gas mass flow rate, and inlet particle mass fraction are positively correlated with the effectiveness reduction as expected. Increasing the deposited mass gain reduces the overall heat transfer coefficient and increases the effectiveness reduction. Gas pressure is negatively correlated with the effectiveness reduction of the tube as expected from Figure 3.7. The critical message on these graphs is that the deposited layer properties do not have a

significant impact on the mass gain prediction while they have a noticeable impact on the heat transfer. Deposit thermal conductivity is negatively correlated with the effectiveness drop because increasing it results in a better heat transfer and a lower drop in effectiveness. Also, deposit layer density is negatively correlated with effectiveness reduction since increasing the layer density reduces the thermal resistance and increases the overall heat transfer (lowers effectiveness drop).

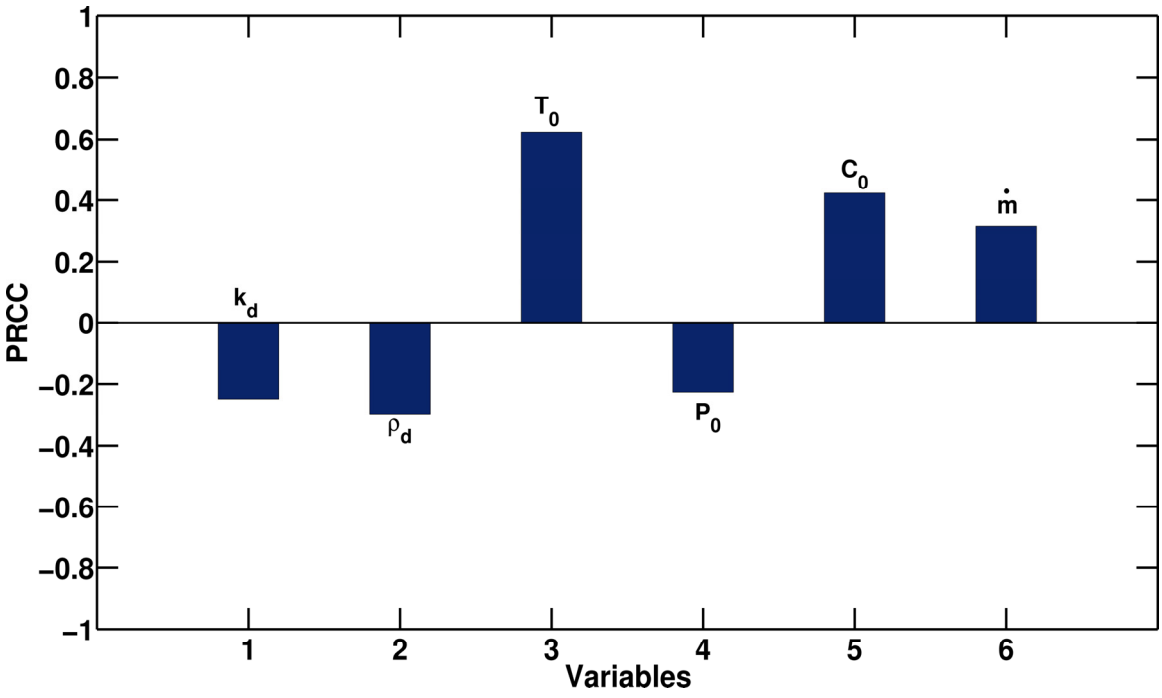

Figure 3.8 – PRCC values for different parameters $k_d, \rho_d, T_0, P_0, C_0, \dot{m}$ effect on effectiveness drop of the tube

3.6.3 Comparison with Experimental Data

To verify the solution, a comparison is also made with experimental measurements of Oak Ridge National Laboratory researchers at different boundary conditions, as listed in Table 3.3. One set of boundary conditions (Experiment No. 8 in Table 3.3) is selected for presenting the results. In the end, a comparison between the current model and experiments at various boundary conditions is made.

Figure 3.9 shows the diameter reduction of the tube due to soot deposition and the deposit layer thickness for the selected experiment (No. 8). It can be seen that the layer thickness reaches approximately150 μm which is quite a noticeable value.

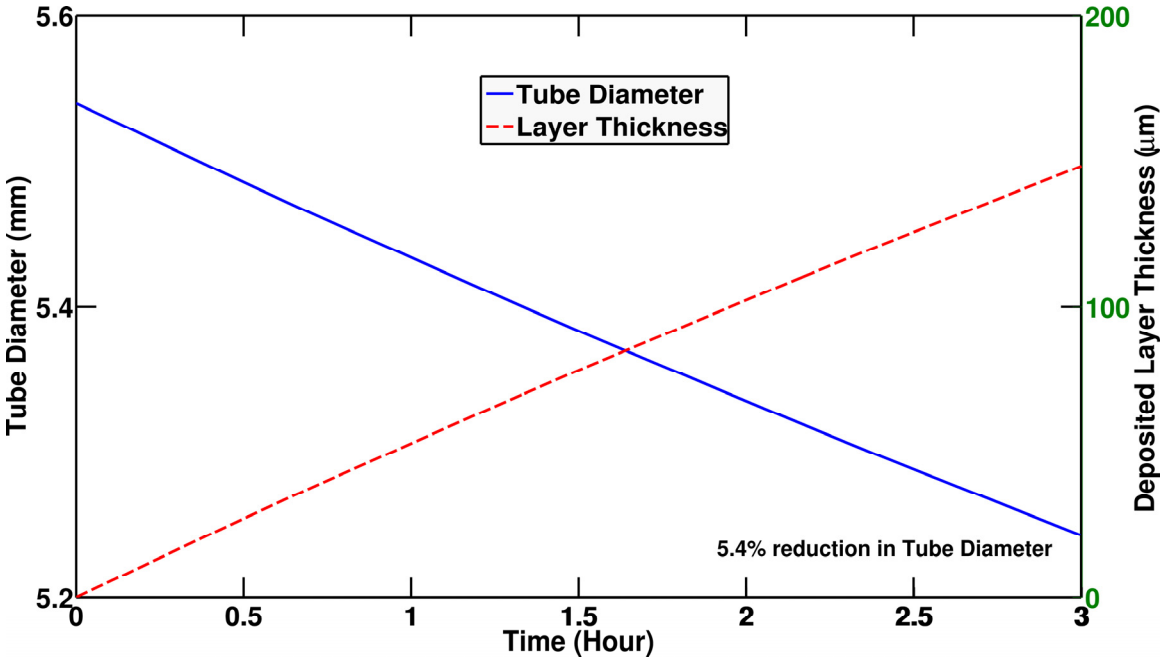

Figure 3.9 – Tube diameter reduction due to soot deposition and deposited layer thickness. $\mathrm{Re}_{t=0} = 8000$, $T_0 = 380^\circ C$, $T_w = 90^\circ C$, $C_0 = 30 mg/m^3$, $P_0 = 196\, Kpa$

A comparison between the analytical solution and experimental results (No. 8) for the effectiveness of the surrogate tube is shown in Figure 3.10. The experiments were run twice for the statistical confidence. The differences between the experiments (especially at t=0) is due to errors in measurements, specifically the exhaust mass flow rate or temperature differential. In the first 5 minutes of the experiments, the effectiveness curve shows an increasing pattern because the fixture was not completely warmed up. The analytical solution predicts the effectiveness drop of the surrogate tube reasonably well in term of both magnitude and slope. That is, the rate of heat transfer reduction of the tube over time is predicted reasonably well by the equations. The effectiveness of the cooler degrades 17% as a result of deposit formation. Although this case is the worst case for

deposition since it has the highest inlet temperature and inlet soot concentration with a high initial Reynolds number, this amount of degradation is quite significant. This is the reason that this problem is getting more attention in industrial applications especially in the automotive industry. Soot particle mass deposited for each experiment and the analytical solution are also shown in Figure 3.10. The numbers show a reasonable consistency between the experimental measurements.

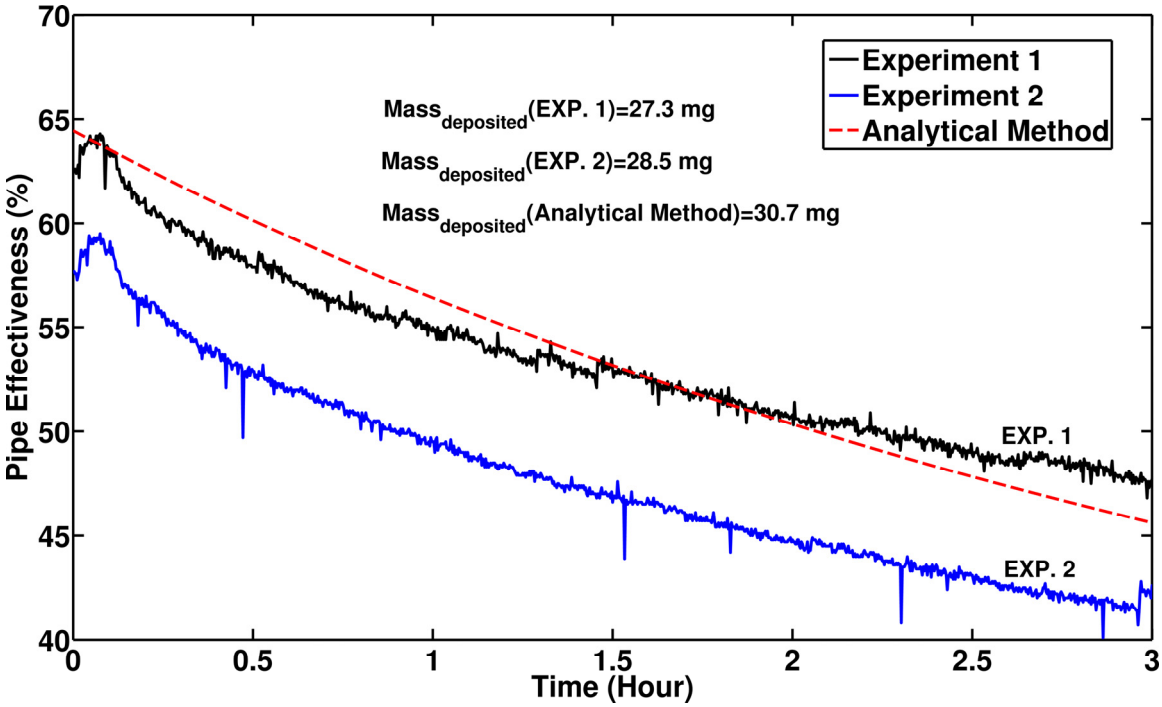

Figure 3.10 – Comparison of effectiveness vs. time.
$\mathrm{Re}_{t=0} = 8000,\ T_0 = 380^\circ C,\ T_w = 90^\circ C, C_0 = 30 mg/m^3, P_0 = 196\, Kpa$

Figure 3.11 shows the deposited soot mass predicted by the analytical solution versus the deposited soot mass measured experimentally for all 8 cases. The values plotted for the experimental results represent the average recorded between the two runs that are almost identical in most cases. If the analytical method predicted the mass gain exactly the same as the experimental results, the "ideal regression line" would have been achieved; however, the other regression line is what the current analytical solution predicts.

Figure 3.12 demonstrates the same comparison for the effectiveness drop. Four experiments (No. 1 to 4 in Table 3.3) have initial Reynolds numbers ($\mathrm{Re}_{t=0}$) between 4000 and 4500; however, the last four experiments (No. 5 to 8 in Table 3.3) are conducted for initial Reynolds number between 8000 and 9000. The results of the analytical solution in the graph are labeled with the corresponding experiment number.

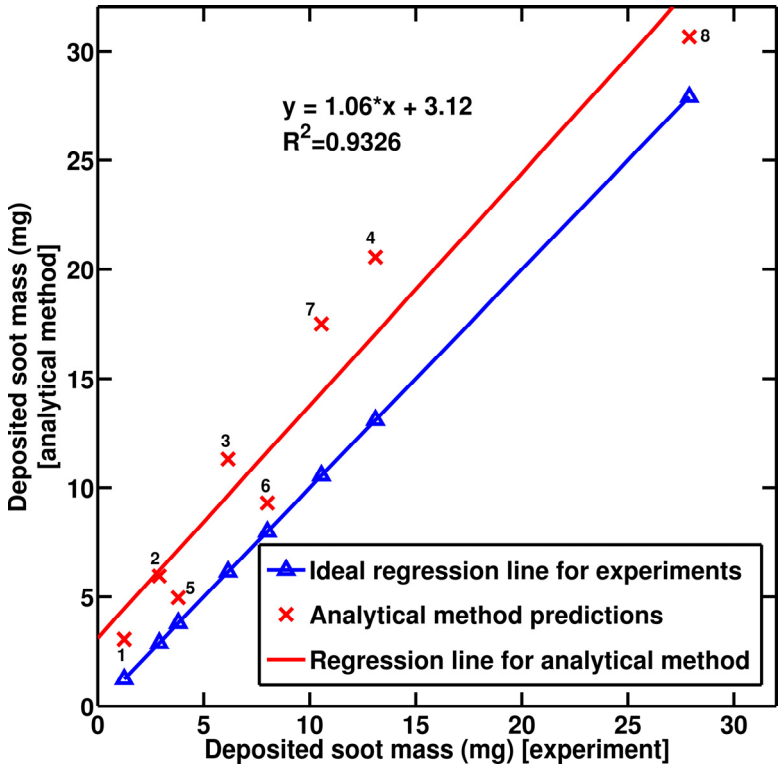

Figure 3.11 – Deposited soot mass gain – model results vs. experimental measurements. Numbers on the data points indicate experimental conditions from Table

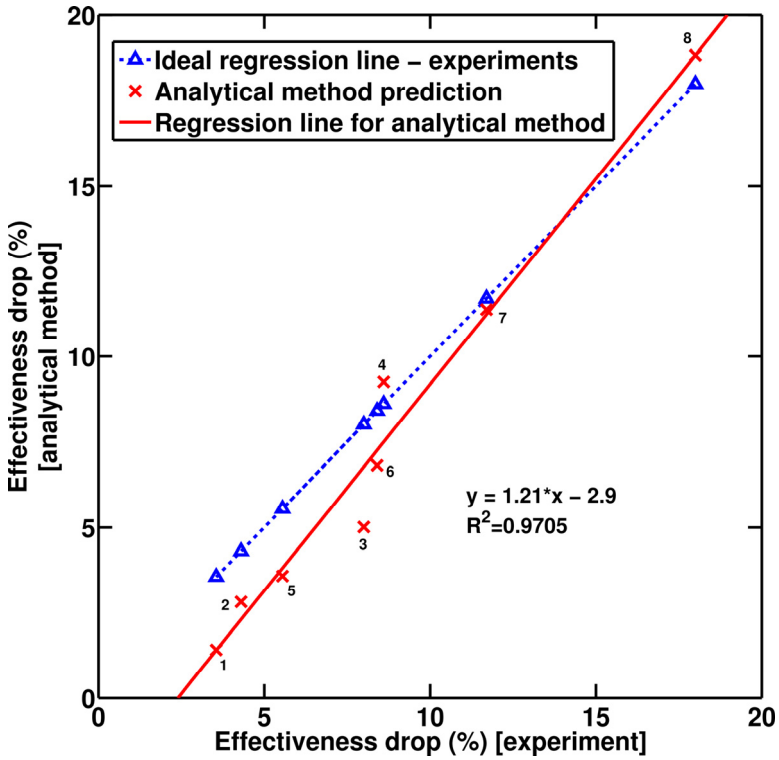

Figure 3.12 – Effectiveness drop – model results vs. experimental measurements. Numbers on the data points indicate experimental conditions from Table 1.

The results show an acceptable agreement (slope and magnitude of predicted curves compared to the measured experimental data in Figure 3.11and Figure 3.12) between the analytical method and experiments for a short exposure time (~3hours). We also learned the effect of different boundary conditions on the deposited mass based on this method. We can improve the analytical method by employing numerical techniques to solve governing equations more accurately. The deposit layer properties, including thermal conductivity and density, are important parameters that affect the results significantly. When the deposit layer grows, the interface temperature is hotter and the layer properties may be a function of the interface temperature and the layer thickness. In this model, the deposit layer properties are non-varying with temperature. The deposit layer is a highly porous medium with a 98% of porosity [32]. There could also be a convective heat transfer mechanism occurring inside the layer at such high porosity. This cannot be accommodated in the analytical method and requires numerical models. CFD

models will improve the results especially for longer exposure times when the analytical methods' prediction in estimating the diameter is not very accurate.

3.7 Concluding Remarks

An analytical solution for thermophoretic deposition of submicron particles in transition and turbulent flow regimes is proposed. An explicit function is offered for the deposited layer thickness (the transient tube diameter).

A parametric study is conducted to investigate the effect of boundary conditions on the amount of particulate mass deposited. It was shown that larger gas inlet temperature, inlet particulate concentration, and initial Reynolds number result in larger particulate mass deposited, while larger gas inlet pressure reduces it when all other boundary conditions are kept constant. A sensitivity analysis is also performed to show how the variables are correlated to the model output (deposit mass gain and effectiveness drop of tubes) after 3 hours exposure time. The sensitivity analysis shows that deposit layer thermal properties are weakly correlated to the deposited mass gain although they have a strong correlation to the effectiveness drop of tubes.

The heat transfer coefficient degradation of the tube over time due to particulate deposition is also predicted as a consequence of the diameter estimation. Particulate deposition can degrade heat transfer effectiveness of a surrogate tube significantly even in a short exposure time (3 hours). Also, the proposed correlation for the particle deposition efficiency shows that it is a function of the transient tube diameter and varies as the layer grows.

Predicted effectiveness drop and soot mass deposited have been compared with data from experiments run at Oak Ridge National Laboratory for particle-laden engine exhaust flowing through a heat exchanger with controlled conditions. The results of the analytical approach are in reasonable agreement with experimental measurements.

The analytical method is developed to find explicit correlations of different variables and it is good for the parametric study of the problem. To incorporate more physics including gas flow and the deposit layer properties variation as a function of temperature along the tube, axial variation of tube diameter as a function of local thermophretic force, and to more accurately solve this complex problem, we need to analyze it numerically. Chapter 4 describes our developed CFD models that are more accurate and complete.

3.8 Nomenclature

C	Mean particle concentration (kg/m^3)
C_0	Inlet particle concentration (kg/m^3)
C_L	Outlet particle concentration (kg/m^3)
C_p	Specific heat of the gas flow ($J/kg\,K$)
D	Transient tube diameter (m)
d_p	Particle diameter (m)
f	Friction factor
h	Convection heat transfer coefficient (W/m^2K)
ID	Inner diameter of a clean tube (m)
Kn	Knudsen number ($=2\lambda/d_p$)
K_{th}	Thermophoretic coefficient
k_d	Deposit layer thermal conductivity (W/mK)
k_g	Gas thermal conductivity (W/mK)
k_p	Particle thermal conductivity (W/mK)
L	Tube Length
MW_g	Gas molar mass
$\dot{m}$	Mass flow rate (Kg/sec)
Nu	Nusselt number
Pr	Prandtl number
$\dot{Q}$	Heat transfer to the tube wall (W)
R	Gas constant ($8.3143\ J/mol\,K$)
R_g	Specific gas constant ($J/kg\,K$)
$R_{conduction}$	Deposit conduction thermal resistance (K/W)
$R_{convection}$	Gas convection thermal resistance (K/W)
Re	Reynolds number
$\text{Re}_{t=0}$	Initial Reynolds number for a clean tube
T	Gas temperature (K)
T_0	Gas inlet temperature (K)
T_{avg}	The average of inlet gas and the tube wall temperatures (K)
$T_{\text{int}erface}$	Deposit-gas interface temperature (K)
T_L	Gas outlet temperature (K)
T_w	Tube wall temperature (K)
t	Time (sec)
U	Mean gas velocity (m/s)
V_{th}	Thermophoretic velocity (m/s)

Greek

Δ	Deposit layer thickness (m)
ε	Tube effectiveness
η_d	Particulate deposition efficiency
λ	Mean free path of a gas molecule (m)
μ	Viscosity of the gas flow ($kg/m\,s$)
ρ	Density of the gas flow (kg/m^3)
ρ_d	Deposit layer density (kg/m^3)
ρ_p	Particle density (kg/m^3)
ν	Gas kinematic viscosity (m^2/s)

3.9 References

[1] Abarham, M., Hoard., J., Assanis, D., Styles, D., Sluder, C. S. , Storey, J. M., "An analytical study of thermophoretic particulate deposition in turbulent pipe flows", Aerosol Sci. and Technol. 44 (9):785-795, 2010.

[2] Walker, K. L., Homsy, G. M., and Geyling, R. T., "Thermophoretic deposition of small particles in laminar tube flow", J. Colloid Interface Sci. 69 (1):138-147, 1979.

[3] Batchelor, G.K., Shen, C., "Thermophoretic Deposition of Particles in Gas Flowing over Cold Surfaces", J. Colloid Interface Sci. 107:21-37, 1985.

[4] Montassier, N., Boulaud, D., and Renoux, A., "Experimental study of thermophoretic particle deposition in laminar tube flow", J. Aerosol Sci. 22(5):677-687, 1991.

[5] Montassier, N., Boulaud, D., Stratmann, F., and Fissan, H., "Comparison between experimental study and theoretical model of thermophoretic particle deposition in laminar tube flow", J. Aerosol Sci.: 21 (Suppl. 1) S85-S88, 1990.

[6] Shimada, M., Seto, T., and Okuyama, K., "Wall deposition of ultrafine aerosol particles by thermophoresis in nonisothermal laminar pipe flow of different carrier gas", Jpn. J. Appl. Phys. 33:1174-1181, 1994.

[7] Stratmann, F., Fissan, H., Papperger, A., and Friedlander, S., "Supperssion of particle deposition to surfaces by the thermophoretic force", Aerosol Sci. Technol. 9:115-121, 1988.

[8] Talbot, L., Cheng, R.K., Schefer, R.W., Willis, D.R., "Thermophoresis of particles in a heated boundary layer", J. Fluid Mech. 101(4):737-758, 1980.

[9] Lin, J.S., Tsai, C.J., "Thermophoretic Deposition Efficiency in a Cylindrical Tube Taking into Account Developing Flow at the Entrance Region", J. Aerosol Sci. 34:569-583, 2003.

[10] Chiou, M. C., "Random eddy model for prediction of thermophoretic effects on particle deposition processes", J. Chinese Soc. Mech. Engng. 17(3):281-288, 1996.

[11] Byers, R. L., Calvert, S., "Particle Deposition from Turbulent Streams by Means of Thermal Force", I. EC. Fundam. 8:646-655, 1969.

[12] Singh, B., and Byers, R. L., "Particle deposition due to thermal forces in the transition and near-continuum regimes", Ind. Engng. Chem. Fundam. 11(1):127-133, 1972.

[13] Nishio, G., Kitani, S., Tkahashi, K., "Thermophoretic Deposition of Aerosol Particles in a Heat-Exchanger Pipe", Ind. Engng Chem. Des. Develop. 13:408-415, 1974.

[14] Romay, F.J., Takagaki, S.S., Pui, D.Y.H., Liu, B.Y.H., "Thermophoretic Deposition of Aerosol Particles in Turbulent Pipe Flow", J. Aerosol Sci. 29:943-959, 1998.

[15] Housiadas, C., Drossinos, Y., "Thermophoretic Deposition in Tube Flow", Aerosol Sci. Technol. 39:304-318, 2005.

[16] He, C., Ahmadi, G., "Particle Deposition with Thermophoresis in Laminar and Turbulent Duct Flows", Aerosol Sci. Technol. 29:525-546, 1998.

[17] Li, W., Davis, E.J., "Measurement of the Thermophoretic Force by Electrodynamics Levitation: Microspheres in Air", J. Aerosol Sci. 26:1063-1083, 1995.

[18] Li, W., Davis, E.J., "The Effects of Gas and Particle Properties on Thermophoresis", J. Aerosol Sci. 26:1085-1099, 1995.

[19] Chen, S. H., "Thermophoretic interactions of aerosol particles with constant temperatures", J. of Aerosol science 33: 1155-1180, 2002.

[20] Lin, S.H., "Particle Deposition due to Thermal Force in a Tube", Appl. Sci. Res. 32:637-647, 1976.

[21] Teng, H., Renger, G., "Particulate fouling in EGR coolers", SAE paper 2009-01-2877, 2009.

[22] Rosner, D. E., and Fernandez de la Mora, J., "Small particle transport across turbulent nonisothermal boundary layers", J. Engng. power 104:885-894, 1982.

[23] Owen, I., El-Kady, A.A., and Cleaver, J. W., "Deposition of sub-micrometer particles onto a heated surface with widely spaced roughness elements", J. Aerosol Sci. 20(6):671-681, 1989.

[24] Berger, C., Horavath, H., and Schindler, W., "The deposition of soot particles from hot gas streams through pipes", J. Aerosol Sci. 26(2):211-217, 1995.

[25] Sluder, C.S., Storey, J., Lewis, S., Styles, D., Giuliano, J., Hoard, J., "Hydrocarbons and Particulate Matter in EGR Cooler Deposits: Effects of Gas Flow Rate, Coolant Temperature, and Oxidation Catalyst", SAE Paper 2008-01-2467, 2008.

[26] Incropera, F. P., Dewitt, D.P., Heat and Mass Transfer, Fifth ed., John Wiley & Sons, New York, p. 491-492, 2002.

[27] Abarham, M., Hoard., J., Assanis, D., Styles, D., Curtis, E., Ramesh, N., Sluder, S., Storey, J., "Numerical modeling and experimental investigations of EGR cooler fouling in a diesel engine", SAE paper 2009-01-1506, 2009.

[28] Kee, R.J., Rupley, F. M., Miller, J. A., Chemkin-II: A FORTRAN Chemical Kinetics Package for the Analysis of Gas-Phase Chemical Kinetics, Sandia National Labs Report SAND89-8009B, 1989.

[29] Kee, R. J., Rupley, F. M., Miller, J. A., The Chemkin Thermodynamic Data Base. Technical Report SAND87-8215, Sandia National Laboratories, 1987.

[30] Bird, R. B., Stewart, W. E., Lightfoot, E. N., Transport phenomena, 2nd Ed., Wiley, New York, 2002.

[31] Mathur, S., Tondon, P. K., Saxena, S. C., "Thermal conductivity of binary, ternary, and quaternary mixtures of rare gases", Mol. Phys. 12:569, 1967.

[32] Lance, M., Sluder, C.S., Wang, H., Storey, J., "Direct Measurement of EGR Cooler Deposit Thermal Properties for Improved Understanding of Cooler", SAE Paper 2009-01-1461, 2009.

[33] Maricq, M., Harris, S., "The Role of Fragmentation in Defining the Signature Size Distribution of Diesel Soot", J. Aerosol Sci. 33:935-942, 2002.

CHAPTER 4

COMPUTATIONAL STUDY OF THERMOPHORETIC PARTICLE DEPOSITION

An analytical method was proposed in chapter 3 for nano-particulate transport in non-isothermal tube flows. Analytical solution was the best method to conduct a parametric study and a sensitivity analysis of the important variables for the problem but it was limited to many assumptions including constant gas properties (incompressible flow assumption). In this chapter, two approaches are used to analyze the problem, a one dimensional model in which the variables are assumed to be uniform in each cross section perpendicular to the tube axis; and an axi-symmetric model with moving boundaries. In the one dimensional model, MATLAB is used via implementing a finite difference scheme. In the axi-symmetric approach, the CFD software ANSYS-FLUENT is employed. In the software environment, a collection of C subroutines are developed to include the thermophoretic transport and the evolution of the boundaries due to the soot deposition. The variation of gas properties in the tube and accurate gas temperature and particle mass fraction gradients are critical factors that were not accommodated in the proposed analytical solution for the sake of simplifying the equations. In the 1D model, we employed empirical correlations for calculating the heat transfer rate to the tube wall exposed to the coolant; however, we solved the Navier-Stokes and energy equations to do so in the axi-symmetric model. We also solved the particulate mass conservation

equation more accurately in the axi-symmetric model. We compared the developed models against experiments conducted at Oak Ridge National Laboratory by comparison of the particulate mass deposited along the tube and the overall heat transfer reduction (effectiveness). Both models show a satisfactory agreement to the experimental results although the axi-symmetric model shows a significantly better estimation of the deposit mass gain in time. That is because of the more accurate estimation of deposition flux in the axi-symmetric model rather than the inaccurate conventional deposition flux in the one dimensional model.

4.1 Introduction

Our proposed analytical correlation for thermophoretic deposition of particles in tube flows is in a reasonably good agreement with experiments but it suffers from many ad-hoc assumptions that we made to simplify the problem. Hence, the current numerical methods are proposed to give a higher level of accuracy with more physics that were not included in the analytical solution.

Several research studies are performed to investigate the particulate deposition and fouling phenomenon in laminar and turbulent flow regimes numerically or experimentally. Thermophoretic particle deposition in tube flows is measured experimentally by Tsai et. al. [1] by using monodisperse NaCl particles under laminar and turbulent flow conditions. The previous empirical equations for thermophoretic deposition are in a good agreement with their experimental measurement. Also, they showed that Talbot's formula [2] for thermophoretic deposition is accurate compared to Waldmann's free molecular formula. Schmidt and Sager [3] studied deposition of particles in turbulent pipe flows numerically.

Messerer et. al. ([4],[5]) investigated thermophoretic submicron soot particles deposition under flow and temperature conditions relevant to heavy duty diesel exhaust

gas. A plate-to-plate thermal precipitation system has been used to investigate the deposition of agglomerate submicron soot aerosol particles in their work. Their experimental results were compared to a recent theoretical study by Rosner and Khalil [6] and showed a good compatibility. In the theoretical study, they proposed a correlation on how total mass deposition rates from a dilute flow stream can be predicted by thermal conductivity ratio, Reynolds number, particle mass loading, and temperature differences.

Epstein studied particle deposition from a suspension flowing parallel to nonporous smooth and rough surfaces in terms of particle attachment, transport, and reentrainment. He also investigated sticking probability of particles to the wall for isothermal and nonisothermal conditions. Referring to the literature, he offered a sticking probability as a ratio of adhesive bond force between particles to average shear force on particles at the surface [7].

Chein and Liao [8] studied diffusion and thermophoretic effects on nano-particle deposition in channel flow numerically. They examined two types of thermal conditions for different nano size particles and calculated particle deposition velocities for various wall temperatures and different inlet temperatures. Lee et. al. [9] simulated the thermophoretic deposition of ultrafine particles in an automobile exhaust pipe. In their study, the experimental data and the numerical simulation reflect the necessity of a new formula for thermophoretic deposition for high concentration polydisperse ultrafine particles in a pipe flow.

Tsai and Liang [10] studied thermophoretic deposition of aerosol particles on a flat cold plate in a laminar flow. The results were correlated from the numerical solutions for similar boundary flows and provided a possible error less than 3% when the mean to wall temperature ratio was between 0.2 and 1. Chomiak and Gupta [11] studied particles behavior in viscous and thermal boundary layer. They showed that the thermophoretic forces on particles with Knudsen numbers smaller than 1 decrease due to the rotations of

particles since the rotation results in a fraction of the particles being in thermal non-equilibrium with the gas flow.

Shams et. al. [12] studied deposition of particles from 10 nm to 50 μm in turbulent duct flows. They developed a sublayer model for the turbulent deposition process that includes the effects of gravity, Brownian, and lift forces. The deposition velocity for a range of particle relaxation times and flow conditions are presented in their work. Shear velocity effects on the deposition rates of various size particles are also investigated in their study.

There is also some recent work done on the modeling of the fouling processe in heat exchangers including EGR coolers ([13]-[18]). Florea et. al. simulated a transient fluid flow and heat transfer in the EGR cooler by using the CFD code FIRE (AVL) and presented temperature gradient and pressure field across the cooler. They then verified their 3D model with experimental measurements and showed the results are comparable in most cases but they did not take into account the effect of fouling in the model explicitly [19].

The novelties of this work compared to numerical models in literature are listed:

- Tube diameter reduction due to the deposited layer, and thermal resistance of the deposited layer are taken into account in the model. In the axi-symmetric model a dynamic subroutine is developed through a collection of user defined functions (UDFs) in ANSYS-Fluent to do this task
- The deposit layer is not considered uniform along the length and its thickness can vary due to the local thermophoretic force (not included in the analytical correlation)
- Accurate calculation of gas temperature and particle mass fraction gradients near the wall for steady state and transient axi-symmetric cases

So, we developed two models for solving mass, momentum, particle mass fraction, and energy equations of gas flow in a tube flow with different boundary

conditions including the inlet temperature, mass flow rate, and inlet particulate mass fraction. To verify the model, data was taken from a controlled test setup with similar tube geometry and boundary conditions [20] as shown in previous chapter.

4.2 One Dimensional Model Description and Governing Equations

In this section, the developed 1D model is described for the particulate transport in non-isothermal turbulent tube flows. Hot gas including solid particles enters into a tube with a lower wall temperature. As the gas passes through the tube, the solid particles are deposited on the wall, forming a solid layer. The thickness of this layer varies along the tube length due the variation in the deposition rate. A schematic of the model is shown in Figure 4.1 where the tube length (L), the inner diameter of a clean tube (ID), the effective inner diameter due to particulate deposition (D), the inlet temperature (T_0), the inlet mass fraction of particles (Y_0), the interface temperature at the gas-deposit interface (T_{int}), and the wall temperature (T_w) are depicted.

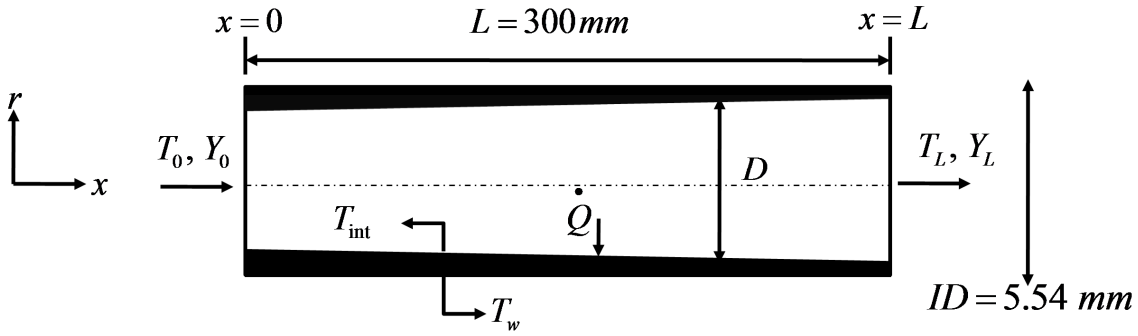

Figure 4.1 – Schematic of the model and the tube geometry

The gas flow and particulate transport are computed through an Eulerian approach to predict particle deposition where the governing equations are as follows. It is also noted that a quasi steady assumption is made in the 1D model to facilitate numerical difficulties. Boundary conditions are time varying and makes the problem a function of time.

4.2.1 Governing Equations

Figure 4.2 shows a schematic of a fluid element in the quasi 1D model. Area variation along the tube forces the problem to be two dimensional in nature but a quasi 1D assumption is made to simplify the equations.

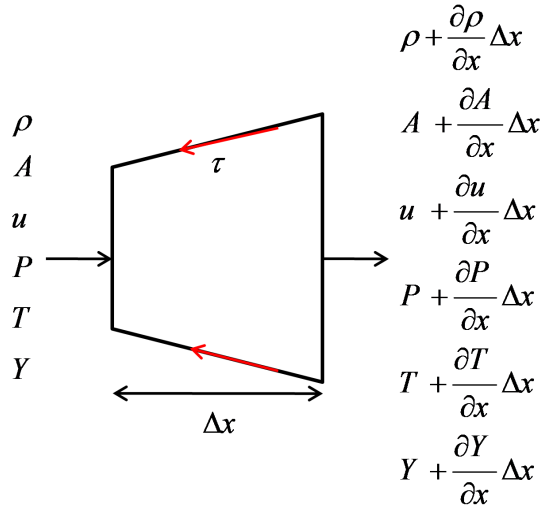

Figure 4.2 – A schematic of a fluid element in the 1D model

Continuity

Deposit layer makes some changes in the cross sectional area of the tube. Also, flow properties vary as a function of mean temperature. As there is a large drop in temperature of bulk gas, the properties variation along the tube length is not negligible. So, the mass conservation equation of the bulk gas flow becomes:

$$\frac{\partial(\rho_g A)}{\partial t}\Delta x + \frac{\partial(\rho_g u A)}{\partial x}\Delta x = 0 \tag{4.1}$$

Neglecting the transient term and particle mass deposition (source term) that is reduced from the main flow, and simplifying the equation yields :

$$\frac{d(\rho_g u A)}{dx} = \frac{d(\dot{m})}{dx} = 0 \tag{4.2}$$

Momentum

In writing the momentum equation, the sum of the pressure forces and shear forces acting on the surface of the control volume must be equal to summation of the rate of change of momentum inside the control volume. Writing the momentum equation of the bulk flow for a unit length of the tube, one obtains:

$$\frac{\partial(\rho_g uA)}{\partial t}\Delta x + \frac{\partial(\rho_g u^2 A + PA)}{\partial x}\Delta x - P\frac{dA}{dx}\Delta x = 0 \tag{4.3}$$

Neglecting the transient term (quasi steady) and considering the friction on the element surface area as the source term yields:

$$\frac{d(\rho_g u^2 A)}{dx}\Delta x + A\frac{dP}{dx}\Delta x = -\frac{1}{8}\rho_g f u^2 \pi D\Delta x \tag{4.4}$$

Combining above equation with mass conservation equation and simplifying the equation results in:

$$\frac{dP}{dx} = -\frac{1}{2}\frac{\rho_g f u^2}{D} - \frac{\dot{m}}{A}\frac{du}{dx} \tag{4.5}$$

Energy

Energy equation for the element of the fluid also yields:

$$\frac{\partial(\rho_g (e + u^2/2)A)}{\partial t}\Delta x + \frac{\partial(\rho_g u(h + u^2/2)A)}{\partial x}\Delta x = \dot{Q} \tag{4.6}$$

Where $\dot{Q}$ acts as a source term and is the heat transfer to the tube wall. Axial conduction in the gas phase is neglected in equation due to the large Peclet number. Neglecting the transient term (quasi steady) and considering the convection heat transfer as the source terms in the equation, one can find:

$$\frac{d(\rho_g u(h + u^2/2)A)}{dx}\Delta x = \dot{Q} \tag{4.7}$$

where the total gas enthalpy is $h = C_p T$, we obtain:

$$\frac{d(\rho_g u c_p T A)}{dx}\Delta x + \frac{d(\rho_g u^3/2\,A)}{dx}\Delta x = \dot{Q} \tag{4.8}$$

Figure 4.3 shows a cross section of a tube with the deposit layer and thermal resistances for an element with the length of Δx . Thermal resistances include conduction resistance of the tube metal, conduction resistance of the deposited layer, and convection resistance between the mean flow and the deposited layer.

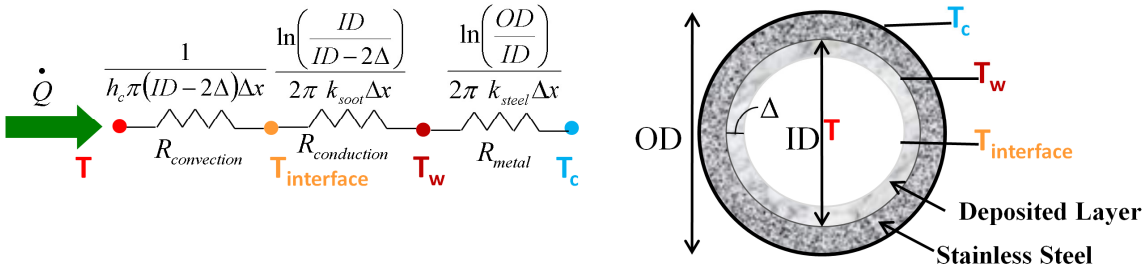

Figure 4.3 – A cross section of a tube with deposit, thermal resistances, and temperatures

So, we can write a simplified form of the energy equation as:

$$\dot{m}\frac{d(c_p T)}{dx} = -\dot{m}\frac{d(u^2/2)}{dx} + \frac{(T - T_w)}{\left(\frac{1}{h_c \pi (ID-2\Delta)} + \frac{\ln\left(\frac{ID}{ID-2\Delta}\right)}{2\pi k_d} + \frac{\ln\left(\frac{OD}{ID}\right)}{2\pi k_{steel}}\right)} \tag{4.9}$$

Conservation of Mass for Particle

By writing mass conservation for soot particles at a segment of the tube, one can balance the changes in particle mass of the mean flow per time step with the amount of deposited particles and the amount of particle mass that re-entrain to the main flow by any possible removal mechanism per time step.

$$\frac{\partial(\rho_g YA\Delta x)}{\partial t}+\frac{\partial(\rho_g YuA)}{\partial x}\Delta x=S_{soot-mass} \tag{4.10}$$

The transient term is neglected (quasi steady), and the total deposition flux due to thermophoresis and diffusion (J) at the wall is considered as the source term:

$$\frac{d(\rho_g YuA)}{dx}\Delta x=\pi D\Delta xJ=\pi D\Delta x(\rho_g D_B\frac{\partial Y}{\partial r}+\rho_g YV_{th})\Big|_{r=D/2} \tag{4.11}$$

Although deposition due to diffusion is not comparable with thermophoretic deposition for small particles based on our scaling analysis, we included the two terms to show their ratio in this model. We neglected the re-entrainment of particles to the main flow in this study since there is not a confirmed experimental evidence behind it for submicron particles. Experimental study of particle removal mechanism is the subject of the next chapter. So, balancing the changes in the particulate mass in the mean flow per time with the amount of deposited particles yields:

$$\dot{m}\frac{dY}{dx}=\pi D(\rho_g D_B\frac{\partial Y}{\partial r}+\rho_g YV_{th})\Big|_{r=D/2} \tag{4.12}$$

The particle Schmidt number is much greater than unity ($Sc_p >> 1$) for submicron particulates [21]. Therefore, the concentration boundary layer of submicron particles is significantly thinner than the hydraulic or thermal boundary layer thickness over the tube surface. So, it is a close estimation in the one dimensional model to use the centerline particulate mass fraction in order to calculate the deposition flux near the wall. The Brownian diffusivity in above equation is defined by [22]:

$$D_B=\frac{k_b C_c T}{3\pi\mu d_p} \tag{4.13}$$

where k_b is the Boltzmann constant and C_c is the correction factor that was defined before.

We start defining the thermophoretic term first. The thermophoretic drift velocity of a small particle is defined by:

$$V_{th} = -K_{th}\frac{\nu}{T}\vec{\nabla}T \tag{4.14}$$

To calculate the thermophoretic velocity, we estimated the temperature gradient in the radial direction at the gas-deposit interface as:

$$\vec{\nabla}T = \left.\frac{\partial T}{\partial r}\right|_{r=D/2} = \frac{h_c(T_{\text{int}} - T)}{k_d} = \frac{Nu(T_{\text{int}} - T)}{D} \tag{4.15}$$

where the difference between the gas and gas-deposit interface temperatures, Nusselt number (Nu) and tube diameter are taken into account to calculate the temperature gradient. Churcill [23] combined the correlations for laminar and turbulent Nusselt numbers and proposed a Nusselt number (employed in this model) for a wide range of Reynolds numbers in transition and turbulent flows:

$$Nu^{10} = Nu_l^{10} + [\frac{\exp((2200 - \text{Re})/365)}{(Nu_{lc})^2} + \frac{1}{Nu_t^2}]^{-5}$$
$$2300 < \text{Re} < 10^6,\ \ 0.6 < \text{Pr} < 10^5 \tag{4.16}$$

Developing laminar and turbulent Nusselt numbers for constant wall temperature tube flows are:

$$Nu_l = 3.657[1 + (\frac{\text{Re}\,\text{Pr}\,D/x}{7.6})^{8/3}]^{1/8} \tag{4.17}$$

$$Nu_t = 5.76 + \frac{0.079\,\text{Re}\sqrt{f/8}\,\text{Pr}}{[1 + \text{Pr}^{4/5}]^{5/6}} \tag{4.18}$$

$$Nu_{lc} = 3.657[1 + (\frac{276\,\text{Pr}\,D}{x})^{8/3}]^{1/8} \tag{4.19}$$

Nu_{lc} is the Nusselt number evaluated at critical Reynolds number of 2100. Reynolds number and Darcy friction factor [23] in the tube are:

$$\mathrm{Re} = \frac{uD}{\nu} \tag{4.20}$$

$$f = \frac{8}{\{\frac{1}{[(\frac{8}{\mathrm{Re}})^{10} + (\frac{\mathrm{Re}}{36500})^{20}]^{1/2}} + (2.21Ln(\frac{\mathrm{Re}}{7}))^{10}\}^{1/5}} \tag{4.21}$$

Tube effectiveness of the tube is defined as:

$$\varepsilon(\%) = \frac{T_0 - T_L}{T_0 - T_w} \times 100 \tag{4.22}$$

To calculate the particle mass fraction gradient in the radial direction, the Sherwood number (Sh) is employed:

$$\left.\frac{\partial Y}{\partial r}\right|_{r=D/2} = \frac{K(Y_{\mathrm{int}} - Y)}{D_B} = \frac{Sh(Y_{\mathrm{int}} - Y)}{D} = -\frac{Sh\,Y}{D} \tag{4.23}$$

Particle mass fraction at the wall of gas-deposit interface is zero and the empirical correlation of Berger and Hau [24] for the turbulent mass transfer in pipe flows is used to calculate the Sherwood number:

$$Sh = 0.0165\,\mathrm{Re}^{0.86}\,Sc_p^{1/3} \tag{4.24}$$

The Schmidt number of particles is defined as the ratio of gas kinematic viscosity to the particles Brownian diffusion coefficient. Having temperature and particle mass fraction gradients, we are able to find the total deposition due to thermophoresis and diffusion in this model.

Another important correlation in this study is particulate deposition efficiency:

$$\eta_d(\%) = \left(1 - \frac{Y_L}{Y_0}\right) \times 100 \tag{4.25}$$

We refer to this parameter in next sections. In correlations (4.22) and (4.25), the outlet temperature and particulate mass fraction are the results of solving the governing equations.

4.2.2 Boundary Conditions

There is a constant mass flow rate, temperature, pressure, and particle mass fraction at the inlet of the tube along with a constant tube wall temperature. Also, particle mass fraction at the gas-deposit interface is zero. We introduce the utilized boundary conditions as it follows:

Inlet

$$\dot{m}(x=0,t)=\dot{m}$$
$$T(x=0,t)=T_0$$
$$Y(x=0,t)=Y_0$$
$$P(x=0,t)=P_0$$

Wall

$$T\big|_{r=ID/2}=T_w$$

Gas-Deposit Interface

$$Y\big|_{r=D/2}=0$$

4.2.3 Solving Methodology

A second order backward differencing method (first order for the first node) is employed for the space in governing equations.

$$u_i^n=\frac{\dot{m}}{\rho_{g,i}^n A_i^n} \tag{4.26}$$

$$\frac{3P_i^n-4P_{i-1}^n+P_{i-2}^n}{2\Delta x}=-\frac{1}{2}\frac{f\,\rho_{g,i-1}^n(u_{i-1}^n)^2}{D_{i-1}^n}-\frac{\dot{m}}{A_i^n}\frac{3u_i^n-4u_{i-1}^n+u_{i-2}^n}{2\Delta x} \tag{4.27}$$

$$\frac{3c_{p,i}^{n}T_{i}^{n}-4c_{p,i-1}^{n}T_{i-1}^{n}+c_{p,i-2}^{n}T_{i-2}^{n}}{2\Delta x}=\frac{\left(T_{i-1}^{n}-T_{w}\right)}{\dot{m}(R_{Convection,i-1}^{n}+R_{conduction,i-1}^{n}+R_{metal,i-1}^{n})} \tag{4.28}$$

$$\frac{3Y_{i}^{n}-4Y_{i-1}^{n}+Y_{i-2}^{n}}{2\Delta x}=\frac{\pi D_{i-1}^{n}\rho_{g,i-1}^{n}D_{AB,i-1}^{n}}{\dot{m}}\left.\frac{\partial Y}{\partial r}\right|_{D,i-1}+\frac{\pi D_{i-1}^{n}\rho_{g,i-1}^{n}Y_{i-1}^{n}V_{th,i-1}^{n}}{\dot{m}} \tag{4.29}$$

The key point in this model is that the deposit layer decreases the effective diameter of the tube and changes the gas-deposit interface temperature and overall heat transfer rate. We take into account this diameter reduction in the consequent time step in order to solve the governing equations as ("n" represents the time step and "i" represents the segment number):

$$\Delta_{i}^{n}=\frac{1}{2}(D_{i}^{n}-\sqrt{(D_{i}^{n})^{2}-\frac{4Mass_{i}^{n}}{\pi\,\Delta x\,\rho_{d}}}) \tag{4.30}$$

$$Mass_{i}^{n}=(\rho_{g,i}^{n}Y_{i}^{n}V_{th,i}^{n}+\rho_{g,i}^{n}D_{B,i}^{n}Y_{i}^{n}Sh_{i}^{n}/D_{i}^{n})\pi\,D_{i}^{n}\Delta x\,\Delta t \tag{4.31}$$

$$D_{i}^{n+1}=D_{i}^{n}-2\Delta_{i}^{n} \tag{4.32}$$

A total number of 150 segments are selected in the one dimensional model. It shows an acceptable mesh independent result. With a 125 segments, the error in calculating the model outputs (mass gain and effectiveness drop) is less than 0.1% (compared to the outputs with 150 segments).

4.3 Axi-symmetric Model Description and Governing Equations

In this model, we employed the CFD software ANSYS-FLUENT (v.12.1, ANSYS, Inc.)to solve Navier-Stokes and the energy equations in an axi-symmetric tube. We defined two zones for the gas (Fluid) and the particulate deposit layer (Solid). The interface boundary splits the zones and it moves when the deposit layer grows. In

following sections, we will describe how the mesh dynamically moves. Figure 4.4 shows a schematic of the domain, zones, and the mesh.

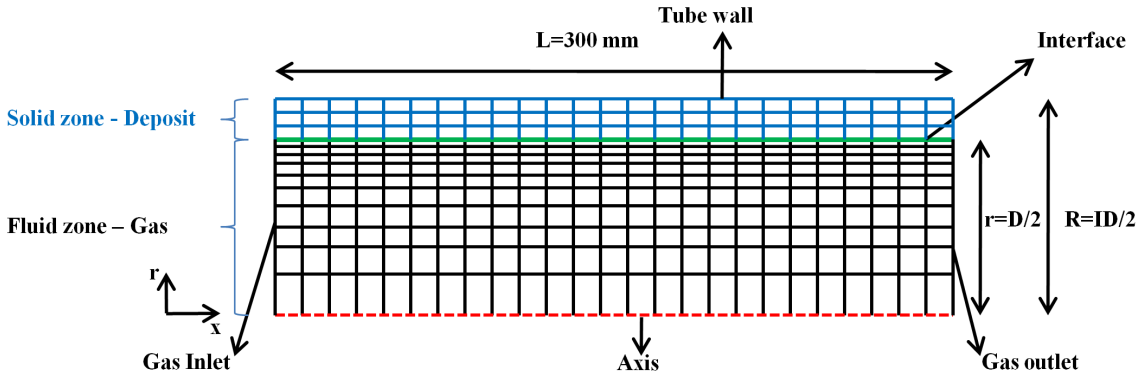

Figure 4.4 – A schematic of the mesh, zones, and boundary conditions in the axi-symmetric model developed in ANSYS-FLUENT

4.3.1 Governing Equations

The Reynolds-average Navier-Stokes (RANS) turbulence model is employed to solve the mean flow. For variable density flows, the averaging process leads to products of density and other variables. To include density variations, a density-weighted Favre averaging is usually used. In classical time averaging, instantaneous flow variables are decomposed into the mean and fluctuating components. As an example for a variable φ, we have $\varphi = \bar{\varphi} + \varphi'$. In Favre time averaging, the variable are decompose as (i.e. $\varphi = \tilde{\varphi} + \varphi''$) where $\tilde{\varphi} = \overline{\rho\varphi}/\bar{\rho}$. Substituting flow variables in Navier-Stokes equations and a Favre time average result in the averaged equations as:

$$\frac{\partial\left(\bar{\rho}_g\right)}{\partial t} + \nabla.\left(\bar{\rho}_g \tilde{\mathbf{v}}\right) = 0 \tag{4.33}$$

$$\frac{\partial\left(\bar{\rho}_g \tilde{\mathbf{v}}\right)}{\partial t} + \nabla.\left(\bar{\rho}_g \tilde{\mathbf{v}}\tilde{\mathbf{v}}\right) = -\nabla \bar{P} + \nabla.\left(\bar{\tau}\right) + \nabla.\left(-\bar{\rho}_g \widetilde{\mathbf{v}''\mathbf{v}''}\right) \tag{4.34}$$

Reynolds stresses $-\overline{\rho}_{\mathrm{g}}\widetilde{\mathbf{v}''\mathbf{v}''}$ representing turbulence are modeled by the Reynolds Stress model (RSM).

The Favre time averaged energy equation can also be written as:

$$\frac{\partial\left(\overline{\rho}_{g}\mathrm{c}_{\mathrm{p}}\widetilde{\mathrm{T}}\right)}{\partial \mathrm{t}}+\nabla.\left(\overline{\rho}_{g}\mathrm{c}_{\mathrm{p}}\widetilde{\mathbf{v}}\widetilde{\mathrm{T}}\right)=\nabla.\left(\mathrm{c}_{\mathrm{p}}\frac{\mu}{\mathrm{pr}}\nabla\widetilde{\mathrm{T}}\right)+\frac{\partial\overline{\mathrm{P}}}{\partial \mathrm{t}}+\nabla.\left(-\overline{\mathbf{v}\boldsymbol{\tau}}\right)+\nabla.\left(-\overline{\rho}_{g}\widetilde{\mathbf{v}''\mathrm{T}''}\right) \qquad (4.35)$$

If particle transport is due to convection, Brownian diffusion, turbulence, and thermophoresis, we can write the particle transport equation as:

$$\frac{\partial\left(\overline{\rho}_{g}\widetilde{\mathrm{Y}}\right)}{\partial \mathrm{t}}+\nabla.\left(\overline{\rho}_{g}\left(\widetilde{\mathbf{v}}+\widetilde{\boldsymbol{V}}_{th}\right)\widetilde{\mathrm{Y}}\right)=\nabla.\left(\overline{\rho}_{g}\mathrm{D}_{\boldsymbol{B}}\nabla\widetilde{\mathrm{Y}}\right)+\nabla.\left(-\overline{\rho}_{g}\left(\widetilde{\mathbf{v}''\mathrm{Y}''}+\widetilde{\mathbf{V}''_{\mathbf{th}}\mathrm{Y}''}\right)\right) \qquad (4.36)$$

Thermophoretic term is included in the advective term on the left hand side of the equation. The second term $\nabla.\left(-\overline{\rho}_{g}\widetilde{\mathbf{v}''\mathrm{Y}''}\right)$ in particle mass fraction equation representing variable fluctuations can be modeled as $\overline{\rho}_{g}\mathrm{D}_{\boldsymbol{T}}\nabla\widetilde{\mathrm{Y}}$. Turbulent diffusivity (D_T) is the mean effect of velocity and particle mass fraction fluctuations in turbulent flows. Turbulent diffusivity is estimated by the turbulence kinematic viscosity (ν_T) in this study. In such a case, the turbulent Schmidt number is one. Turbulent viscosity is a function of turbulence dissipation rate and turbulence kinetic energy. The last term $\nabla.\left(-\overline{\rho}_{g}\widetilde{\mathbf{V}''_{\mathbf{th}}\mathrm{Y}''}\right)=\nabla.\left(-\overline{\rho}_{g}\mathrm{k}_{\mathrm{th}}\nu\widetilde{\nabla\ln\left(\mathrm{T}''\right)\mathrm{Y}''}\right)$ is neglected compared to the other terms.

4.3.2 Boundary Conditions

Boundary conditions for governing equations in two phases are listed as:

Gas phase inlet:

$\dot{m}\left(x=0,\ 0\le r\le D/2\ ,t\right)=\dot{m}$

$P\left(x=0,\ 0\le r\le D/2\ ,t\right)=P_0$

$T\left(x=0,\ 0\le r\le D/2\ ,t\right)=T_0$

$Y(x=0,\ 0\le r\le D/2\ ,t)=Y_0$

Gas phase outlet:

$$\frac{\partial u}{\partial x}\left(x = L,\ 0 \le r \le D/2\ ,t \right) = 0$$

$$\frac{\partial T}{\partial x}\left(x = L,\ 0 \le r \le D/2\ ,t \right) = 0$$

$$\frac{\partial Y}{\partial x}\left(x = L,\ 0 \le r \le D/2\ ,t \right) = 0$$

Gas-deposit interface:

$$u\left(0 \le x \le L,\ r = D/2\ ,t\right) = 0 \quad (no\ slip)$$

$$-k_g \frac{\partial T_g}{\partial r}\left(0 \le x \le L,\ r = D/2\ ,t \right) = -k_d \frac{\partial T_d}{\partial r}\left(0 \le x \le L,\ r = D/2\ ,t \right)$$

$$Y\left(0 \le x \le L,\ r = D/2\ ,t\right) = 0$$

Deposit layer:

$$T\left(x = 0,\ D/2 \le r \le ID/2\ ,t\right) = T_0$$

$$T\left(x = L,\ D/2 \le r \le ID/2\ ,t\right) = T_w$$

Coolant wall:

$$T\left(0 \le x \le L,\ r = ID/2\ ,t\right) = T_w$$

We wrote a C user defined subroutine in ANSYS-Fluent to define the new advective term $\left(\overline{\rho}_g\left(\tilde{\mathbf{v}} + \widetilde{V}_{th}\right)\widetilde{\mathrm{Y}}\right)$ and solve a new user defined scalar (UDS) as the particle mass fraction (Y). The deposition flux in both laminar and turbulent flows near the wall can be calculated as (just radial component is taken into account):

$$J = \overline{\rho}_g D_B \left.\frac{\partial \overline{Y}}{\partial r}\right|_{r=D/2} \tag{4.37}$$

Deposition occurs in a very thin layer near the wall and turbulent diffusivity does not play any role in deposition because turbulent properties are zero there (gas-deposit interface).

It should be noted that the correlation between particle concentration and particle mass fraction is defined by:

$$Y = \frac{C}{\rho_g} \tag{4.38}$$

4.3.3 Solving Methodology

We used a second order upwinding method to discretize the equations spatially. The calculations were carried out using a dynamic grid. Equations (4.33) to (4.36) for the exhaust and the deposit layer were solved using the commercial software Ansys-Fluent 12. The momentum and energy equations are discretized with a second-order upwind method, and the SIMPLE algorithm [25] was used for the pressure correction. The resulting algebraic equations were solved using an iterative-segregated method to reduce the memory allocation.

We also activated the enhanced wall treatments to match the initial effectiveness of tubes with experimental data that will be discussed. The enhanced wall treatment is designed to extend the validity of near-wall modeling beyond the viscous sub-layer. This method is employed in general to resolve the laminar sub-layer. There is a requirement to have at least 10 cells within the viscosity-affected near-wall region to be able to resolve the mean velocity and turbulent quantities in that region. More details are explained in the software user manual. Turbulent intensity is the ratio of the root mean square of the velocity (u'_{rms}) fluctuations to the mean flow velocity. We chose the inlet boundary condition for the turbulence model to be a turbulent intensity of 10%. This number is used in CFD simulations [26] of turbulence in after-treatment systems (diesel particulate filters and diesel oxidation catalyst) that are close to our work.

4.3.4 Dynamic Mesh in the Axi-Symmetric Model

A collection of C subroutines are written to dynamically move the gas-deposit interface and reconstruct the mesh when the deposit layer grows. The technique was

previously used in a numerical study on fabrication of fiber-optics [27]. To initiate the solution and solve the steady state equations for a two zone model, we considered a layer of 10 microns for the deposit layer before deposition starts in a clean tube. This is because 10 micron was the minimum distance recognized as a line by the mesh generator software. We did not include this initial layer in the final deposit mass gain results but it causes a very small error (less than 2%) in predicting the initial effectiveness of a clean tube in the steady state solution. Figure 4.4 shows a schematic of the mesh constructed in ANSYS-Gambit (version 2.4.6, ANSYS, Inc.).

A total number of 140 nodes in the radial direction for the fluid zone (with a successive ratio of 0.95) and 11 nodes in the radial direction for the solid zone are used along with a total number of 601 nodes in the axial direction to generate the initial mesh. Above numbers showed an acceptable mesh independency without causing numerical instabilities in calculating gradients near the gas-deposit interface. Then, the new mesh is constructed with the same number of nodes in axial and radial directions. A quasi-steady variation of the interface is assumed for the mesh motion. The distance between nodes in axial direction always remains constant. In both zones, the ratio of the radial coordinate of nodes to the effective diameter is always kept constant while reconstructing the mesh at each time step. A schematic of how the mesh moves in radial direction is shown in Figure 4.5 at two consequent time steps. The wall and axis boundaries stay stationary while the interface moves.

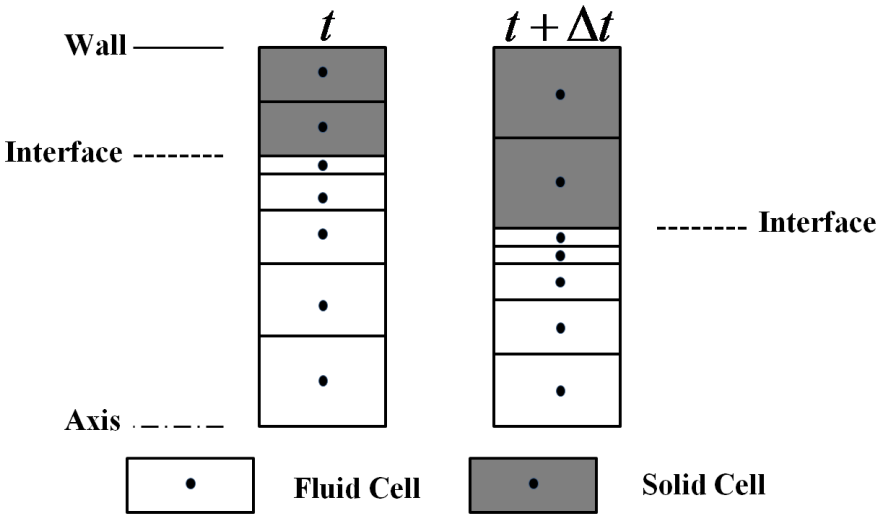

Figure 4.5 – A schematic of the mesh reconstruction when the deposit layer grows

4.3.5 Validation of the Steady State Axi-Symmetric Model

To validate our steady state models with current literature, we compared our results with the results presented in [28]. In their work, they proposed a theoretical correlation for particle deposition in laminar and turbulent flows and conducted experiments and performed several experiments for a various range of particle diameters. We took their data for 100 nm NaCl particles for validation. Figure 4.6 is a comparison between their experiments (figure 8 in their work) and our proposed one dimensional and axi-symmetric models for a flow rate of 20 L/min and a wall temperature of 293 K. The tube length in their tests was 0.965 m with a diameter of 4.9 mm.

Figure 4.7 depicts the same comparison for particle deposition efficiency for a different gas flow rate of 35 L/min and a wall temperature of 293 K. We see a satisfactory agreement between our models and Romay et. al. experiments.

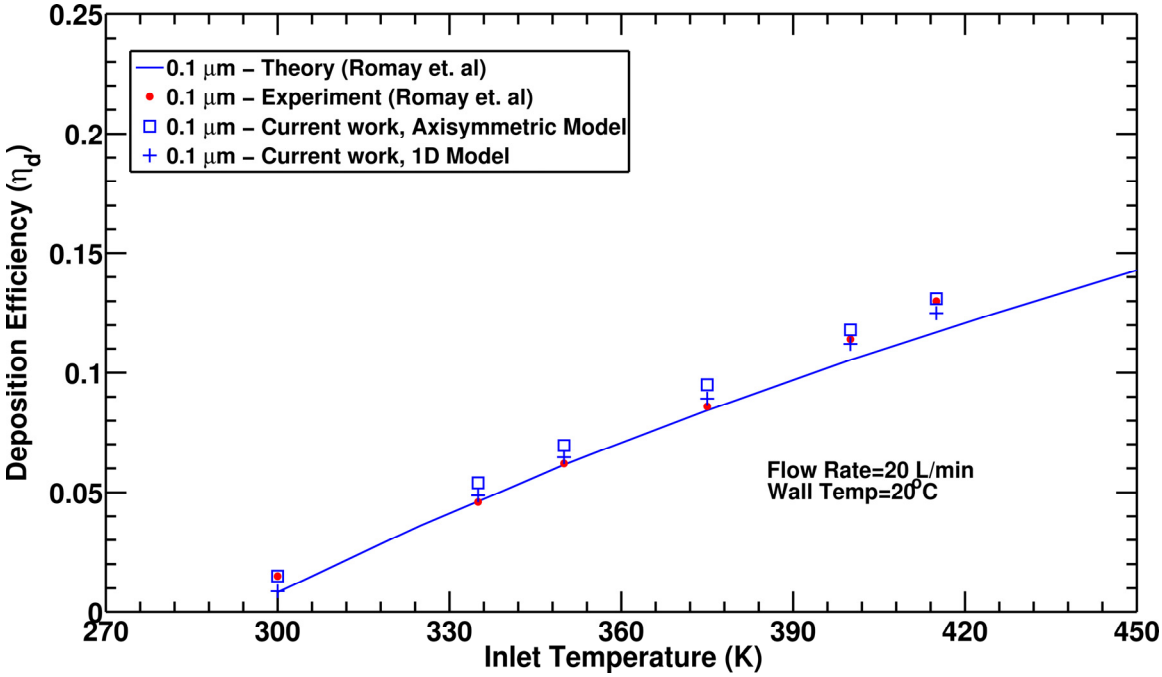

Figure 4.6 – Comparison of deposition efficiency between our models and Romay et. al.[28] $Q = 20\,L/\min, T_w = 293\,K, P_0 = 101\,kPa, ID = 4.9\,mm, L = 0.965\,m$

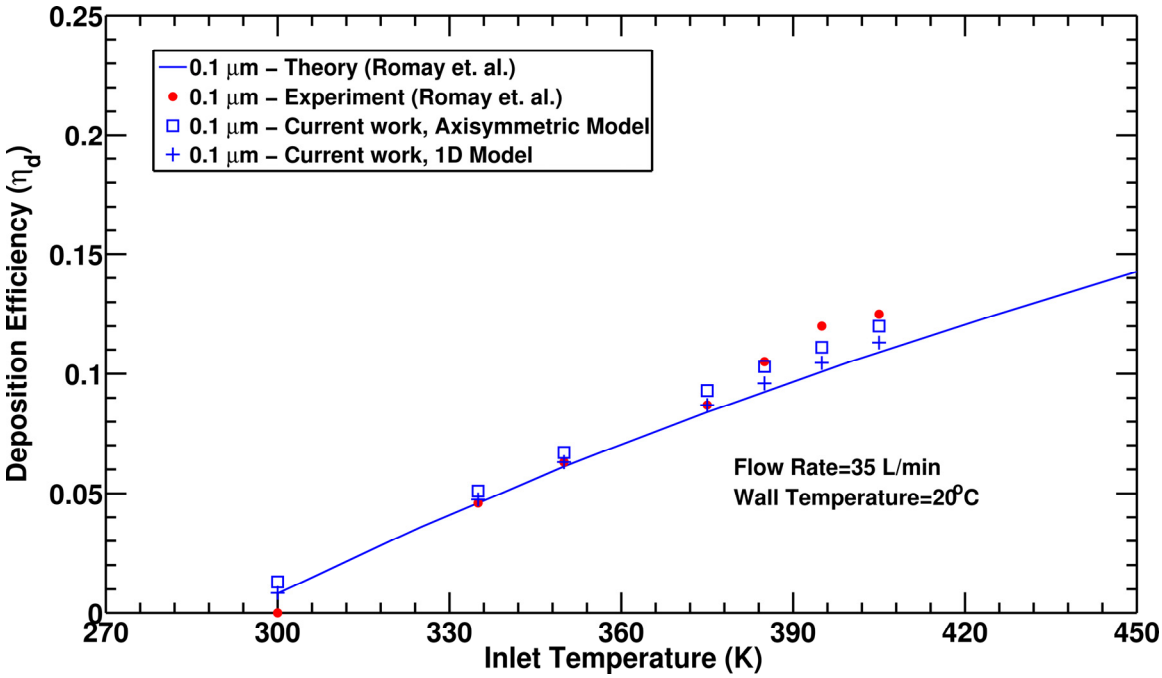

Figure 4.7 – Comparison of deposition efficiency between our models and Romay et. al. [28] $Q = 35\,L/\min, T_w = 293\,K, P_0 = 101\,kPa, ID = 4.9\,mm, L = 0.965\,m$

It is claimed that thermophoresis is the dominant deposition mechanism for submicron particles compared to other deposition mechanism including diffusion. To verify this in our model, we compared the particle mass fraction where thermophoresis exists (new advective term) and when it is not present in the model. Figure 4.8 demonstrates the two profiles at the half length (x=L/2) of a tube (geometry in Figure 4.1) where the boundary conditions are:

$\dot{m} = 9\times10^{-4}\ kg/s$, $T_0 = 653K$, $T_w = 363K$, $P_0 = 196\,Kpa$, $Y_0 = 28.9\times10^{-6}$.

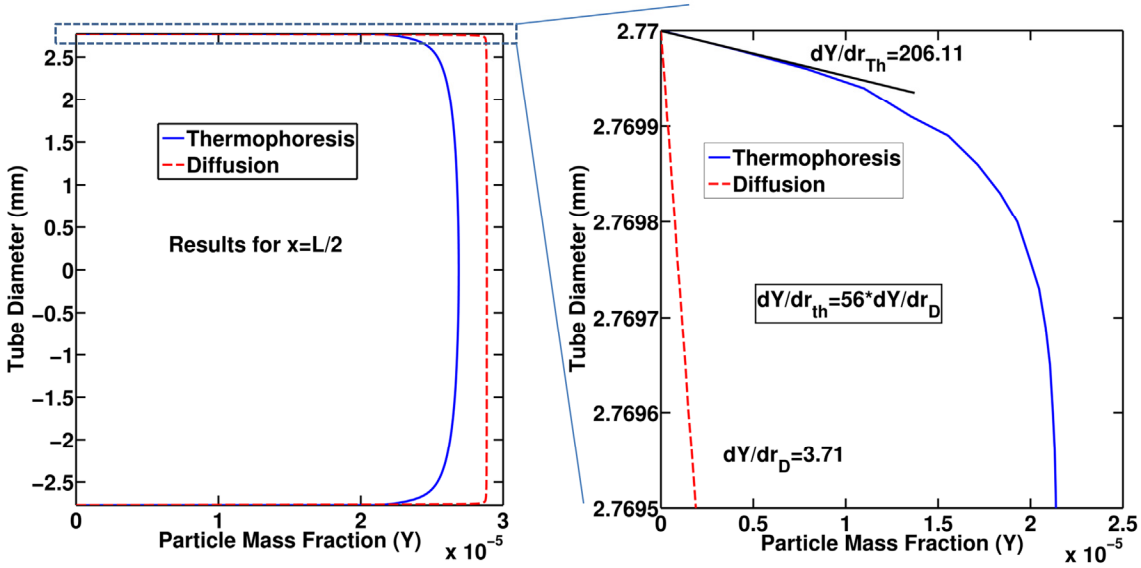

Figure 4.8 – Left: Comparison of particle mass fraction gradient in presence and absence of thermophoresis at x=L/2 at the given set of boundary condition, right: the magnified version of the left figure at 500 nm from the wall

$\dot{m} = 9\times10^{-4}\ kg/s, T_0 = 653\,K, T_w = 363\,K, P_0 = 196\,kPa, Y_0 = 28.9\times10^{-6}$

When thermophoresis is not included in the model, the centerline mass fraction is very close to the inlet mass fraction ($Y_0 = 28.9\times10^{-6}$) since deposition efficiency is nearly zero (less than 1%). When thermophoresis is present, the centerline mass fraction (also averaged mass fraction) drops due to deposition upstream. In the zoomed graph (right side of Figure 4.8), it is demonstrated that the particle mass fraction gradient is 56 times larger when thermophoresis is introduced to the model through user defined

functions (UDFs). It implies that thermophoresis enhances the particle mass fraction gradients (deposition flux) by carrying them very close to the wall. The same comparison for the one dimensional model (at the same boundary conditions and axial location (x=L/2)) resulted in:

$$\frac{J_{th}}{J_D} = \left. \frac{\rho_g Y V_{th}}{\rho_g D_B \left. \frac{\partial Y}{\partial r} \right|_{r=\frac{D}{2}}} \right|_{x=\frac{L}{2}} = 36.0 \tag{4.39}$$

After validation of our model for steady state cases, we proceeded with the transient tests that were performed in Oak Ridge National Laboratory. Then, we activated the dynamic mesh subroutines to address the deposit layer growth and its effect on heat transfer drop of the surrogate tubes in our models.

4.4 Oak Ridge National Laboratory Experiments

To verify the models, the Oak Ridge National Laboratory tests are selected as it was discussed thoroughly in chapter 2. Tests were done in a controlled engine test set up. Details of the test set up and measurement procedures are fully described before. The exhaust gas was divided to a few tubes and different designed boundary conditions selected to specify the range of practical conditions for diesel EGR coolers (Table 4.1). In all performed experiments, the gas inlet absolute pressure was kept at 196 KPa. Experiments ran at normal engine coolant temperature (90°C). At this temperature, there is no water condensation in the tube.

Table 4.1 – Boundary conditions

Experiment NO.	Coolant temperature (°C)	Flow rate (kg/sec)	Inlet particles concentration (mg/m3)	Inlet particles mass fraction	Inlet gas temperature (°C)
1	90	4.5×10^{-4}	7.5	5.5×10^{-6}	220
2	90	4.5×10^{-4}	7.5	7.2×10^{-6}	380
3	90	4.5×10^{-4}	30	21.8×10^{-6}	220
4	90	4.5×10^{-4}	30	28.9×10^{-6}	380
5	90	9×10^{-4}	7.5	5.5×10^{-6}	220
6	90	9×10^{-4}	7.5	7.2×10^{-6}	380
7	90	9×10^{-4}	30	21.8×10^{-6}	220
8	90	9×10^{-4}	30	28.9×10^{-6}	380

There is also another long exposure time experiment that will be presented in later sections.

4.5 Exhaust Gas and Deposit Layer Properties

A detail explanation on calculating the exhaust gas properties is given in chapter 3 and is repeated here. The correlations are listed as:

$$R_g = \frac{R}{MW_g},\ MW_g = 28.89\ \frac{g}{mol} \tag{4.40}$$

$$\rho_g = \frac{P}{R_g T} \tag{4.41}$$

$$\mu = 3.07\times10^{-7} T^{0.7126} \tag{4.42}$$

$$C_p = 0.2168T\ + 960.49 \tag{4.43}$$

$$k_g = 5.43\times10^{-5}T + 0.01084 \tag{4.44}$$

The porosity of deposits layer is measured by Oak Ridge National Lab researchers and determined to be 98%. It shows that the layer is a high porous media. In the first look at the literature for turbulent boundary layer over permeable or rough surfaces ([29]-[35]), we notice that "no slip condition" is not valid anymore at the interface. But it is claimed that for Darcy numbers of less than 10^{-5}, the flow in the porous medium is very weak and can be neglected without considerable loss of accuracy [36]. This conclusion is made for a laminar flow inside a circular duct partially filled with a porous material. Overall, no slip condition is considered at the gas-deposit interface in this study as an assumption.

The thermal conductivity of the deposit layer (solid zone in axi-symmetric model) as a highly porous medium consisting of a solid (graphite) and a fluid phase (trapped gas) is calculated here. Thermal conductivity of each phase of the layer is calculated at the local cell temperature in the axi-symmetric model and at the averaged temperature of the interface and tube wall in the one dimensional model. The correlation for thermal conductivity of the gas phase comes from (4.44). So, we calculated the thermal conductivity of the deposit layer as [37]:

$$k_d = (1-\phi)^{1.5} k_{Graphite} + \phi^{0.25} k_{EGR}\big|_T \tag{4.45}$$

$$k_{Graphite} = 13.0839 - 0.03495\times T + 3.82\times10^{-5}T^2 - 1.48\times10^{-8}T^3 \tag{4.46}$$

Figure 4.9 shows the deposit layer thermal conductivity as a function of temperature and the layer porosity. Calculations for 98% porosity line up with Oak Ridge National Lab (ORNL) measurements of the deposit thermal conductivity at room temperature (0.041 W/mK) [38]. The deposit layer density is 35.4 kg/m^3 [38].

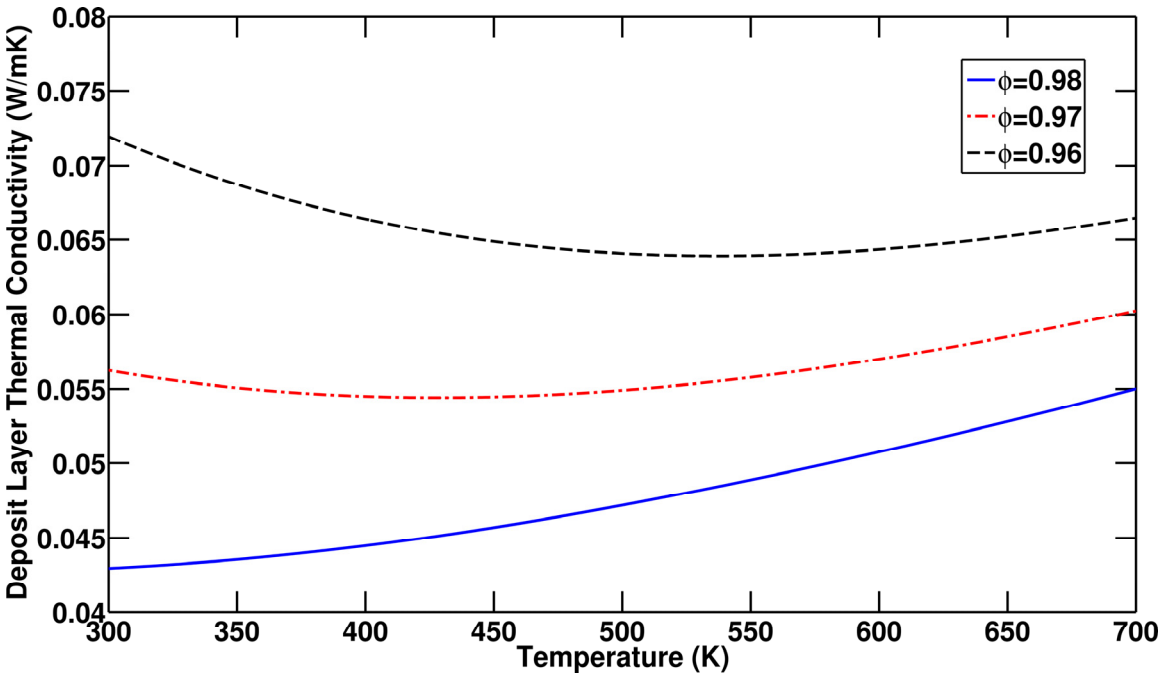

Figure 4.9 – Deposit thermal conductivity as a function of temperature and layer porosity

4.6 Results and Discussion

In chapter 3, we described in detail how different boundary conditions can affect the particle deposited mass and the overall heat transfer reduction in a tube flow. Here, we discuss the results of the developed models and compare them with experimental measurements at different selected conditions. We made a comparison for the effectiveness drop of the tube flow at the given boundary condition (Experiment No. 4 in Table 4.1) in Figure 4.10. Each experiment ran twice to improve statistical confidence. The effectiveness of the cooler degrades as a result of the deposit formation. It is seen that models predict the initial effectiveness (better prediction by axi-symmetric model) and the effectiveness drop of the tube quite well.

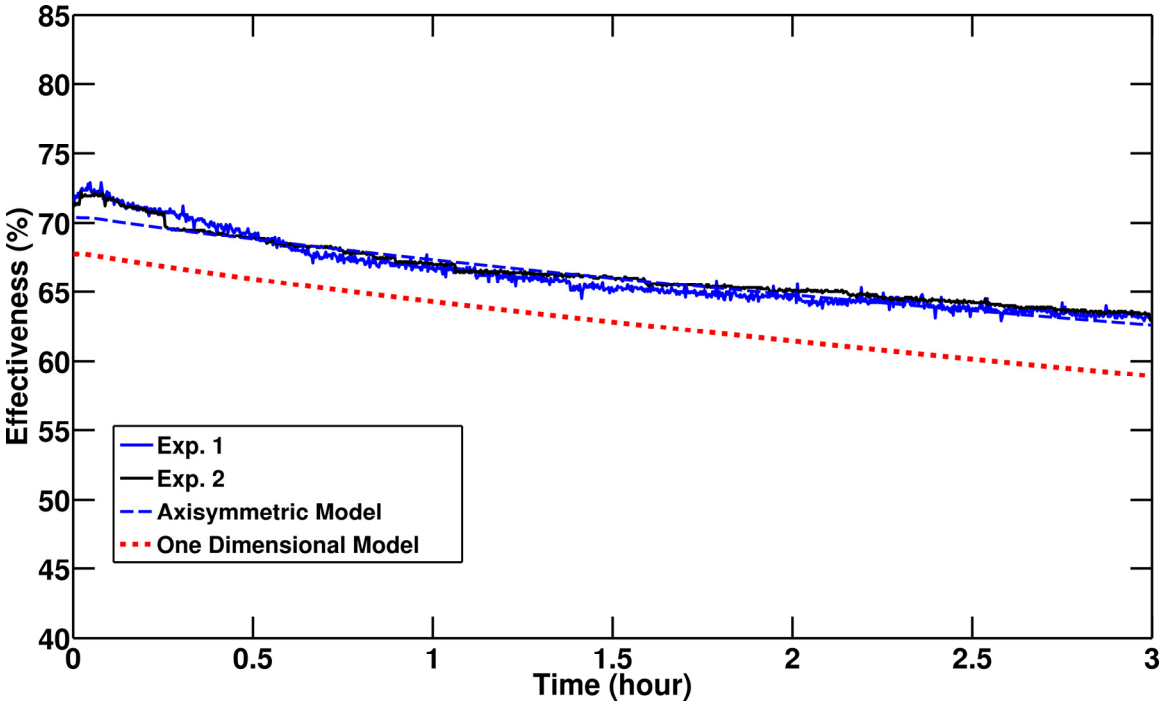

Figure 4.10 – Comparison of effectiveness vs. time (Experiment No. 4 in Table 4.1) - $\dot{m} = 4.5 \times 10^{-4}\ kg/s, T_0 = 653\ K, T_w = 363\ K, P_0 = 196\ kPa, Y_0 = 28.9 \times 10^{-6}$

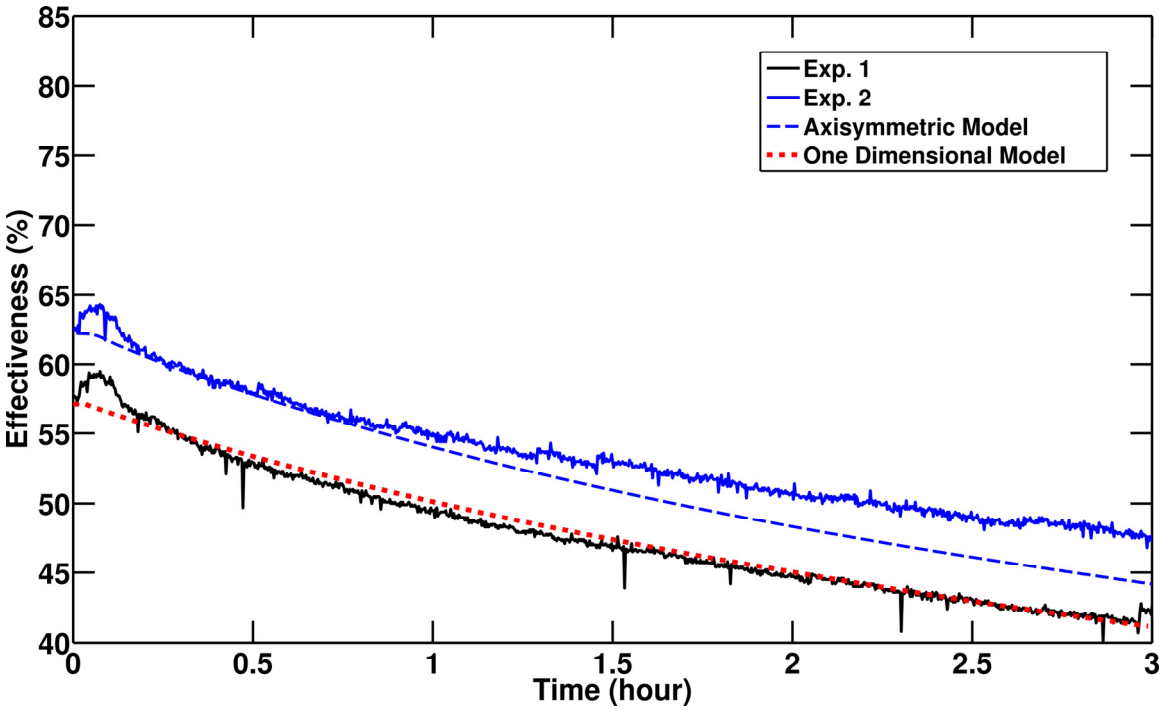

Figure 4.11 – Comparison of effectiveness vs. time (Experiment No. 8 in Table 4.1) - $\dot{m} = 9 \times 10^{-4}\ kg/s, T_0 = 653\ K, T_w = 363\ K, P_0 = 196\ kPa, Y_0 = 28.9 \times 10^{-6}$

Figure 4.11 shows the same comparison for Experiment No. 8. The initial effectiveness for this experiment is lower compared to experiment No. 4 because the flow rate is larger and there is a smaller residence time for gas molecules in the tube to transfer heat. In the first 5 minutes of the experiments, the effectiveness curve shows an increasing pattern because the fixture was not completely warmed up. The discrepancy between the experiments in Figure 4.11 comes from experimental sources of error including the location of thermocouples in the gas flow, or error in the mass flow rate measurement.

Figure 4.12 shows the soot particle mass gain predicted by the models versus mass gain measured experimentally for all eight experiments in Table 4.1. If the model predicted the mass gain exactly as the experimental results, the ideal regression line would have been achieved. It is seen that in most cases, the axi-symmetric model delivers a closer prediction of mass gain and its predicted results are within the experimental error bars.

The better prediction of mass gain by the axi-symmetric model arises from the calculation of the deposition flux in each model. In the one dimensional model, the thermophoretic flux in (4.12) is computed from the centerline particle mass fraction ($\rho_g Y V_{th}$); however, particle mass fraction near the wall is zero. Also, thermophoretic velocity is calculated from empirical correlations for Nusselt number. In the axi-symmetric model, the total deposition flux (diffusion and thermophoretic) in (4.37) is calculated accurately by computing the near wall particle mass fraction. This is the reason for a better prediction of deposited mass gain by the axi-symmetric model.

Overall, the axi-symmetric model shows a 52% improvement in predicting the deposited mass gain compared to the proposed analytical solution (discussed in chapter 3) and a 14% improvement compared to the one dimensional model.

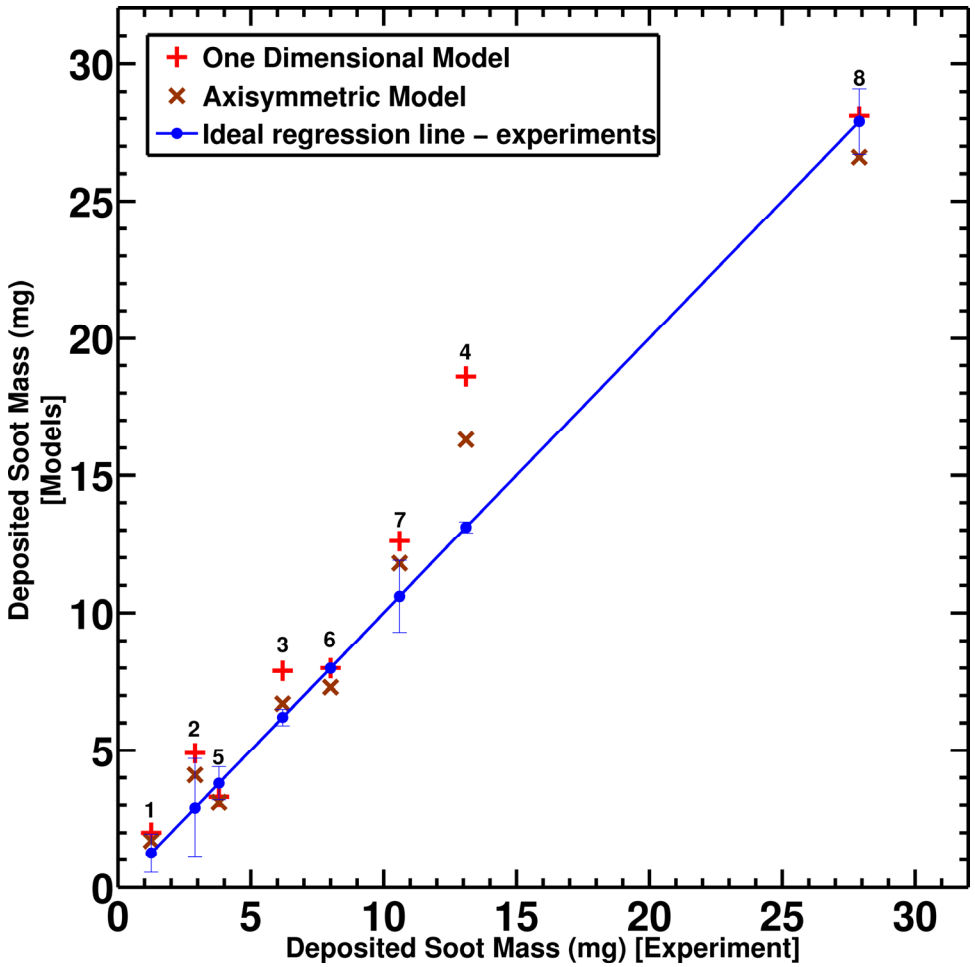

Figure 4.12 – Deposited soot mass gain – models vs. experimental measurements. Numbers on the data points indicate experimental conditions from Table 4.1

Figure 4.13 demonstrates a similar comparison for the effectiveness drop. The average value of two sets of experiment at the end of 3 hours exposure is used for each case to show the experimental results in Figure 4.12 and Figure 4.13. Hence, the error bars in these graphs are calculated based on the deviation of each test from the average value. Overall, the axi-symmetric model gives a better estimation of the heat transfer reduction in tubes compared to the one dimensional model (3%). Comparing the two models, we notice that the results of the axi-symmetric model in four cases (mostly high flow rate flows experiments 6-8 and experiment 4) are within the error bar range of experiments while in only two cases the one dimensional model prediction is within the

range of experimental data. Overall, the axi-symmetric model prediction is closer to experiments especially for the experiments with high gas mass flow rates.

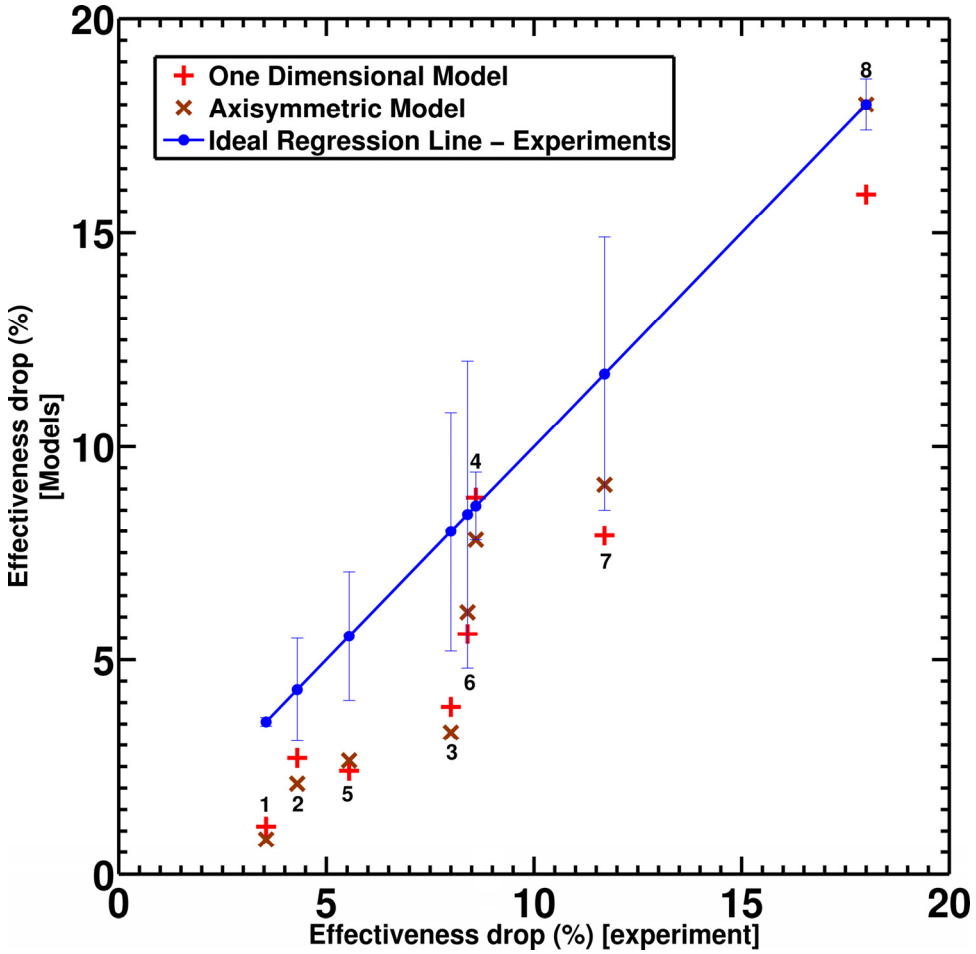

Figure 4.13 – Effectiveness drop – models vs. experimental measurements. Numbers on the data points indicate experimental conditions from Table 4.1.

The above experiments ran for a relatively short exposure time (3 hours). Experimental measurements for a longer period of time will help to improve the understanding of layer property variation or possible removal mechanisms of the deposited layer. Figure 4.14 shows the effectiveness comparison for a longer time exposure of 12 hours (Experiment No. 8 in Table 4.1). It is seen that the effectiveness is predicted well by models but experiment shows a sharper slope change over time compared to the models prediction. There can be following reasons for this small

discrepancy in the slope. The deposited layer properties including thermal conductivity and density are important parameters affecting the results significantly. Our correlation is based on what is in literature. In-situ measurements of deposit thermal conductivity and density will help to investigate how the layer properties vary when it builds up. Also, experimental evidences and microscope images show a higher layer density in the bottom than in the top of the deposited layer (as discussed in chapter 2) [39]. More experimental measurements are required to clear these ambiguities although current prediction is quite good. We describe in the next chapter how we approached to study the deposit stabilization mechanism(s) for long exposures through a visualization test rig that we designed and built at the University of Michigan.

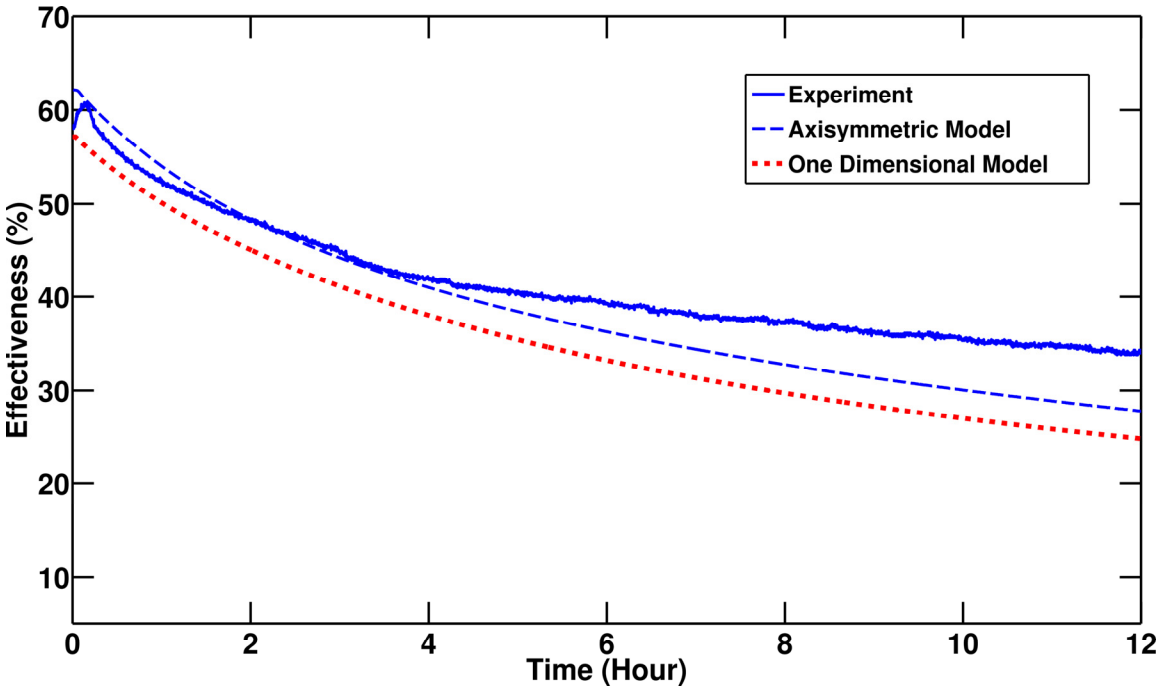

Figure 4.14 – Comparison of effectiveness vs. time (long exposure experiment) - $\dot{m} = 9 \times 10^{-4}\ kg/s, T_0 = 653\ K, T_w = 363\ K, P_0 = 196\ kPa, Y_0 = 28.9 \times 10^{-6}$

Figure 4.15 shows the particulate deposition efficiency predicted by the two models. There is a significant reduction in deposition efficiency when the deposit layer forms.

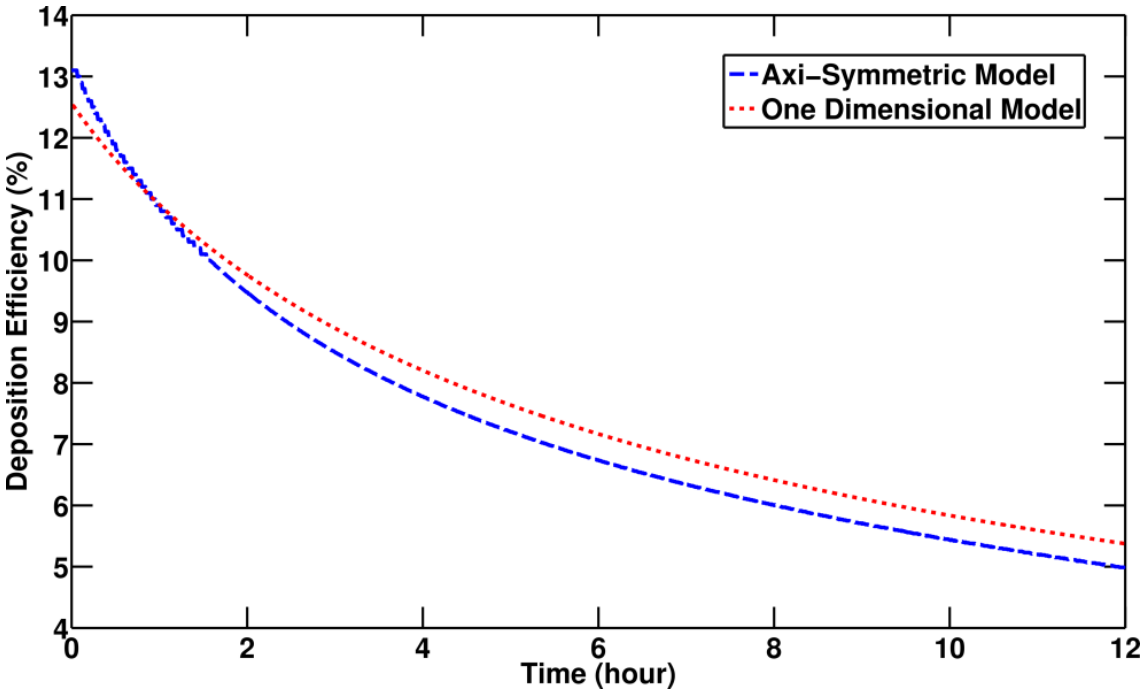

Figure 4.15 – Particulate deposition efficiency vs. time (long exposure experiment) - $\dot{m} = 9 \times 10^{-4}\ kg/s, T_0 = 653\ K, T_w = 363\ K, P_0 = 196\ kPa, Y_0 = 28.9 \times 10^{-6}$

Figure 4.16 depicts the comparison between the deposited soot mass gain in long exposure experiment over time. The axi-symmetric model shows a significantly better prediction in this graph for longer exposures (8 and 12 hours). There is a 4% error in the axi-symmetric prediction after 12 hours exposure when the error of the 1D model is 17%.

Figure 4.17 also shows the deposit thickness comparison predicted by models. As expected from Figure 4.16, the one dimensional model predicts a thicker deposit layer at the end of 12 hours especially at the inlet but the axi-symmetric model shows a lower thickness with a more uniform axial distribution that is closer to ORNL microscope images in general.

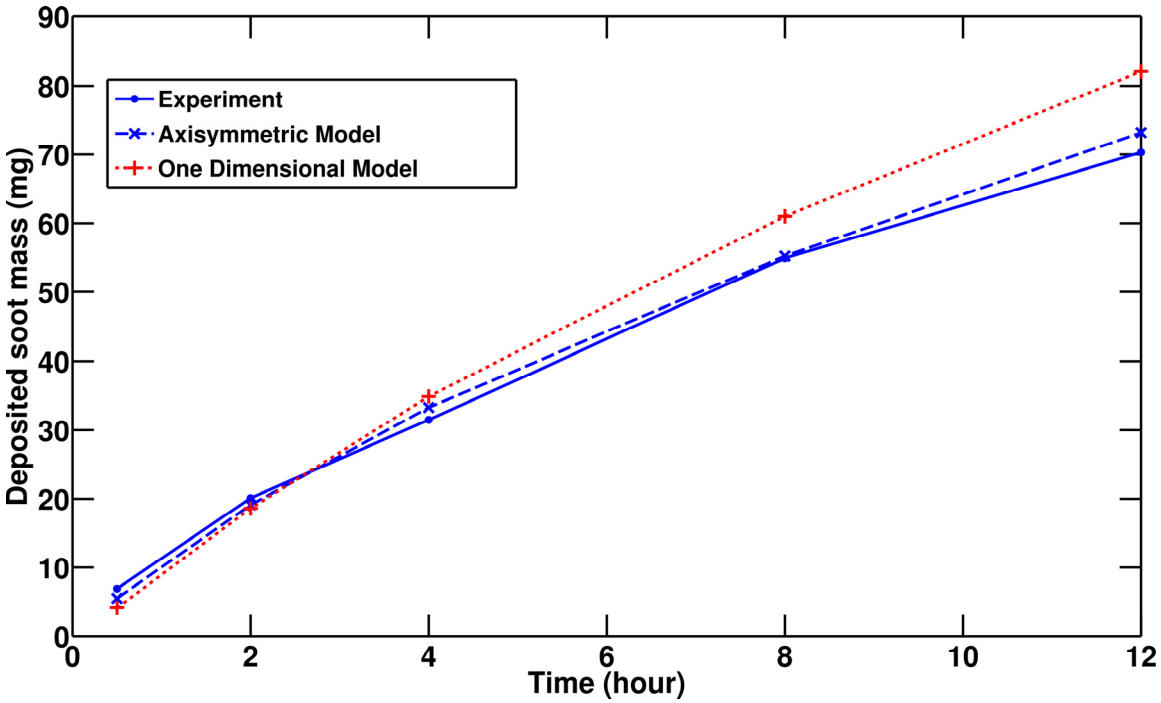

Figure 4.16 – Comparison of deposited soot mass vs. time (long exposure experiment) - $\dot{m} = 9 \times 10^{-4}\ kg/s, T_0 = 653\ K, T_w = 363\ K, P_0 = 196\ kPa, Y_0 = 28.9 \times 10^{-6}$

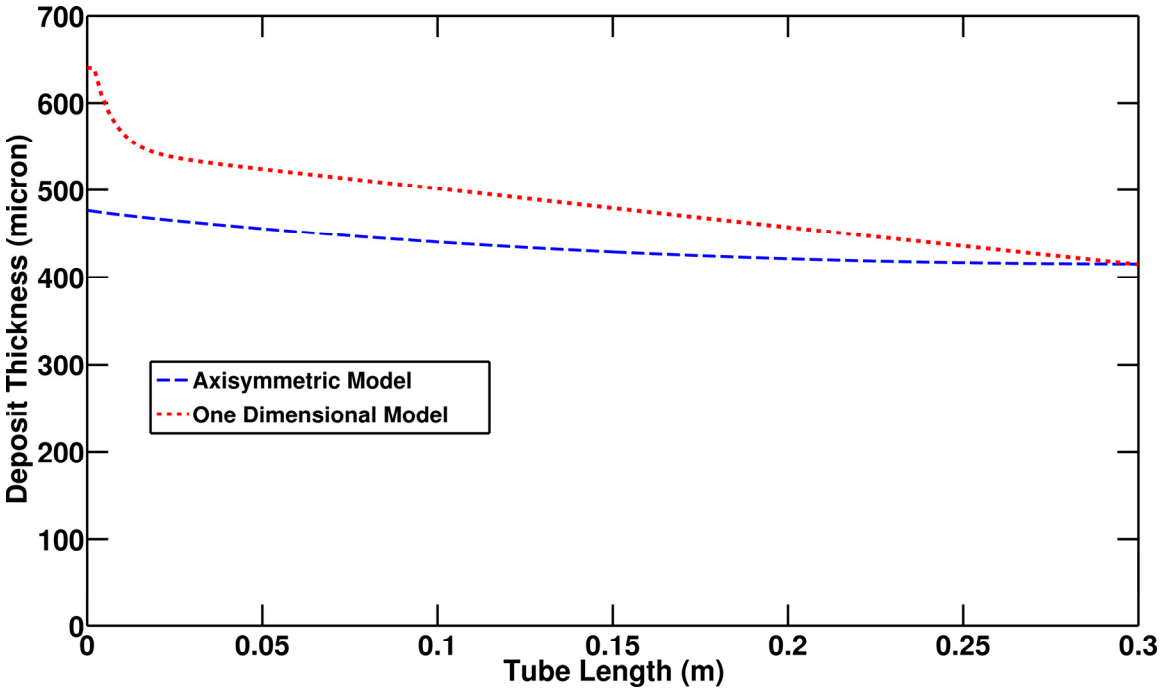

Figure 4.17 – Comparison of deposited soot thickness vs. tube length (long exposure experiment) - $\dot{m} = 9 \times 10^{-4}\ kg/s, T_0 = 653\ K, T_w = 363\ K, P_0 = 196\ kPa, Y_0 = 28.9 \times 10^{-6}$

We do not have the experimental data to support the predicted thickness for the experimental condition in Figure 4.16 but it is worth looking at the available measurement (courtesy of Michael Lance at ORNL) that were conducted for a square tube, 1/4" across. Shown data in Figure 4.18 summarizes the average data for the deposit thickness in the entire length of tubes at various tests where exposure time, HC level, and fuel type were varied. The error bars in this figure represent the minimum and maximum values for the four tube samples in each experiment.

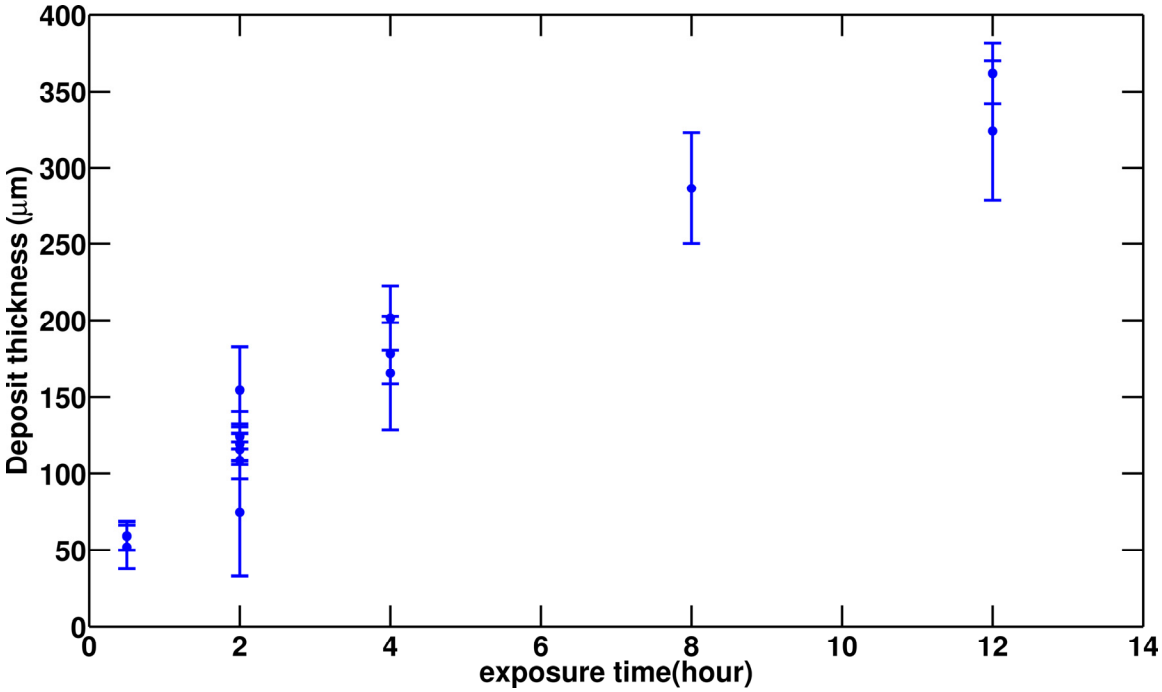

Figure 4.18 – Average deposit layer thickness in entire tube length for various exposure times (courtesy of Michael Lance, ORNL)

Figure 4.19 shows the deviation from the tube average value for deposit thickness (closed circles) and mass (open circles) for 17 model cooler tubes (0: is the inlet). The thickness was measured at six cross-sections along the length of the tube and the mass was measured along 4 1-inch sections of tube. In y axis, 1 is a reference point that corresponds to the average value for the thickness (mass) in entire length of the tube at various experiments (boundary conditions). Then, for each point (for thickness) and

segment (for mass) along the length, the deviation from this average value is calculated. Thereafter, an average value of the deviations is calculated and presented in Figure 4.19. The results in this graph show that there is not a significant deviation from the average from the inlet to the outlet.

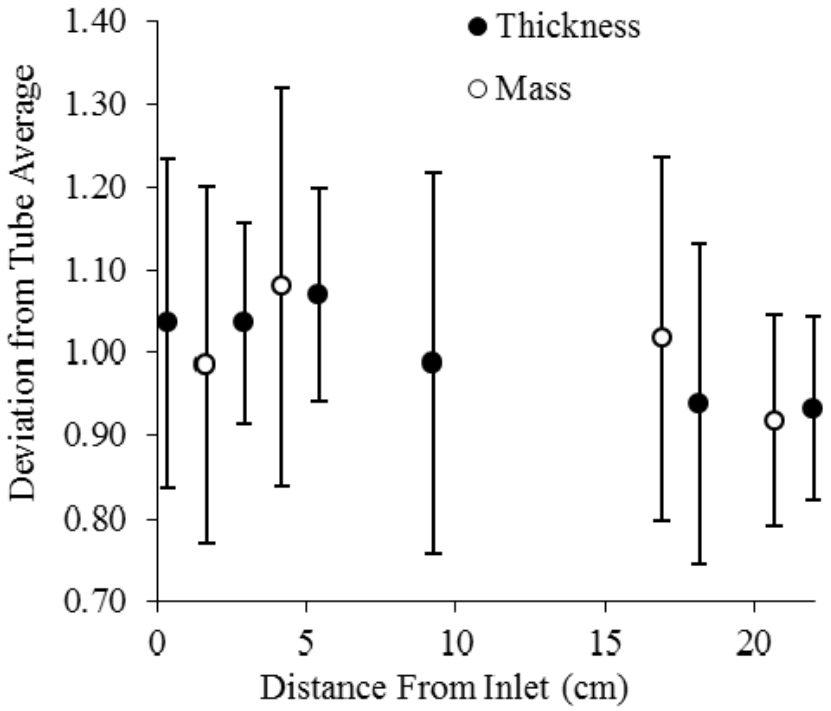

Figure 4.19 – The deviation from the tube average value for deposit thickness (closed circles) and mass (open circles) for 17 model cooler tubes (courtesy of Michael Lance, ORNL)

Although our modeling study was performed for tube flows, in reality EGR coolers have turbulent generator functions like wavy channels with/without winglets. One dimensional model cannot accurately predict the flow fields inside the complex geometries. The developed axi-symmetric model is most comprehensive solution in current literature and is the only way to predict the effect of geometrical designs on the dynamics of particle deposition in real EGR coolers with wavy channels and winglets.

4.7 Concluding Remarks

We developed a one dimensional model in MATLAB and an axi-symmetric Eulerian model in ANSYS-FLUENT to study the particle transport in tube flows under influence of thermophoretic forces. They are the most complete models in literature taking into account the cross section area variation of the tube due to deposition, gas and deposit properties variation as a function of temperature, axial conduction in the deposit layer, and accurately calculated near wall gradients.

A comparison between isothermal and non-isothermal (when thermophoresis is present) flow conditions in tube flows (Figure 4.8) shows that in the non-isothermal condition, the deposition flux is 1-2 order of magnitude larger than that of isothermal cases by comparing the mass fraction gradients near the wall.

Engine exhaust is selected as a particle-laden flow to verify the developed models. Eight experiments are designed and conducted in a controlled engine test set up in Oak Ridge National Laboratory to vary the exhaust gas inlet temperature, particle mass fraction, and the gas mass flow rate. Exhaust gas was passed in surrogate tubes for a certain time exposure. Effectiveness drop of surrogate tubes and deposited soot mass gain in tubes are the variables employed for verification.

Both models show acceptable agreement with experimental measurements but the axi-symmetric model gives a closer prediction of deposited mass gain, the deposit thickness, and heat transfer reduction in tubes. Better prediction of deposited mass gain by the axi-symmetric model arises from the fact that the deposition flux in the axi-symmetric model is accurately computed through calculation of gas temperature and particle mass fraction gradients near the wall while in the 1D model the deposition flux is approximately calculated by empirical correlations. Axi-symmetric model is the only way to approach time evolution of the deposition process in real heat exchangers simulations with wavy channels and a more complex geometry than simple tubes.

4.8 Nomenclature

Symbols

A	Tube cross sectional area (m^2)
C	Particle concentration (kg/m^3)
C_C	Correction factor
C_p	Gas specific heat ($J/kg\,K$)
D	Transient tube diameter (m)
D_B	Browonian diffusivity ($m^2/\sec$)
D_T	Turbulent diffusivity ($m^2/\sec$)
d_p	Particle diameter (m)
f	Friction factor
h	Gas enthalpy (J/kgK)
h_c	Convection heat transfer coefficient (W/m^2K)
ID	Inner diameter of a clean tube (m)
J	Deposition flux ($kg/m^2\,s$)
k_b	Boltzmann's constant
k	Thermal conductivity ($W/m\,K$)
K_{th}	Thermophoretic coefficient
K	Mass transfer coefficient ($m/\sec$)
Kn	Knudsen number
L	Tube Length
MW_g	Gas molecular weight
$\dot{m}$	Gas mass flow rate ($kg/\sec$)
Nu	Nusselt number
OD	Outer tube diameter (m)
P	Gas pressure (N/m^2)
Pr	Prandtl number
$\dot{Q}$	Heat transfer to the tube wall (W)
R	Gas constant ($J/mol\,K$)
$R_{conduction}$	Deposit conduction thermal resistance (K/W)
$R_{convection}$	Convection thermal resistance (K/W)
R_{metal}	Metal conduction thermal resistance (K/W)
Re	Reynolds number
r	Radial direction
Sc_p	Particles Schmidt number
Sh	Sherwood number
T	Absolute temperature (K)
t	Time (sec)

$\mathbf{v}$	Gas velocity vector (m/s)
$\mathbf{V}_{th}$	Thermophoretic velocity (m/s)
x	Axial direction
Y	Particle mass fraction

Greek

Δx	Tube segment length (m)
Δt	Time step (sec)
Δ	Deposited layer thickness (m)
ε	Surrogate tube effectiveness (%)
η_d	Deposition efficiency (%)
λ	Mean free path of a gas molecule (m)
μ	Gas viscosity ($kg/m\,s$)
ρ	Density (kg/m^3)
ν	Gas kinematic viscosity (m^2/s)
φ	Deposited layer porosity

Superscript

n	Time step

Subscripts

0	Inlet
d	Deposit
i	Segment number
int	interface
g	Gas
L	Outlet
p	Particle
T	Turbulent
w	Wall

4.9 References

[1] Tsai, C. J., Lin, J. S., Aggarwal, S.G., Chen, D.R., "Thermophoretic deposition of particles in laminar and turbulent tube flows", Aerosol Science and Technology 38:131-139, 2004.

[2] Talbot, L., Cheng, R.K., Schefer, R.W., Willis, D.R., "Thermophoresis of particles in a heated boundary layer", Journal of Fluid Mechanics 101(4):737-758, 1980.

[3] Schmidt, F., Sager, C., "Deposition of particles in turbulent pipe flows", J. Aerosol Sci. 31(Suppl. 1): S847-848, 2000.

[4] Messerer, A., Niessner, R., Poschl, U., "Thermophoretic deposition of soot aerosol particles under experimental conditions relevant for modern diesel engine exhaust gas system ", J. of Aerosol science 34:1009-1021, 2003.

[5] Messerer, A., Niessner, R., and Poschl, U., "Miniature pipe bundle heat exchanger for thermophoretic deposition of ultrafine soot aerosolparticles at high flow velocities", Aerosol Science and Technology 38(5):456–466, 2004.

[6] Ronser, D., Khalil, Y.F., "Particle morphology-and Knudsen transition-effects on thermophoretically dominated total mass deposition rates fromcoagulation-aged aerosol population", J. of Aerosol science 31:273-292, 2000.

[7] Epstein, N., "Elements of particle deposition onto nonporous solid surfaces parallel to suspension flows", Experimental Thermal and Fluid Science 14:323-334, 1997.

[8] Chein, R., Liao, W., "Thermophoretic effects on nano-particle deposition in channel flow", Heat and Mass Transfer 42:71-79, 2005.

[9] Lee, B.U., Byun, D.S., Bae, G.N., Lee, J.H., "Thermophoretic deposition of ultrafine particles in a turbulent pipe flow: simulation of ultrafine particle behavior in an automobile exhaust pipe", Journal of Aerosol science 37:1788-1796, 2006.

[10] Tsai, R., Liang, L.J., "Correlation for thermophoretic deposition of aerosol particles onto cold palates ", J. of Aerosol science, vol. 32, pp. 473-487, 2001.

[11] Chomiak, J., Gupta, A.K., "Thermophoresis in boundary layer flows", J. of Aerosol Science 20:1-5, 1989.

[12] Shams, M., Ahmadi, G., Rahimzadeh, H., "A sublayer model for deposition of nano- and micro- particles in turbulent flows", Chemical Engineering Science 55:6097-6107, 2000.

[13] Brahim, F., Augustin, W., Bohnet, M., "Numerical simulation of the fouling process", Internation Journal of Thermal Sciences 42:323-334, 2003.

[14] Yang, M., Young, A., Niyetkaliyev, A., Crittenden, B., "Modelling of the fouling induction period", Proceedings of International Conference on Heat Exchanger Fouling and Cleaning VIII, Schladming, Austria, June 14-19, 2009.

[15] Cussac, F. C., Lister, D. H., "Modelling of particulate fouling on heat exchanger surfaces: influence of bubbles on iron oxide deposition", Proceedings of 7th International Conference on Heat Exchanger Fouling and Cleaning -Challenges and Opportunities, Tomar, Portugal, July 1 - 6, 2007.

[16] Charles, E., Cotton, J. S., Gerges, I. E., Chang, J. S., "Comparison of the effect of soot deposition on the flow and thermal characteristics of finned-plate-type and shell-and-tube-type exhaust gas recirculation cooling devices", Proc. IMechE part D: Automobile Engineering 223:1093-1100, 2009.

[17] Eiris, A., Saurez, E, Concheiro, M., "CFD numerical simulation of HP-EGR cooler performance under pulsating engine conditions", SAE paper 2011-26-0073, 2011.

[18] Nagendra, K., Tafti, D., Viswanathan, A. K., "Modelling of soot deposition in wavy-fin exhaust gas coolers", Int. J. Heat and Mass Transfer 54:1671-1681, 2011.

[19] Florea, R., Taraza, D., Henein, N.A., Bryzik, W., "Transient fluid flow and heat transfer in the EGR cooler", SAE 2008-01-0956.

[20] Sluder, C.S., Storey, J., Lewis, S., Styles, D., Giuliano, J., Hoard, J., "Hydrocarbons and Particulate Matter in EGR Cooler Deposits: Effects of Gas Flow Rate, Coolant Temperature, and Oxidation Catalyst", SAE paper 2008-01-2467, 2008.

[21] Crowe, C. T., Multiphase flow handbook, first ed., Tylor & Francis, New York, 2006, pp. 6-6.

[22] Einstein, A., "On the motion of small particles suspended in liquids at rest required by the molecular-kinetic theory of heat", Ann. Phys. 17:549-560, 1905.

[23] Churchill, S. W., "Comprehensive correlating equations for heat, mass and momentum transfer in fully developed flow in smooth tubes", Industrial Engineering Chemical Fundamentals 16:109-116, 1977.

[24] Berger, E. P., Hau, K. F., Mass transfer in turbulent pipe flow measured by electrochemical method, Int. J. Heat Mass Trasnfer 20:1185-1194, 1977.

[25] Patankar, S. V., Numerical heat transfer and fluid flow, Hemisphere Publishing Incorporation, 1980.

[26] Strom, H., Sasic, S., Andersson, B., "Effects of the turbulent-to-laminar transition in monolithic reactors for automotive pollution control", Ind. Eng. Chem. Res. 50(6): 3194-3205, 2011.

[27] Zamankhan P., Denn, M. M., "Simulation of non-iso thermal draw and twist of a bi-component chiral glass fiber", Chemical Engineering Science 64:1687-1694, 2009.

[28] Romay, F.J, Takagaki, S.S., Pui, D.Y.H., Liu, B.Y.H., "Thermophoretic Deposition of Aerosol Particles in Turbulent Pipe Flow", J. Aerosol Sci. 29:943-959, 1998.

[29] Mendoza, C., Zhou, D., "Effect of porous bed on turbulent stream flow above bed", J. of Hydraulic Engineering 118(9):1222-1240, 1992.

[30] Beavers, G., Joseph, D. D., "Boundary conditions at a neaturally permeable wall", J. Fluid Mech. 30(1):197-207, 1967.

[31] Cebeci, T., "Behavior of turbulent flow near a porous wall with pressure gradient", AIAA Journal 8(2):2152-2156, 1970.

[32] Zippe, H. J., and Graf, W. H., "Turbulent boundary-layer flow over permeable and non-permeable rough surfaces", J. of Hydraulic Research 21 (1):51-65, 1983.

[33] Wooding, R. A., "Rayleigh instability of a thermal boundary layer in flow through a porous medium", J. Fluid Mech. 9:183-192, 1960.

[34] Zhou, D., Mendoza, C., "Flow through porous bed of turbulent stream", J. Engineering Mechanics 119(2):365-383, 1993.

[35] Dvorak, F. A., "Calculation of turbulent boundary layers on rough surfaces in pressure gradient", AIAA Journal 7(9):1752-1759, 1969.

[36] Poulikakos, D., Kazmierczak, M., "Forced convection in a duct partially filled with a porous material", Journal of Heat Transfer 109:653-662, 1987.

[37] Ciro, W.D., Eddings, E.G., Sarofim, A.F., "Experimental and Numerical Investigation of Transient Soot Buildup on a Cylindrical Container Immersed in a Jet Fuel Pool Fire", Combust. Sci. and Tech. 178:2199-2218, 2006.

[38] Lance, M., Sluder, C.S., Wang, H., Storey, J., "Direct measurement of EGR cooler deposit thermal properties for improved understanding of cooler", SAE paper 2009-01-1461, 2009.

[39] Lance, M., Sluder, C.S., Lewis, S., Storey, J., "Characterization of field-aged EGR cooler deposits", SAE Int. J. Engines. 3 (2):126-136, 2010.

CHAPTER 5

IN-SITU MONITORING OF PARTICLE TRANSPORT IN CHANNEL FLOW

It is shown in previous publications that the formed layer due to particulate deposition in duct flows tends to stabilize after a long exposure time ([1]-[3]). The mechanisms leading to this stabilization are not clearly understood and there is no published article discussing deposit removal of sub-micron particles in the sub-sonic flow range. There may be deposit removal mechanisms, or it may be that the rate of deposition decreases as deposits build (or both). It can also be the deposit layer thermal properties variation when the layer grows. The lack of literature on this subject and many uncertainties in this complex problem led us towards this fundamental experimental investigation.

Our developed CFD models are in a good agreement with Oak Ridge National Laboratory experiments for short exposure times. Despite the good agreement for short exposures, the results of developed models show a deviational trend for longer exposure times. Therefore, we decided to investigate the physics of long exposure experiments and deposit stabilization mechanism(s) by monitoring the deposit layer in-situ. The aim of this experimental study is to find enhancing mechanisms for deposit removal and effectiveness recoveries in EGR coolers by visualizing the events happening at different conditions. In the following section the experimental test fixture and the tests are described.

Little experimental study of fouling (particle deposition) phenomenon in EGR coolers exists in literature for different aspects including effectiveness reduction and pressure increment due to fouling ([4]-[6]). Most of these experiments were blind tests in which the inlet and outlet temperature and pressure of real EGR coolers were measured at different boundary conditions. Despite the good quality of these studies, the dynamics of the fouling process is not clear in them. Also, there have been a few attempts in simulation, prediction, and measurement of deposit growth in a combustion chamber by extensive micrographic study ([7]-[9]) but current novel investigation is done to observe the dynamics of particle deposition and removal in-situ.

5.1 Experimental Apparatus

A unique experimental apparatus is designed and built for in-situ monitoring of deposition formation and removal of diesel engine exhaust particulates in a channel flow. A 2008 model year 6.4L Ford PowerStroke® diesel engine is used to generate exhaust for the visualization test fixture. Hot engine exhaust carrying particles flows through a rectangular channel with one wall made of Pyrex and the other of stainless steel. The Pyrex wall gives an opportunity to monitor the deposit growth on the opposite wall made of stainless steel.

If thermophoresis is the only deposition mechanism for submicron particles, then imposing a zero temperature gradient (in the radial direction) on the Pyrex wall should result in no deposition. A Ford proprietary method is used to heat the glass. Figure 5.1 depicts a schematic of the surrogate channel carrying exhaust flow and Figure 5.2 shows a real image of the experimental setup. As shown, coolant is circulated below the metallic wall to cause thermophoretic deposition due to the temperature gradient. Although our main target is to study real EGR coolers, this study is limited to a surrogate channel. Moreover, the heated air stream transfers the heat to the exhaust flow and does not let the

metallic channel act as a cooler. Therefore, the focus is to visualize and record the deposition/removal events and not the effectiveness measurement of the channel.

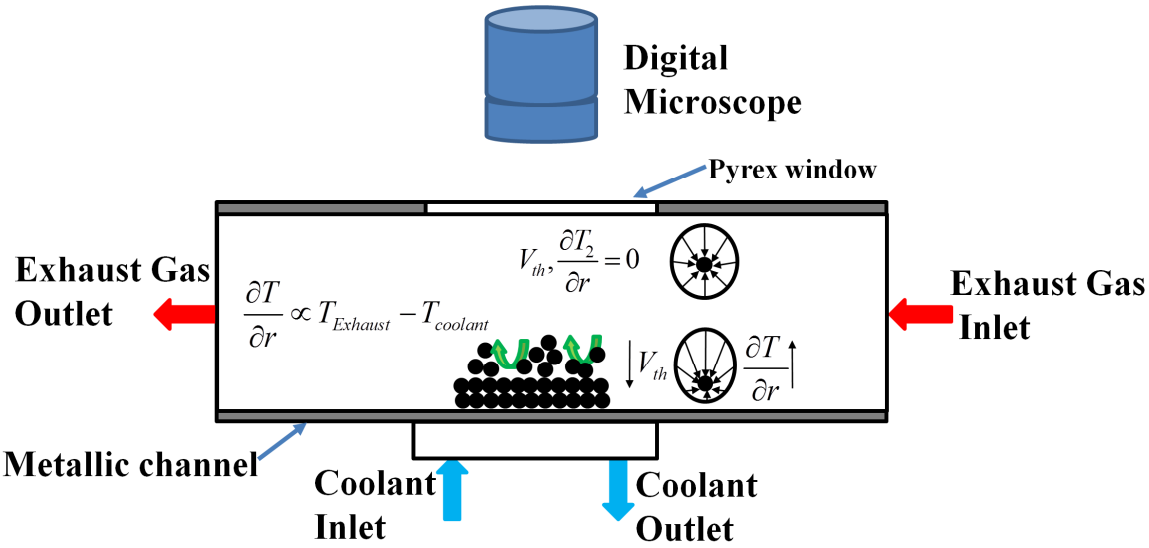

Figure 5.1 – Principle of the visualization test rig – Metallic channel caries exhaust (or compressed air) and glass window allows visualization

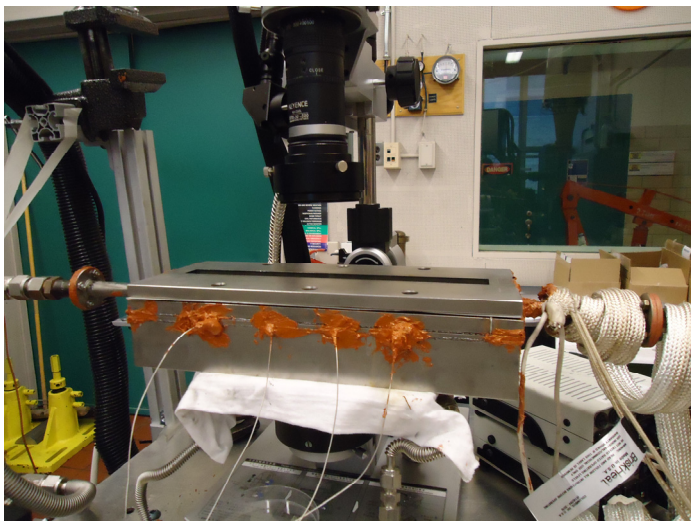

Figure 5.2 – A picture of the experimental setup – digital microscope, metallic channel, thermocouples below the specimen, coolant and gas inlets and outlets. Exhaust flow direction is from right to left.

A digital microscope (Keyence, VHX-1000E) is located on the top of the Pyrex wall and tracks the deposit growth caused by thermophoresis on the opposite wall. The

camera can record individual pictures or videos; we typically recorded time lapse videos with one image captured per minute. Monitoring the deposit layer over the time exposure of the experiments and recording the events on the surface with the digital microscope shows that there can be a removal mechanism in the form of deposit flaking. There are four thermocouples to measure the metal temperature below the specimen (opposite wall) in which deposition occurs. Since the metal deposit surface is thin (~1 mm stainless steel) we expect the deposit-side metal temperature to be very close to the temperature measured by these thermocouples.

Besides the exhaust gas stream in the metallic channel, we also designed another gas line for compressed air that can replace exhaust as needed. Figure 5.3 shows schematics of how these two lines switch and how pressure transducers, thermocouples, flow meters, and heaters are controlled by a computer program. A Labview® program is written to control the flows at the desired temperature, pressure, and flow rate. The exhaust flow is filtered and the flow measured by a Siemens flow meter (SITRAN F C MASSFLOW 2100 DI 6). Also, the compressed air line flow rate is measured by a MKS mass controller (1579A00832LR1BV). The purpose of compressed air line in our design is to 1) warm up the system before flowing exhaust in order to avoid any possible condensation of water and hydrocarbons if not needed, 2) to investigate removal mechanisms caused by shear forces at higher flow rates, 3) to cool down the system with no water condensation at low temperatures (the compressed air has a dryer and filter upstream of the fixture). Using hot air at an almost identical condition as exhaust (temperature, pressure, and flow rate) lets us study the effect of shear force on removal enhancement with no deposition (no particulate in compressed air).

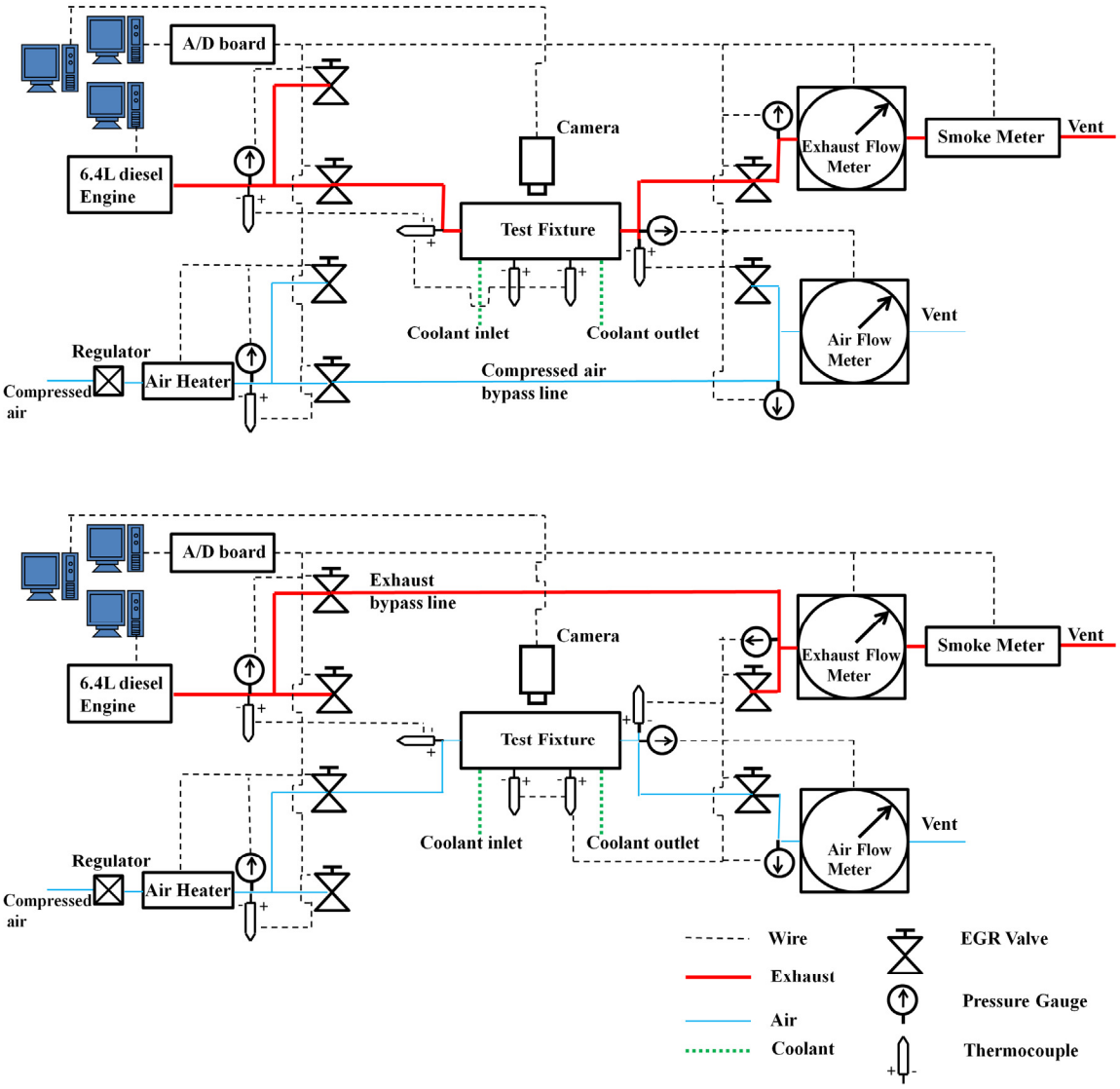

Figure 5.3 – Schematics of gas lines and wires – Exhaust mode on top and compressed air mode in bottom

Engine exhaust is sampled from the engine high pressure EGR pipe upstream of the EGR catalyst and cooler. This pipe is at exhaust pressure upstream of the turbocharger turbine. This pressure drives the exhaust flow through the system without need for a sampling pump. A heated line is used between the engine and the fixture to keep the exhaust temperature high enough (190^{o}C). The purpose of this heated line is to 1) prevent hydrocarbons condensation in the path 2) Prevent heat loss from the exhaust flow to the ambient 3) prevent thermophoretic PM deposition in the line.

5.2 Long Deposition Test

A series of experiments was performed to visualize the soot particle deposition and removal at various boundary conditions. First, the deposition tests are described and thereafter different designed experiments for removal observation are discussed. Although a few removal tests were successful and just one was practical for real EGR coolers recovery, this apparatus can be used for further investigations on this field.

5.2.1 Long Deposition Test

A steady state load/speed condition (1200 RPM, 7.5 BMEP with post injection, 1.57 bar pressure at turbine inlet, air fuel ratio 20) of the diesel engine representative of a highly loaded cruise is selected for the deposition test. This point is selected to produce a higher particulate level of FSN=1.1 (20.4 mg/m^3) as PM is known to be the significant exhaust constituent that degrade EGR cooler performance. A series of long runs (with the maximum of 18 hours continuous run) were conducted to observe possible obvious removal mechanism with the deposition is occurring. Some tests were performed in different days and some were conducted continuously in one day to make sure the observed results are not affected by deposit aging over time. If the tests were continued in different days, we made sure to have an initial warm up time with hot compressed air and a cool down period with hot air at a similar condition after each test. This is to avoid possible water or hydrocarbon condensation and keep the layer unaffected by condensed species.

In deposition tests, exhaust gas passed through the metallic channel at the given boundary condition in Table 5.1 (properties in estimating Reynolds number are calculated at the average temperature of the coolant and inlet exhaust temperature).

Table 5.1 – Channel geometry and boundary condition

Channel width (mm)	21.5
Channel height (mm)	12
Channel length (mm)	300
Exhaust inlet pressure (bar)	1.25
Exhaust inlet temperature (^{o}C)	350
Coolant temperature (^{o}C)	80
Mass flow rate (kg/hr)	3
Re	2800

A 1/16" thermocouple is used to measure temperature near the surface of the Pyrex window at the glass channel outlet. This temperature of the heated glass was kept larger than the inlet temperature of exhaust in the metallic channel.

Gas lines are round ½" Swagelok tubes and fitting and the channel is rectangular (Table 5.1). The channel inlet and outlet adaptors are designed so that recirculation at the inlet and outlet is minimized.

The significant observation from deposition tests is that we were quite successful in keeping the Pyrex window clean and could observe the opposite wall. The fact that the glass remains clear apparently shows that as the only expected deposition mechanism for small soot particles in exhaust is thermophoresis and other mechanisms do not play an important role. This trend was expected from literature and our aforementioned scaling work discussed before.

Figure 5.4 shows a clean surface at half-length of the channel before deposition and after 2 hours of soot particle deposition at the aforementioned engine condition. It is clearly seen that in a course of two hours, soot particles completely covered the metallic surface where the camera was recording images (magnification of 50 – Image size is 6.88mm$\times$5.16 mm).

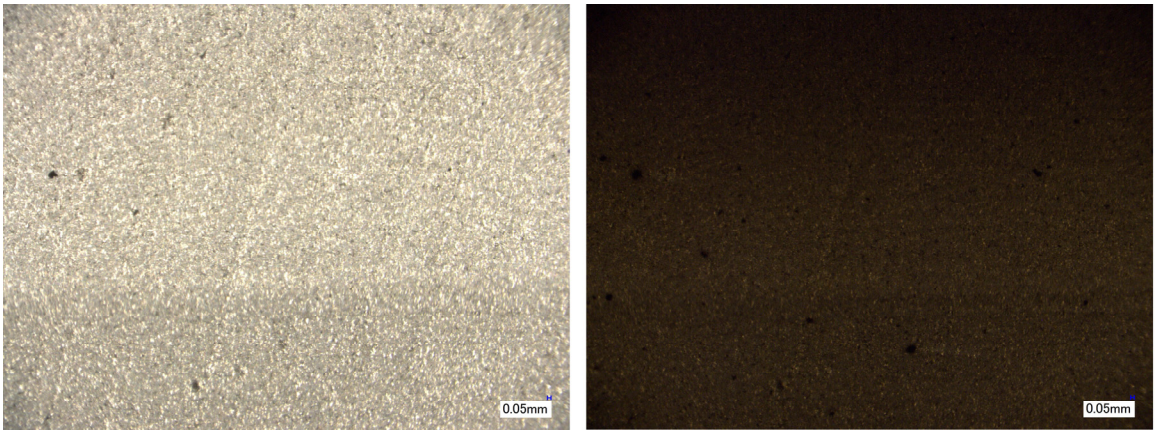

Figure 5.4 – Two images taken from the surface before and after deposition within a two hour interval – (magnification 50)

In another deposition test, we used the microscope to measure the deposit thickness. To do so, we made a scratch mark on the surface to have a reference (clean metal surface) for this measurement. After 2 hours of soot deposition a 3D image of the deposit layer was taken. Figure 5.5 depicts a real image of the layer and its 3D images from two different views. The deposit thickness was measured to be 69.3 micron. The thickness was also measured by a commercial thickness measurement probe and the results were quite close (65 micron).

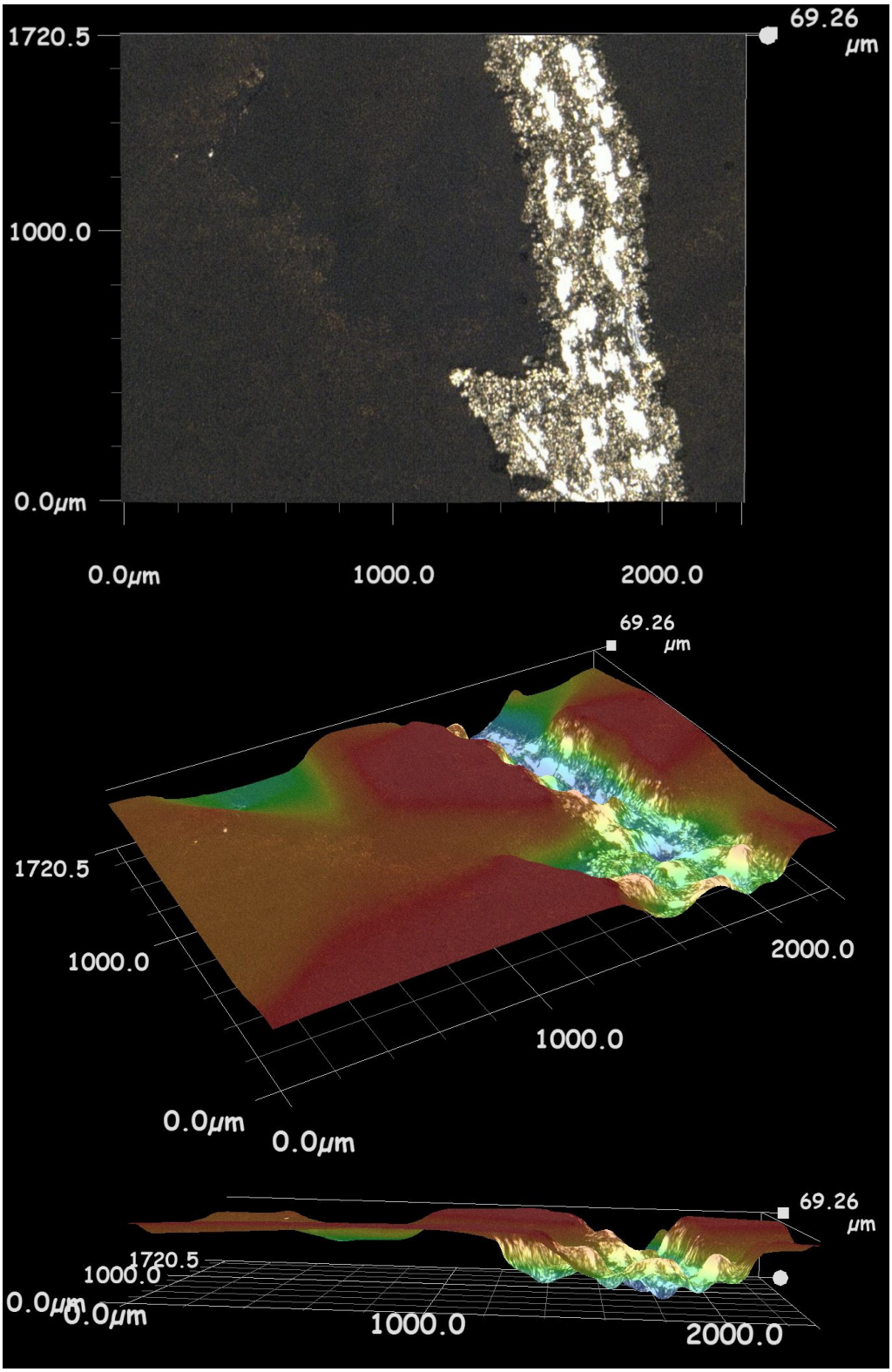

Figure 5.5 – A real image of the deposit layer with a scratch mark for the reference – 3D images of the layer (150x magnification)

During the long steady state tests, no significant removal in the form of flaking occurred but the morphology of the layer changed once when the deposit sat in ambient condition for two days. We hypothesize that it can be either due to chemical reactions in the layer or hydrocarbon evaporation from the deposit layer. Further investigation of this phenomenon is planned as future work.

To make sure that the observations are consistent, we repeated the deposition tests several times at the same conditions. The deposition tests were always the same and no obvious removal or recovery was observed except a few small random flakes ranging from a few to a hundred micron. These flakes occurred (along the tube length including where the camera was looking) just a few times over a long test and the resulting spot was covered in about an hour. We do not consider these types of flakes as a removal mechanism. In addition, there were seen a few big particles with the maximum diameter of a few hundred microns landing on the layer (see Figure 5.4). These particles may be flakes of deposits from the cylinder or exhaust system, and are not normally measured by typical particulate measuring instruments. We hypothesize that small flakes discussed above were also caused by these big particles that are not in the range of exhaust soot particles reported in literature.

Besides random big particles flowing in the exhaust flow, we observed small flakes when we switched the line. Due to the fact that there is a tee connection between the exhaust and the air line and particles can be trapped in the tee fitting, once in awhile removal was observed in the form of small flakes when we switched the lines. We hypothesize those particles hitting the surface (when switching the lines) come from the tee fitting upstream of the channel and not from the engine.

A collection of big particles were observed either when switching the lines or randomly in the exhaust flow. Therefore, we studied the existence of big particles in the exhaust flow. The conventional understanding is that soot particles range from 10 to 300

nm [10] but our study show that there are big particles in the flow and those are the ones filtered in the cyclones of devices in which distribution analysis is done.

We passed the exhaust gas through a fiberglass filter of 2.7 micron pore size and 60 mm diameter at different locations; at the sample tap in the EGR line, through 20 feet of heated sample line just before the test fixture inlet, and in the air line which is used to pre heat the test fixture. We exposed the filter to exhaust for two minutes in each test. This data demonstrates the presence of large particles not previously documented. Figure 5.6 demonstrates the filter-holder used in this study and Figure 5.7 shows a sample filter exposed to the exhaust flow for two minutes.

Figure 5.6 – Filter holder for the particle distribution study

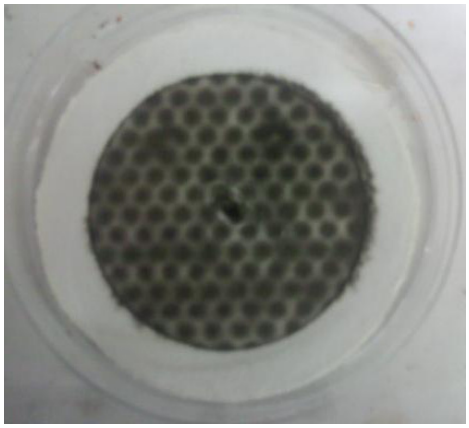

Figure 5.7 – A sample filter that is exposed to exhaust for two minutes

Many filters were used to sample the particles at different engine conditions. Interestingly, those big particles were observed under the microscope in most of the sample filters. Figure 5.8 shows a filter at the magnification of 200. Big particles are clearly seen in this image.

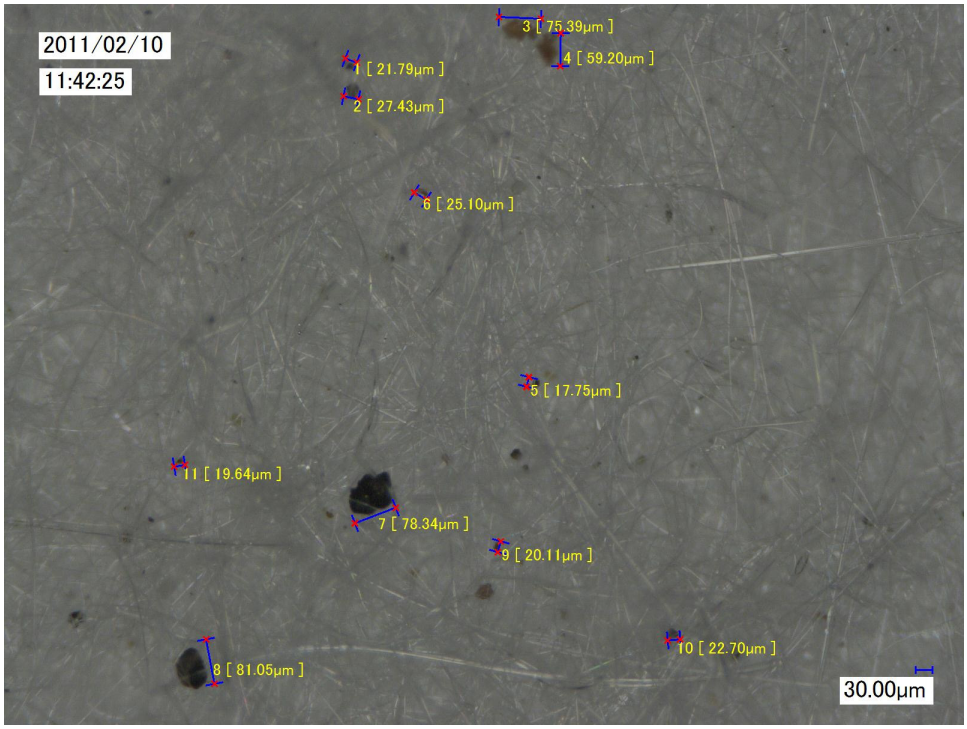

Figure 5.8 – Large trapped particles in the filter – Image taken by the microscope - Image size 1.74mm×1.29 (200x magnification)

5.2.2 Thermal Cycling Test

One hypothesis for removal is potential thermal stress cracking of the deposit. To experiment this, we performed a thermal cycling test. After the deposition period for 18 hours, this test was conducted with hot compressed air to avoid the chance for water condensation. We monitored the effect of temperature variation of the layer by reducing the coolant temperature (turning off the water heater). Consequently, the specimen temperature gradually dropped to 40^{o}C over 26 minutes. We heated up the coolant again to 80^{o}C and repeated this experiment once more. We did not observe any flakes or

significant change in the layer because of thermal cycling. Either thermal cycling does not have a significant impact on deposit removal or the temperature variation range was not sufficient or fast enough due to large heat capacity of the fixture.

5.2.3 Water Condensation Test

The criterion for water condensation to occur is that the mole fraction of water in the main flow is equal or larger than the mole fraction at the wall surface and that the surface is below the dew point temperature. Water mole fraction in the flow is defined by:

$$y_w = \frac{P_v}{P} \tag{5.1}$$

where water vapor pressure can be calculated by using its Antoine coefficients (A, B, C) as:

$$Log_{10} P_v = A - \frac{B}{T_C + C}, \quad A = 10.23,\ B = 1750,\ C = 235 \tag{5.2}$$

Pressure is in Pascal and the surface temperature is in Celsius in above equations. Water mole fraction in the exhaust flow can be estimated from the ideal diesel fuel combustion (H:C ratio CH = 1.809) when the air fuel ratio is 20 in our experiment:

$$CH_{1.809} + 2(O_2 + 3.76N_2) \rightarrow CO_2 + 0.9045H_2O + 7.521N_2 + 0.548O_2$$

Having water mole fraction in the flow (0.091) and the exhaust pressure (1.25 bar), one can calculate the dew point for water condensation in the fixture to be 47^{o}C.

The system ran a total of 18 hours of deposit accumulation with engine operating conditions as described above. This total accumulation was done over a period of five days. At each shut down the flow was switched from exhaust to heated air. On the initial start and subsequent restarts, the system was preheated with hot air before exhaust flow was routed through the test fixture.

After 18 hours of the deposition test, we gradually reduced the coolant temperature from 80°C to 40°C over 16 minutes while flowing exhaust gas. Soon after the temperature below the specimen reached 42°C (approximately the dew point) over 31 minutes, we observed a fracture in the deposit and its growth. Image of the fracture growth are presented in Figure 5.9. There is a 5 minute interval between each from image (a) to image (d). The real size of each image is 6.88mm×5.16mm and the magnification is 50.

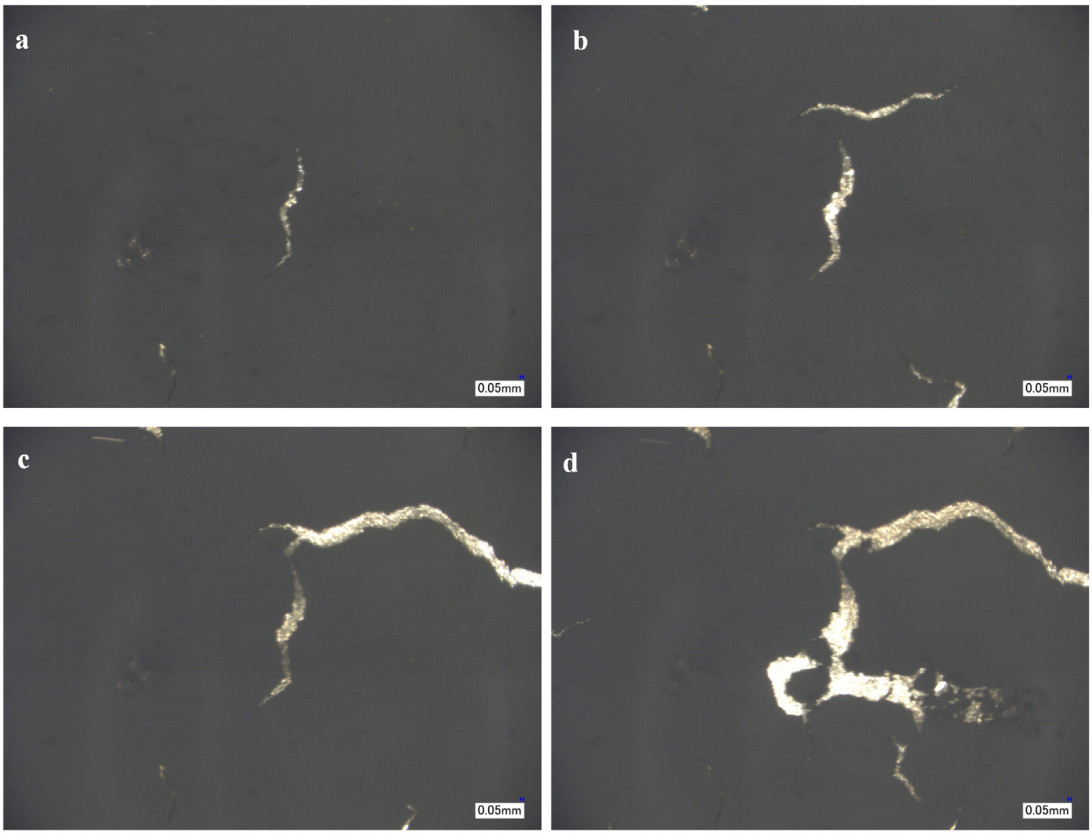

Figure 5.9 – Fracture in deposit when coolant reached the critical temperature (42°C). There is 5 minutes interval between successive images. The real size of each image is 6.88mm×5.16mm (50x magnification). Gas flows from bottom to top.

In the next test, we circulated very low coolant temperature (9°C) while flowing compressed air. No further changes were observed. Then, we switched the flow from compressed air to exhaust gas through the channel. Immediately after exposing the

channel to exhaust flow (containing water molecules), significant deposit flakes were observed so that a clean metal surface was easily seen. In other words, water droplet formation below the deposit layer weakened the bond forces and caused the deposit layer to float until they were removed by gas flow in the form of flakes. The consequence of this process can be seen in Figure 5.10. It is seen that there are no droplets on top of the deposit. Condensed water diffuses through the porous layer and forms droplets underneath.

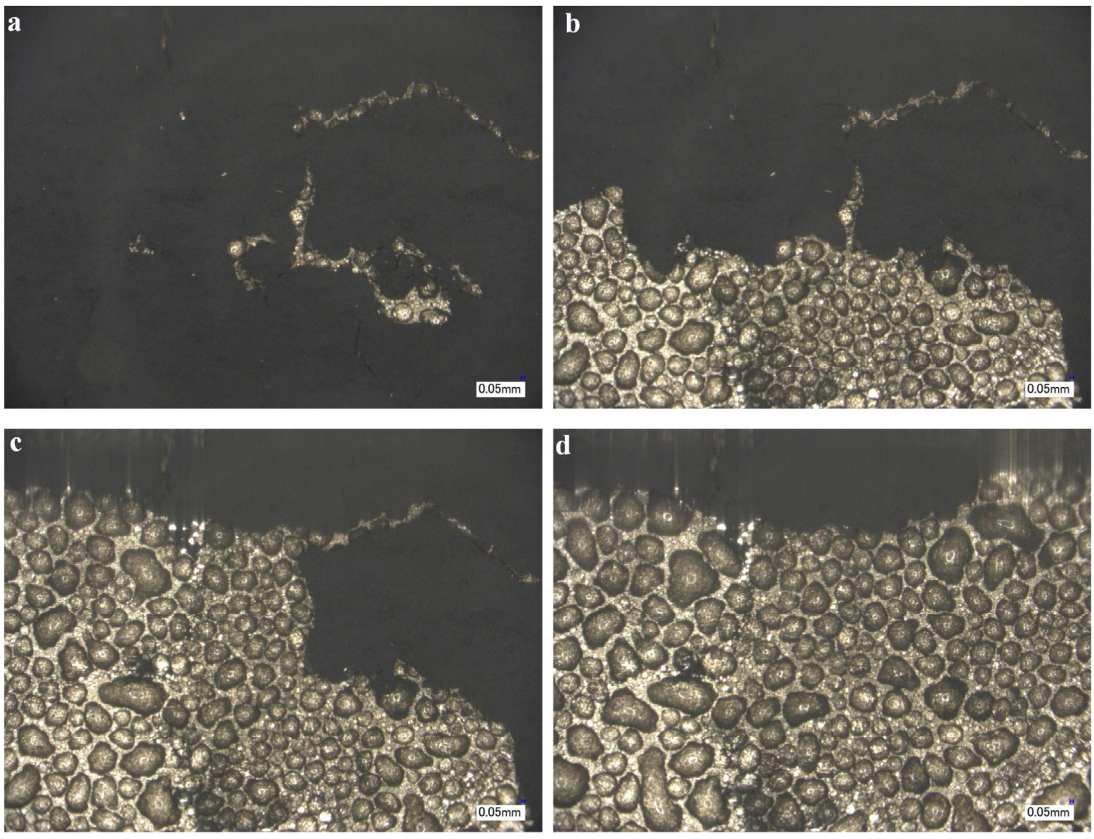

Figure 5.10 – Deposit flakes when specimen temperature was really low (20^{o}C). There is 1 minute interval between successive images. The real size of each image is 6.88mm×5.16mm (50x magnification). Gas flows from bottom to top.

This test was repeated twice; in the second test, the deposition part was shorter (6 hours) and the formed layer in 6 hours was exposed to low coolant temperature. Similar results for recoveries were observed.

The only ex-situ investigation on removal of exhaust soot particles are conducted by Kalghatgi in [11] to [13]. He investigated the effect of water drops on combustion chamber deposits. Although his research was not directly related to the EGR cooler deposits, one can find it really helpful in understanding the flake off mechanism. He observed that cylinder deposits flake when exposed to water droplets.

5.3 Discussion

In these experiments, long tests ran for forming a deposit layer in a channel. In deposition tests, small random flakes were observed because of large particles landing on and hitting the deposit layer. These big particles can be deposit flakes formed in the engine. Our qualitative study showed that big particles (micrometer) exist in the exhaust flow; they are not captured in distribution analysis instruments. It is hypothesized that these big particles cause random small flakes.

A thermal cycling test was performed in air flow. No significant removal was observed. It can be because thermal cycling does not have an effect on removal or it was not done fast enough in our fixture due to the large heat capacity of the rig.

We observe that deposits can be removed from the surface by operation at low coolant temperature with water condensation. It may be difficult to do this in real vehicle systems, since engines have limited EGR tolerance when cold. Also, coolant temperatures increase rapidly on engine start. In our experiment, as water condensed on the surface the deposit layer appeared dry as observed by the camera, but we saw water droplets on the surface when the flakes blew away. This seems to indicate that water diffuses through the porous deposit layer and condenses on the relatively colder metal surface. The deposits seem to be hydrophobic. It is believed that small particles are held on the surface by Van der Waals forces. It may be that the condensation of water creates

an environment where those forces are reduced, so that the deposit layer can crack and blow away.

It is also noted that the deposit layer acts as a porous solid, rather than as either fluffy dry carbon soot or liquid condensed hydrocarbons. This seems to imply some chemical reaction in the deposit layer over time and is probably related to the reason why similar effects may not be present on early deposit layers. Kalghatgi ([11]-[13]) similarly noted that flaking occurs only on aged deposits.

The fixture is not designed for large gas velocities due to the large channel size. Therefore, shear force test at the highest velocity possible in the test fixture (5 m/s) did not result in any removal of particles.

5.4 Concluding Remarks

An apparatus is designed and built to monitor soot particle deposition and removal in channel flows. This novel experimental study is a unique method that has not been conducted before and can provide significant physical insight into the removal/flaking mechanisms of submicron particle.

An exhaust stream is sampled from a 2008 model year medium duty diesel engine to resemble particle-laden channel flows. This test rig has the capability to vary boundary conditions and observe its effect on deposit. Coolant temperature, gas temperature, pressure, and flow rate, engine condition (i.e. load, speed) are the parameters that can be controlled in our fixture. Each of the aforementioned parameters might have a significant impact on the enhancement of deposit removal and must be studied thoroughly in our future tests.

Long deposition tests were performed with the hope of observing removal, flakes, or fractures in the layer. It was occasionally observed in deposition tests that large particles (a few hundred microns) hit the layer and caused flakes.

Then, a thermal cycling test was done and no removal was observed during the test. It can be because of the large heat capacity of the fixture that does not let fast temperature change inside the layer or thermal cycling does not have a significant effect on removal of young deposit.

Deposit removal in the form of flakes was observed when an aged (18 hours of deposition) deposit layer was exposed to exhaust flow at a low coolant temperature. We were quite successful in preventing deposition on one wall (Pyrex) and observing deposit formation and removal of particles on the channel wall. We repeated our test with a shorter deposition period (6 hours) and made sure that water condensation is responsible for deposit removal in the form of flakes.

5.5 References

[1] Epstein, N., "Elements of particle deposition onto nonporous solid surfaces parallel to suspension flows", Experimental Thermal and Fluid Science 14:323-334, 1997.

[2] Stolz, A., Fleischer, K., Wolfgang, K., Jens, N., Roland, S., "Developmentof egr coolers for truck and passenger car application". In .Vehicle Thermal Management Systems Conference and Exposition, SAE paper 2001-01-1748, 2001.

[3] Lepperhoff, G., Houben, M., "Mechanisms of deposit formation in internal combustion engines and heat exchangers", SAE paper 931032, 1993.

[4] Chang, D. K., Sobh, A. J., Tjong, J. S., Styles, D. J., Szente, J. J., "Diesel EGR cooler fouling with Ni-Fe-Cr-Al DPF at Freeway cruise", SAE paper 2010-01-1955, 2010.

[5] Abd-Elhady, M. S., Malayeri, M. R., Steinhagen, H. M., "Fouling problems in exhaust gas recirculation coolers in the automotive industry", Proceedings of International Conference on Heat Exchanger Fouling and Cleaning VIII, Schladming, Austria, June 14-19, 2009.

[6] Ismail, B., Charles, F., Ewing, D., "Mitigation of the diesel soot deposition effect on the exhaust gas recirculation (EGR cooling devices for diesel engines", SAE paper 2005-01-0656, 2005.

[7] Price, R. J., Spink, C. D., Morely, C., "Prediction of combustion chamber deposit growth in SI engines", SAE paper 972835, 1997.

[8] Cheng, S. S., "A micrographic study of deposit formation process in a combustion chamber", SAE paper 962008, 1996.

[9] Price, R. J., Wilkinson, J. P. T., Jones, D. A. J., Morely, C., "A laboratory simulation and mechanism for the fuel dependence of SI combustion chamber deposit formation", SAE paper 952445, 1995.

[10] Harris, S.J., Maricq, M.M., "The role of fragmentation in defining the signature size distribution of diesel soot", J. of Aerosol Science 33:935-942, 2002.

[11] Kalghatgi, G.T., Price, R.J., "Combustion chamber deposit flaking", SAE 2000-01-2858, 2000.

[12] Kalghatgi, G.T., "Combustion chamber deposit flaking-Studies using a road test procedure", SAE 2002-01-2833, 2002.

[13] Kalghatgi, G.T., "Combustion chamber deposit flaking and startability problems in three different engines", SAE 2003-01-3187, 2003.

CHAPTER 6

CONCLUSIONS AND FUTURE WORK

6.1 Summary and Concluding Remarks

In chapter 1, the problem of EGR cooler fouling was introduced and the research studies in the field were discussed. Deposit in EGR coolers mainly consists of soot, condensed hydrocarbons and acids. It was shown that the majority of deposit is soot particles. Therefore, we limited our modeling work to particulate transport in particulate-laden flows to understand the dominant deposition mechanisms in EGR coolers. EGR cooler deposit is shown to have a stabilization trend after a long running time. The reason for the stabilization might be that the rate of deposition decreases when the layer builds up, or possible removal mechanisms that balance with deposition mechanisms, or thermal properties of deposit varies as a function of layer growth.

In chapter 2, a scaling analysis of various deposition and removal models in literature were discussed and it was shown that thermophoresis is the dominant deposition mechanisms of submicron soot particles in exhaust flow. We showed that removal mechanisms (for larger particles) proposed in literature does not seem to be responsible for stabilization of EGR coolers deposit. A simple calculation on forces acting on an attached particle to a surface shows that Van der Waals forces are strong enough for submicron particles so that they cannot be easily re-entrained by shear force, turbulent bursts or the lift force. This scaling analysis led us towards modeling of thermophoretic deposition of particles by using analytical correlations. Since most EGR

coolers are shell-and-tube heat exchangers, we limited our study to surrogate tubes to resemble real EGR coolers. This reduced the complexity of problem and helped us understand the physics of the fouling dynamic.

In chapter 3, particulate deposition under thermophoretic forces in tube flows is studied analytically by solving the energy equation for the gas and particle mass conservation. The flow regimes are either turbulent or in the transition. For various boundary conditions including inlet gas temperature and pressure, wall temperature, inlet particle concentration and gas mass flow rate, the problem was solved by using the proposed analytical correlations. The deposited layer was treated as a solid layer with a constant thermal conductivity and density. A parametric study was done and showed that larger particle concentration, larger inlet temperature, and larger gas mass flow rates increases the deposited mass along the tube while increasing pressure reduces the deposited mass. We compared the results of the analytical method with experiments conducted in Oak Ridge National Laboratory (ORNL) and the results are in a satisfactory agreement. Although proposed analytical correlations predict the mass deposited and heat transfer drop of the tube flows for a relatively short exposure time (3 hours) quite well, it cannot predict the stabilization of the deposit for longer exposure times due to the fact that no removal term in the governing equations was included and the layer properties were constant. At this point, we moved one step forward to CFD modeling of the problem.

In chapter 4, we used two approaches to analyze the problem, a one dimensional model in which the variables are assumed to be uniform in each cross section perpendicular to the tube axis; and an axi-symmetric model with moving boundaries. In the one dimensional model, MATLAB is used via implementing a finite difference scheme. In the axi-symmetric approach, the CFD software ANSYS-FLUENT is employed. In the software environment, a collection of C subroutines are developed to include the thermophoretic transport and the evolution of the boundaries due to the soot

deposition. The variation of gas properties in the tube and accurate gas temperature and particle mass fraction gradients are critical factors that were not accommodated in the proposed analytical solution for the sake of simplifying the equations. We compared the developed models against experiments conducted at Oak Ridge National Laboratory by comparison of the particulate mass deposited along the tube and the overall heat transfer reduction (effectiveness) for a short exposure time (3 hours). Both models show a satisfactory agreement to the experimental results although the axi-symmetric model shows a better estimation of the deposited mass gain in time. It is because the deposition flux is computed more accurately in the axi-symmetric model. Also, both models were examined for a longer exposure time (12 hours). The axi-symmetric model showed a significantly closer prediction of the deposited mass gain at the end of 12 hour exposure compared to the 1D prediction. Furthermore, Both models showed a good prediction of the heat transfer reduction for long exposure times. Despite of the good prediction for short exposures, there was a slight deviation in the effectiveness slope prediction by models starting after 4 hours. It shows that either there must be a removal source term in governing equations (not yet understood) or the deposit properties correlations based on literature are not well matched with real properties of EGR cooler deposit. At this point, we decided to study possible removal mechanisms or recovery methods experimentally. So, we developed an experimental apparatus for visualization of the growing layer over time under various boundary conditions. It is noted that the axi-symmetric model is the most comprehensive model in current literature and is the only way to predict the flow field and dynamics of particle deposition in real EGR coolers with complex geometries (wavy channel and winglets).

In chapter 5, an experimental study is performed to visualize the dynamics of fouling process in-situ. Exhaust gas was passed through a rectangular channel with a wall made of Pyrex for visualization purposes. The deposition and removal of deposit is monitored by a digital microscope that can record time lapse images or high quality

movies at various magnifications ranging from 50 to 500. Long deposition tests were performed with the hope of observing removal, flakes, or fractures in the layer. It was occasionally observed in deposition tests that large particles (a few hundred microns) hit the layer and caused flakes. This led us towards a series of tests to capture possible big particles. It was seen that large particles on the order of micron exist in the exhaust flow and they can cause flakes in deposit randomly over deposition tests. Then, a thermal cycling test was done and no removal was observed during the test. It can be because of the large heat capacity of the fixture that does not let fast temperature change inside the layer or thermal cycling does not have a significant effect on removal of young deposit. The formed deposit was not exposed to ambient air or hydrocarbon condensation and it did not go through aging process. It is the reason we call it a young deposit. By passing a low coolant temperature (40°C), fractures were observed in the layer. At even lower coolant temperatures (20°C), already fractured deposit was totally removed due to formation of water droplets underneath of the layer. The layer is hydrophobic and water droplets were always formed below the deposit layer. Water droplets loosen the bond forces of the deposit and made the layer prone to removal by the gas flow. In another test, we found a recovery method that seems very promising for real EGR coolers. It resulted in a significant removal of the already formed layer. This method remains confidential to Ford Motor Company at this point. We plan to disclose this practical recovery method for a potential patent.

6.2 Recommendations for Future Work

- By installing an IR camera on the top of the window and looking at the same area that digital microscope is adjusted for, the layer surface temperature can be tracked as the layer builds up. Having surface temperature (measured by IR camera) and the layer thickness

measured by the digital microscope, and knowing the coolant temperature and the heat flux (using thermocouples and heat flux probes underneath of the specimen), gives us the ability to quantify the thermal conductivity of the deposit layer over the exposure time of an experiment. This is a novel study with a significant impact on this field that helps understanding if the stabilization of the deposit layer is related to the thermal properties variation of the layer over time. Having the surface temperature, we can prove or disprove our hypothesis on higher kinetic energy of the top layer.

- Deposit mechanical properties measurement would be beneficial in investigation of deposit removal theories including spalling, spadering, and fractures in the deposit layer due to the thermal stress.
- We hypothesized that the gas-deposit interface temperature might reach a critical value in which removal occurs. The possible reason for removal might be that high kinetic energy of particles at the interface possibly overcomes Van der Waals potential energy and results in removal of particles. This theory can be investigated by measuring the gas-deposit interface temperature and the deposit thickness over a long exposure test.
- Various engine conditions including different load and speed and post injection with different level of hydrocarbon helps us understand the effect of wetting by hydrocarbon or possible chemical reactions with soot.
- Proposing a fouling map based on the engine load/speed curves and highlighting the high and low risk regions for fouling depending on the engine operating condition would be an interesting and useful task for the auto industry.

- Pulsation may have a huge impact on the flow and the deposited layer. In our long heated line, the pulsation is somewhat damped. Installing a pulsation driver at the inlet or outlet of the fixture and making pulsation at various frequencies can lead towards finding more practical ways to mitigate or prevent deposition.
- Shaking the fixture at different high frequencies with the purpose of finding the natural frequency of the deposit layer can be another significant investigation in this field. Using the natural frequency may prohibit the layer growth or may remove the layer after certain time exposures in real engines.
- Effect of different fuels can be investigated and the deposit layer can be analyzed using TGA techniques to see if the layer thickness, morphology, and constituents are a function of the fuel used.
- Another task can be measurement of the inlet and outlet particulate concentration for the modeling validation. Oak Ridge National Laboratory experiments did not have the outlet concentration of particles. This number can significantly help the model validation. It also shows how deposition efficiency reduces over time when the layer builds up.
- In the models, the layer is treated as a highly porous zone that no-slip condition is valid at the gas-deposit interface. Treating the deposit layer as a permeable zone that can include a convective form of heat transfer inside is another subject for future work.
- After understanding the layer thermal properties as a function of the gas-deposit interface developed CFD models can be revisited for improvements.

- Employing the developed model in ANSYS-FLUENT to investigate the effect of winglets in tubes or wavy tubes is another task that can be done. Experimental results for comparison exist (from ORNL) for the thickness measurement of these cases. In the next step actual EGR cooler geometries can be modeled.

APPENDIX A

CONDENSATION MODEL FOR SPECIES IN INTERNAL FLOWS

A.1 Hydrocarbon and Acids Condensation Model

Diesel exhaust contains a wide range of hydrocarbon and hydrocarbon-derived species. These include unburned and partially burned fuel and lube oil. Some of these compounds can condense on cooler surfaces. Condensation occurs when the surface of the cooler is below the dew point for the partial pressure of the compound. Thus, heavier species and higher concentration species will condense most.

In addition, acids are known to contribute to chemical reactions with hydrocarbons, leading to hard deposits. It is possible that acids play a role in aging of deposits, although there does not seem to be any literature confirming this mechanism.

In a free stream of a gas at (P,T) containing some different species and flowing over a surface (below the dew point of the species), a condensate film forms on the surface as shown in Figure A.1.

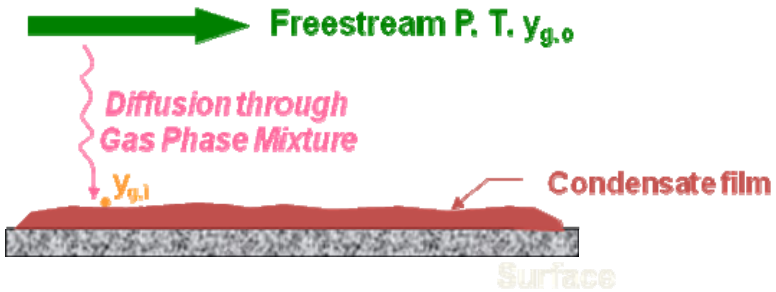

Figure A.1 – Condensation film forms on a surface

The phenomenon of interface mass transfer can be seen from the point of kinetic theory as a difference between two quantities: a rate of arrival of molecules from the vapor phase to the interface and a rate of departure of molecules from the liquid surface towards the vapor phase. When condensation occurs, the arrival rate is larger than departure rate [1]. During evaporation, the departure rate is larger than arrival rate. It is obvious that during equilibrium the two rates are the same. In case of condensation, mass condensation flux from the gas stream to the surface is defined by [1]:

$$j_{g,i} = K\rho \ln\left(\frac{1-y_{g,i}}{1-y_{g,o}}\right) \tag{A.1}$$

Where K is a mass transfer coefficient defined by analogy between heat and mass transfer as:

$$K = \left(\frac{h_c}{\rho C_p}\right)\left(\frac{\mathrm{Pr}}{Sc}\right)^{2/3} \tag{A.2}$$

$$Nu = \frac{h_c D}{k_g} = \frac{(\mathrm{Re}-1000)\,\mathrm{Pr}\, f/8}{1.0+12.7\sqrt{\mathrm{f}/8}(\mathrm{Pr}^{2/3}-1.0)} \tag{A.3}$$

By employing the above definitions, Equation A.1can be rewritten as:

$$j_{g,i} = \frac{(\mathrm{Re}-1000)\, f/8}{1.0+12.7\sqrt{\mathrm{f}/8}(\mathrm{Pr}^{2/3}-1.0)}\left(\frac{\mathrm{Pr}^2}{Sc}\right)^{1/3}\frac{\alpha}{D}\rho \ln\left(\frac{1-y_{g,i}}{1-y_{g,o}}\right) \tag{A.4}$$

The mass flux is a function of the species mole fraction in the main flow and that of at the interface. The total mole fraction of all hydrocarbons (C1 based) in the exhaust flow is measured by ORNL. The total count of each species is also given in Figure A.2. So, one is able to calculate the mass fraction of each species as described step by step in the next section.

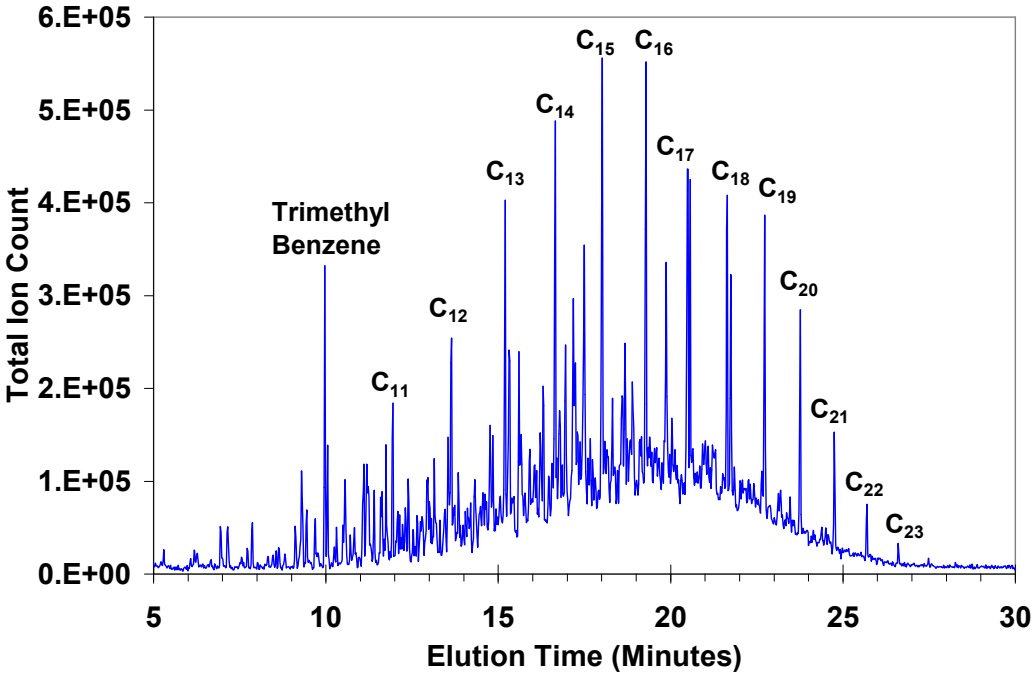

Figure A.2 – Hydrocarbon speciation in EGR flows

There is a wide range of hydrocarbons in the exhaust and it is not really necessary to model every single species of them. C22 represents C21 to C24; C18 represents C17 to C20; and C15 represents C13 to C15 in the model. The model shows that there is no condensation for hydrocarbons lighter than C12 in the range of coolant temperature (313 K-363 K). So, only heavy hydrocarbons (>C12) are taken into account in the model.

It should be noted that the mole fraction of each species at the interface of liquid and gas can be calculated as the ratio of the partial pressure of the compound at the interface to the total pressure of the mean flow:

$$y_{g,i} = \frac{P_{g,i}}{P_{total,m}} \tag{A.5}$$

Partial pressure can be calculated by utilizing the Antoine coefficients of the species as:

$$Log_{10}P_{g,i} = A - \frac{B}{T_{\text{int}erface} + C} \tag{A.6}$$

where A, B, and C are the Antoine coefficients of each species. Pressure in above equation is in mm-Hg and temperature is in $^{\circ}$C in equation.

It is assumed when HC condenses on the wall, it diffuses through the porous fouled layer and stays near the cold wall. Cold wall temperature does not let HC molecules evaporate. However, the interface temperature is the critical factor in calculating HCs condensed mass, it does not play a role in evaporating HC molecules. It is an assumption in the model and it is compatible with experimental observations. Also, there is no evaporation since the HC molecules have diffused through the porous layer and sit near the cold wall.

A.2 Calculating Mole Fraction of Each HC Species in the Gas Flow

$$CH_{1.809} + 4.12(O_2 + 3.76N_2) \rightarrow CO_2 + 0.9045H_2O + 15.491N_2 + 2.667O_2$$

$$n_{total} = 20.105$$

$X(ppm) - C1$	Inlet PPM – C1 Based
C_i	Number of carbon in the species
$X(ppm) = \frac{X(ppm) - C1}{\sum_i C_i y_i}$	Mole fraction of all HC species in the bulk gas flow
x_i	Mass fraction of each species in the fuel
MW_i	Molecular weight of each species
MW_{Flow}	Molecular weight of the bulk flow

$\dot{m}_{flow} = \dot{n}_{total}\, MW_{Flow}$	Mass of flow per unit time step
$\dot{m}_{HC} = X(ppm)\dot{n}_{total}\, MW_{Fuel}$	Mass of hydrocarbons (fuel) per unit time step
$\dot{m}_i = x_i X(ppm)\dot{n}_{total}\, MW_{Fuel}$	Mass of each species per unit time step
$\dot{n}_i = \frac{x_i X(ppm)\ \dot{n}_{total}\, MW_{Fuel}}{MW_i}$	Total mole of each species per unit time step
$y_{i-flow} = \frac{x_i X(ppm) MW_{Fuel}}{MW_i}$	Species mole fraction in the flow

A.3 References

[1] Collier, J.G., J.R., Thome, Convective Boiling and Condensation, 3rd Ed., 1996.